

Alma Mater Studiorum – Università di Bologna

DOTTORATO DI RICERCA IN

Ingegneria Biomedica, Elettrica e dei Sistemi

Ciclo 32°

Settore Concorsuale: 09/E4

Settore Scientifico Disciplinare: ING-INF/07

TITOLO TESI

Integration of conventional and unconventional Instrument
Transformers in Smart Grids

Presentata da: Alessandro Mingotti

Coordinatore Dottorato

Supervisore

Prof. Daniele Vigo

Prof. Lorenzo Peretto

Esame finale anno 2020

Preface

This thesis concludes a three-years work. It contains the main achievements, result of study and effort aimed at contributing, with a little step further, to the scientific knowledge.

To this purpose, the reader will be guided towards the role of Instrument Transformers inside the always evolving Smart Grid scenario. In particular, even non-experts or non-metrologists will have the chance to follow the main concepts presented; this, because the basic principles are always presented before moving to in-deep discussions.

The chapter including the results of the work is preceded by three introductory chapters. These, contain the basic principles and the state of the art necessary to provide the reader the tools to approach the results chapter.

The first three chapters describe: Instrument Transformers, Standards, and Metrology. In the first chapter, the studied Instrument Transformers are described and compared with particular attention to their accuracy parameters. In the second chapter instead, two fundamental international documents, concerning Instrument Transformers, are analysed: the IEC 61869 series and the EN 50160. This has been done to be completely aware of how transformers are standardized and regulated. Finally, the last introductory chapter presents one of the pillars of this work: metrology and the role of uncertainty. As a matter of fact, it is fundamental to provide an accuracy parameter together with the result of a measurement. Therefore, this aspect is stressed and highlighted along the results description to confirm their meaningfulness.

In the core of the work Instrument Transformers integration in Smart Grid is distinguished in two main topics. The first assesses the transformers behaviour, in terms of accuracy, when their normal operation is affected by external quantities (either electric or environmental). The second exploits the current and voltage measurements obtained from the transformers to develop new algorithm and techniques to face typical and new issue affecting Smart Grids.

In the overall, this thesis has a bifold aim. On one hand it provides a quite-detailed overview on Instrument Transformers technology and state of the art. On the other hand, it describes issues and novelties concerning the use of the transformers among Smart Grids, focusing on the role of uncertainty when their measurements are used for common and critical applications.

CONTENT

Page

1. Instrument Transformers	1
1.1. Inductive Instrument Transformers	1
1.1.1. Basic Principles	1
1.1.1.1. Ideal configuration	1
1.1.1.2. Real configuration	2
1.1.2. Current Transformers	3
1.1.2.1. From the equivalent circuit to the ratio and phase-angle	3
1.1.2.2. Current transformers types	4
1.1.2.3. Current transformers accuracy	5
1.1.3. Voltage Transformers	5
1.1.3.1. From the equivalent circuit to the ratio and phase-angle	5
1.1.3.2. Voltage transformers types	7
1.1.3.3. Voltage transformers accuracy	8
1.1.4. Combined Transformers	8
1.2. Low-Power Instrument Transformers	9
1.2.1. Introduction	9
1.2.1.1. LPITs accuracy	10
1.2.2. Current Transformers: Rogowski Coils	10
1.2.2.1. Basic principles	10
1.2.2.2. Advantages and disadvantages	12
1.2.3. Voltage Transformers: Capacitive Dividers	12
1.2.3.1. Basic principles	12
1.2.3.2. Advantages and disadvantages	13
2. International Standards	15
2.1. IEC 61869	15
2.1.1. IEC 61869-1 and IEC 61869-6	16
2.1.1.1. Operating conditions and rated values	16
2.1.1.2. Tests on the ITs	17
2.1.2. IEC 61869-2 and IEC 61869-3	17
2.1.3. IEC 61869-4 and IEC 61869-12	20
2.1.4. IEC 61869-10 and IEC 61869-11	20
2.2. EN 50160	21
2.2.1. Medium and Low Voltage supply characteristics	21
3. The Role of Uncertainty	23
3.1. Basic Principles	23
3.2. Guide to the Expression of Uncertainty in Measurements	25
3.2.1. Introduction	25
3.2.2. The GUM	25
3.2.2.1. Basic definitions and concepts	25
3.2.2.2. Evaluating standard uncertainty	26
3.2.2.3. The Monte Carlo method	27
3.2.2.4. The central limit theorem	28
4. Instrument Transformers & Smart Grids	30
4.1. ITs vs. Influence Quantities	30
4.1.1. Inductive VT, Verification of Accuracy Depending on Temperature	30
4.1.1.1. Introduction	30
4.1.1.2. Experimental setup	31
4.1.1.3. Experimental tests & results	35
4.1.1.4. Conclusion	37

4.1.2. Inductive CT, Verification of Accuracy Depending on Temperature	38
4.1.2.1. Introduction	38
4.1.2.2. Automatic measurement setup	38
4.1.2.3. Tests & results	40
4.1.2.4. Conclusion	44
4.1.3. Accuracy vs. multiple influence quantities verification of passive LPCT	45
4.1.3.1. Introduction	45
4.1.3.2. Automatic measurement system	45
4.1.3.3. Experimental tests	46
4.1.3.4. Experimental results	48
4.1.3.5. Conclusion	54
4.2. ITs Integration into Smart Grid Operation	56
4.2.1. A novel approach for assessing the time reference in asynchronous measurements	56
4.2.1.1. Introduction	56
4.2.1.2. The approach	57
4.2.1.3. Numerical example	60
4.2.1.4. Final remarks	65
4.2.1.5. Appendix	64
4.2.2. Uncertainty analysis of an equivalent synchronization method for phasor measurements	66
4.2.2.1. Introduction	66
4.2.2.2. Line modelling: PI-section line schematization	66
4.2.2.3. The proposed approaches	67
4.2.2.4. Simulations results	71
4.2.2.5. Measurement setup	72
4.2.2.6. Numerical examples	72
4.2.2.7. Conclusion	76
4.2.3. A general expression for uncertainty evaluation in residual voltage measurement	78
4.2.3.1. Introduction	78
4.2.3.2. Residual voltage	79
4.2.3.3. Uncertainty evaluation	81
4.2.3.4. Experimental setup	86
4.2.3.5. Experimental tests & results	87
4.2.3.6. Conclusion	90
5. Conclusion	92

Chapter 1

INSTRUMENT TRANSFORMERS

In this chapter the key element of the thesis is presented: the instrument transformer (IT). It is “a transformer intended to transmit an information signal to measuring instruments, meters and protective or control devices”, here a transformer is “an electric energy converter without moving parts that changes voltages and currents associated with electric energy without change of frequency” [1]. ITs were developed at the end of the nineteenth century and their improvement continues even today. To understand their evolution over the years, the following section provides an overview of the main technologies and their working principles. This will help the reader to understand the structure of the document and clarify some aspects useful to master the core of this thesis.

1.1 Inductive Instrument Transformers

1.1.1 Basic Principles

The transformer [2, 3] is a static electric machine and can be represented by Fig. 1.1. It consists of a magnetic core, typically obtained by joining several thin metallic layers, and of two copper windings: the primary and the secondary. Its working principle is based on Faraday’s law, Lenz’s law, and conservation of energy law. It is important to understand the difference between its ideal and real configuration to grasp the concept of ITs.

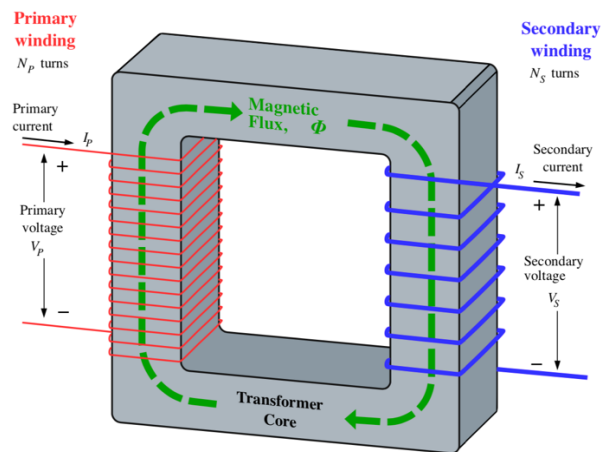


Fig. 1.1. Main components of a generic transformer

1.1.1.1 Ideal configuration

By applying an alternate voltage source V_p to the primary windings, as in Fig. 1.1, a varying magnetic flux ϕ is generated by the current of the winding I_p and transmitted via the infinite magnetic permeability of the transformer core. Then, such a varying flux induces an electromotive force on the secondary windings which results in a current I_s generated in the secondary windings, hence in a secondary voltage V_s . In light of this behavior, the ratio between the primary and secondary quantities depends on the number of turns of the primary and secondary, N_p and N_s , respectively. In particular, it is:

$$\frac{V_p}{V_s} = \frac{I_s}{I_p} = \frac{N_p}{N_s}, \quad (1.1)$$

where (1.1) holds only under two ideal hypotheses on the magnetic material of the core: linearity (hence with a permeability μ far higher than the one of free space μ_0) and null conductivity (no iron

losses). This results in two possible behaviors, a step-down transformer is obtained if $N_P > N_S$, whereas a step-up one is the result of $N_P < N_S$.

1.1.1.2 Real configuration

A better representation of a transformer can be provided if nonidealities are considered. By referring to Fig. 1.2, which shows the equivalent circuit of a transformer, these can be detailed as:

- Joule Losses. Primary and secondary windings are made of copper; hence losses can be represented as resistors (R_P and R_S' for the primary and secondary, respectively).
- Leakage Flux. This includes the amount of flux which does not concatenate with the secondary windings, hence it is lost and not transferred in the secondary. Such phenomenon is represented with a reactance for both the primary (X_P) and secondary (X_S') circuits.
- Eddy Currents. These loss currents rise in the magnetic material of the core, due to its not-null conductivity. They are proportional to the square of the thickness of the laminated layers, which represent the magnetic material.
- Hysteresis Losses. Due to the nonlinearity of the magnetic material, a percentage of energy is lost at every polarity change of the magnetic field.

The last two aspects are also known as core losses, because they arise from phenomena taking place in the core of the transformer. Their effect is represented by a resistor R_C considering that the physical effect is heat production, and then a current I_C is flowing through the resistor.

- Magnetizing reactance. A reactance X_M is introduced in the equivalent circuit of the transformer (Fig. 1.2) to include a further nonideality. The iron used for the core has a very small reluctance, but clearly not zero. Therefore, a magnetizing current I_M is required to maintain the mutual flux inside the transformer core.

Finally, the two currents (I_C and I_M) originated from the transformer's nonidealities can be combined to a current I_0 , referred to as the no-load condition current.

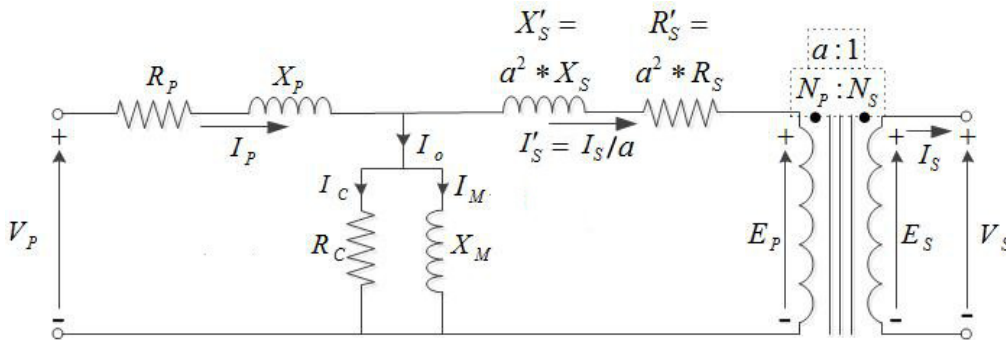


Fig. 1.2. Transformer equivalent circuit, referred to the primary windings

Considering the nonidealities introduced above, from the equivalent circuit referred to the primary windings of Fig. 1.2, it can be emphasized that:

- The secondary current of a transformer is not exactly proportional to the transformer ratio a due to the presence of the core losses.
- The secondary voltage of a transformer is not exactly proportional to the transformer ratio a due to the presence of the primary and secondary windings impedance.
- In primary or secondary equivalent circuits, it is essential to consider the effects of the impedance on the other side. In an equivalent primary circuit, a weight of a^2 for R_S is considered. In an equivalent secondary circuit, $1/a^2$ for R_P is applied.

After describing the main principles of the transformer, the following subsections discuss in detail some peculiarities of both current and voltage transformers.

1.1.2 Current Transformers

1.1.2.1 From the equivalent circuit to the ratio and phase-angle

The Current Transformer (CT) is used in series to the main circuit, as shown in Fig. 1.3. The primary current I_p is scaled to the secondary one I_s , which is typically closed on a resistive burden B . The CT burden is almost a short circuit and in most of the applications it has one point connected to ground. As for the number of coil's turns, typically the primary circuit only has few of them (or even none, as explained in the following), whereas the number of coil turns in the secondary circuit is much higher depending on the desired transformation ratio.

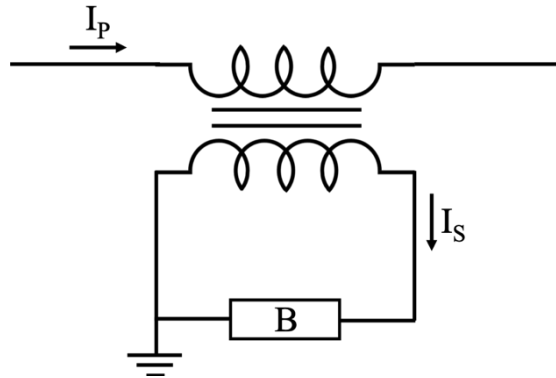


Fig. 1.3. Connection of the CT in series to the main circuit

From Fig. 1.2 and 1.3, it is possible to build a simple vector diagram of the CT. Let \bar{E}_S be the phasor of voltage induced in the secondary windings by the primary current; then its relation with the overall secondary burden \bar{Z}_S is $\bar{E}_S = \bar{I}_S * \bar{Z}_S$. As for the angles, \bar{E}_S is 90° shifted from the flux ϕ , and leading \bar{I}_S of an angle φ_S . To complete the vector diagram of the CT, depicted in Fig. 1.4, the primary current \bar{I}_p and the overall core leakage current \bar{I}_0 must be defined: the former is the sum of \bar{I}_0 and the secondary current referred to the primary circuit \bar{I}_S' , by being multiplied by $N_T = 1/a$. The latter current, \bar{I}_0 , is obtained by summing the magnetizing current \bar{I}_M , in phase with ϕ and the loss current \bar{I}_C , 90° leading ϕ . Hence:

$$\bar{I}_S' = N_T * \bar{I}_S, \quad (1.2)$$

$$\bar{I}_p = \bar{I}_0 + \bar{I}_S', \quad (1.3)$$

$$\bar{I}_0 = \bar{I}_M + \bar{I}_C. \quad (1.4)$$

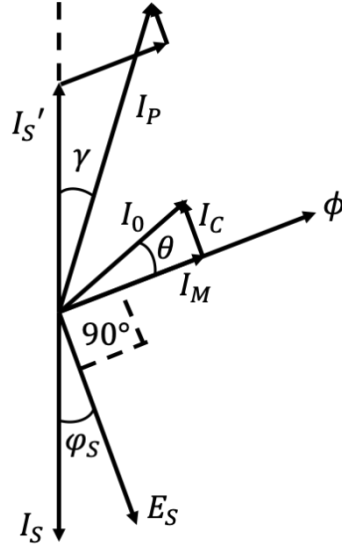


Fig. 1.4. Vector diagram of the CT

At this point, the expressions of the actual transformer ratio N and phase-angle between currents γ [4], both function of the CT parameters, can be written as:

$$N = N_T \left[1 + \frac{2(I_M \sin \varphi_S + I_C \cos \varphi_S)}{I_S N_T} + \frac{I_0^2}{I_S^2 N_T^2} \right]^{1/2}, \quad (1.5)$$

$$\gamma = \frac{I_0 \cos(\varphi_S + \theta)}{I_S N_T}, \quad (1.6)$$

where θ is the angle between \bar{I}_0 and the flux, whereas the quantities without the vector symbol refer to the correspondent magnitudes. From (1.5) and (1.6) it is clear that both N and γ depend on several CT parameters which basically result from the geometry of the transformer. A further simplification of those equation can be done under the hypotheses of (i) a mainly resistive burden with a slight inductive component and (ii) a very small φ_S . Then:

$$N \approx N_T \left(1 + \frac{I_C}{I_P} \right), \quad (1.7)$$

$$\gamma \approx \frac{I_M}{I_P}. \quad (1.8)$$

These last expressions provide at a glance which CT parameters affect the most N and γ .

1.1.2.2 Current transformers types

The basic principle detailed above can be implemented in more than one type of CTs. In particular, three main types of CT can be distinguished in typical applications: wound-type, bar-type, and toroidal-type. An example of each has been collected in Fig. 1.5.



Fig. 1.5. From left to right: wound-type, bar-type, toroidal-type CT

The wound-type CT has to be installed in series to the main circuit through its terminals; then the main case contains the primary and the secondary windings, insulated one from another. The bar-type differs from the previous by the fact that the primary “bar” that composes the CT is the only primary winding available, hence constitutes a single turn configuration. Again, it has to be installed in series to the main circuit. As for the toroidal-type, it differs from the others, because here the primary conductor has to be inserted into the hole of the CT. Hence, the conductor constitutes of the primary winding only, whereas in the CT case, the secondary wires are wound around the toroidal base.

In terms of carried current, the bar-type is used for carrying very high currents, whereas the wound-type is the mostly used for low ratios and low current values.

1.1.2.3 Current transformers accuracy

The described technologies for manufacturing CTs share common definitions when dealing with CTs accuracy: ratio (or current) error ε and phase displacement $\Delta\varphi$. From [1], the ratio error is “the error which a current transformer introduces into the measurement of a current and which arises from the fact that the actual transformation ratio is not equal to the rated transformation ratio”, whereas the phase displacement is “the difference in phase between the primary and secondary currents, the positive direction of the primary and secondary currents being so chosen that this difference is zero for a perfect transformer”. The two accuracy indicators are defined in the Standard IEC 61869-2 dedicated to the inductive current transformers [5] (detailed in the next chapter) as:

$$\varepsilon = \frac{k_r I_S - I_P}{I_P} * 100, \quad (1.9)$$

$$\Delta\varphi = \hat{I}_S - \hat{I}_P, \quad (1.10)$$

where k_r is the CT nominal ratio, I_P and I_S are the rms values of the primary and secondary currents, respectively. As for (1.10), \hat{I}_P and \hat{I}_S are the phase-angles of the primary and secondary current phasors. The accuracy parameters ε and $\Delta\varphi$ allow to determine the performance of a CT, according to the Standard, by referring to standardised accuracy classes collected in [5] and described in the following.

1.1.3 Voltage Transformers

1.1.3.1 From the equivalent circuit to the ratio and phase-angle

Conversely to current transformers, Voltage Transformers (VTs) [4] are much similar to power transformers which are spread among the network nodes to appropriately scale the voltage. As Fig. 1.6 shows, the connection of the VT to the network is different from the CT link. In fact, the primary windings of the VT are connected to both lines of the main circuit; this way the VT is subjected to the line voltage. This leads to another peculiarity of the VT: by considering the voltage stability of

the network, the VTs primary input varies in a very limited range compared to the CTs, which can experience a variety of different currents depending on the load demand of a particular time-slot. Therefore, the flux inside the core of a VT can be considered as almost constant, whereas the one of the CTs cannot.

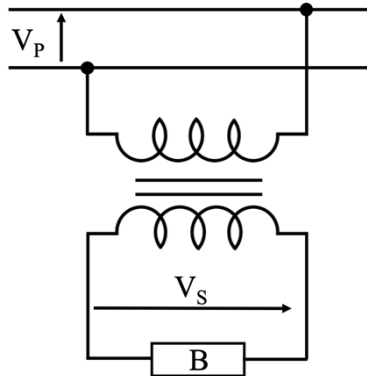


Fig. 1.6. Connection of the VT in parallel to the main circuit

As for the burden of a VT, there is another interesting comparison: whereas the CTs work under almost short-circuit conditions, the VTs work under near open-circuit conditions, with relatively high burdens (instrumentation) connected to the secondary terminals.

Even for the VTs, it is worth to consider a vector diagram to comprehend the main quantities that have an important role in the VT operation. Note the VT vector diagram in Fig. 1.7. Distinguish these parameters: the flux ϕ and the 90° lagging voltage \bar{E}_S induced in the secondary windings. In turn, \bar{E}_S generates the secondary current \bar{I}_S , hence a secondary voltage \bar{V}_S at the secondary output terminals of the VT, by considering the presence of the secondary impedance \bar{Z}_S . Then there is $\bar{E}'_S = a\bar{E}_S$, the secondary induced voltage reflected to the primary side of the VT by the transformer ratio. This component summed to the voltage drop caused by the primary impedance \bar{Z}_P originated the primary voltage \bar{V}_P . Finally, the primary current \bar{I}_P is obtained by summing \bar{I}_0 and the secondary current referred to the primary circuit $\bar{I}'_S = \bar{I}_S/a$.

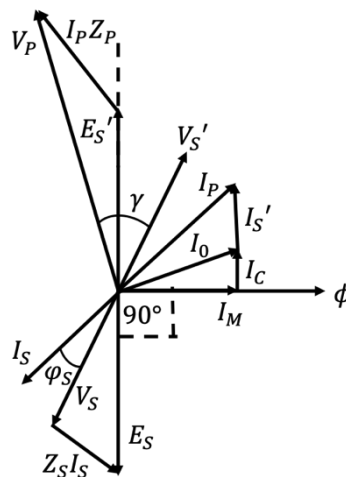


Fig. 1.7. Vector diagram of the VT

In the case of a VT, the quantities of interest are the ratio between the primary and secondary terminal voltages N and the phase-angle between them γ (\bar{V}_P and \bar{V}'_S , respectively). Their approximated expression, without detailing the computation step because out of the aim of this work, are:

$$N = a \left[1 + \frac{I_S(R_{TS}\cos\varphi_S + X_{TS}\sin\varphi_S) + \frac{I_C R_P + I_M X_P}{a}}{V_S} \right], \quad (1.11)$$

$$\gamma = \frac{I_M R_P - I_C X_P}{a V_S} - \frac{I_S}{V_S} (X_{TS}\cos\varphi_S - R_{TS}\sin\varphi_S). \quad (1.12)$$

Where R_{TS} and X_{TS} are two equivalent impedances defined as:

$$R_{TS} = R_S + \frac{R_P}{a^2} \quad (1.13)$$

$$X_{TS} = X_S + \frac{X_P}{a^2} \quad (1.14)$$

From a first comparison between (1.5)-(1.6) and (1.11)-(1.12), note the complexity of the VT expressions and their dependence on more VT parameters.

1.1.3.2 Voltage transformers types

By starting from the working principle of the transformer, in what follows are described two of the most spread types of VTs that can be found in the market, which differ one from the other by slight peculiarities. The two typologies are: wound-type, and capacitive-type transformers, and they are collected in Fig. 1.8. It is sometimes difficult to distinguish one type from the other from their construction.



Fig. 1.8. From left to right: wound-type, capacitive-type VT

The wound-type voltage transformer is exactly the application described in the previous sections: two sets of windings are used to scale the voltage to match with the measuring/protective instruments inputs.

The capacitive-type voltage transformer (CVT) is basically a VT not directly connected to the power line. In between a series of two capacitors (C_1 and C_2) is installed; in particular, the VT is connected to the C_2 terminals (as depicted in Fig. 1.9), whereas the power line voltage is applied to the series of the two capacitors. This way it is possible to reduce extra-high voltages guaranteeing the safety properties of a standard VT.

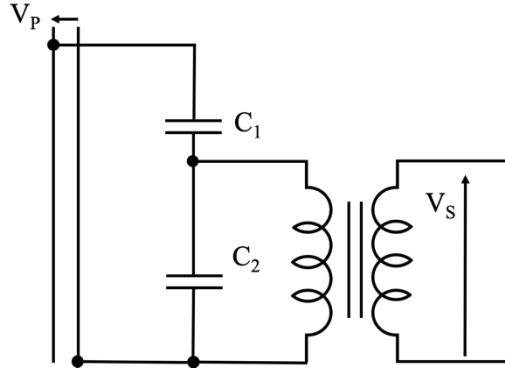


Fig. 1.9. Schematic of a capacitive voltage transformer

1.1.3.3 Voltage transformers accuracy

As it is standardized in [5] for CTs, the accuracy parameters, ratio error and phase displacement, of a VT are defined in IEC 61869-3 [7]. They are defined as:

$$\varepsilon = \frac{k_r U_S - U_P}{U_P} * 100, \quad (1.15)$$

$$\Delta\varphi = \hat{U}_S - \hat{U}_P, \quad (1.16)$$

where U_P and U_S are the primary and secondary rms voltage of the VT under test, whereas k_r is its nominal ratio. In (1.16) the circumflexed quantities \hat{U}_P and \hat{U}_S refer to the phase of the primary and secondary voltages.

Based on this, it is clear how the performance scenario of the inductive ITs has been well uniformized by International Standards. As a matter of fact, both kinds of ITs (including the unconventional ones, as described in the following chapters) are assessed by always referring to the same expressions.

1.1.4 Combined Transformers

An instrument that includes the features of VTs and CTs is the combined transformer. By definition, it is an “instrument transformer consisting of a current and a voltage transformer in the same enclosure” [1], hence it does not introduce novelties from a technological point of view but only in the application of different technologies. It is largely adopted in High Voltage (HV) primary stations, but it can be found even in Medium Voltage (MV) applications. They are typically installed in places with limited free space, as fewer mechanical structures are needed. In addition, the cost of combined transformers is lower than for single transformers. Fig. 1.10 includes a picture (left) and a simple schematic diagram (right) of the combined transformer.

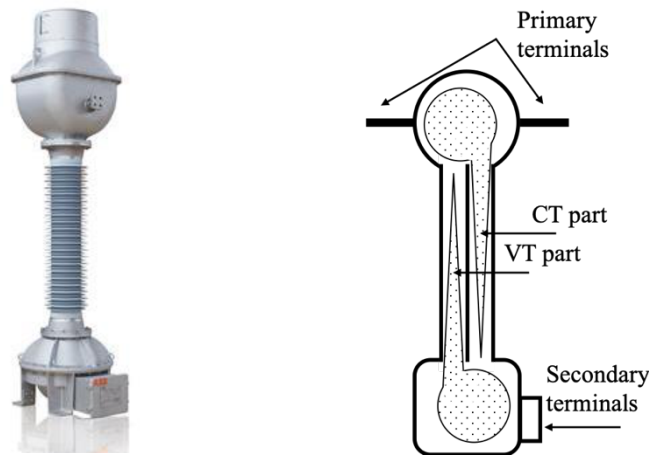


Fig. 1.10. Picture (left) and simple schematic (right) of a combined transformer

The upper part of the transformer is dedicated to the primary terminals; in fact, the voltage is applied on just one of the current terminals. The main central part of the instrument provides the main connections for the two measured quantities: there is proper physical separation between the voltage and the current. This is also the main drawback of the combined solution: the two parts are separately insulated and contained inside the external insulation. Therefore, parasitic capacitances arise and are subjected to an electric field distributed in the height of the combined transformer. Finally, the lower part of the transformer contains the secondary voltage and current terminals, including the ground connection.

For the accuracy of the combined transformer, refer to Standard IEC 61869-4 [8]. In particular, the Standard assesses the transformer accuracy by using the ratio error and phase displacement expressions defined singularly for VTs and CTs.

1.2 Low-Power Instrument Transformers

1.2.1 Introduction

A new generation of ITs has been developed and spread in the last few decades. Initially, they have been referred to as non-conventional ITs; while after their standardization, they are referred to as Low-Power Instrument Transformers (LPITs) or simply “sensors” as another accepted term. The general aspects of LPITs are regulated by Standard IEC 61869-6 [9], defining these devices as: “arrangement, consisting of one or more current or voltage transformer(s) which may be connected to transmitting systems and secondary converters, all intended to transmit a low- power analogue or digital output signal to measuring instruments, meters and protective or control devices or similar apparatus”. In addition to this definition, it is essential to clarify the meaning of “low-power”. The Standard [9] states that an IT can be considered low-power if its output is typically lower than 1 VA. So, it is clear that the Standard has not been strict in defining the LPITs; therefore, the classification of ITs is not as straightforward as it seems, there is some degree of freedom to the manufacturer and user of such devices.

The LPITs structure, is shown in Fig. 1.11 in the block diagram, where the upper block-chain describes the general components of a passive LPIT, while the bottom blocks only apply to active LPITs. However, the block diagram, defined in [9], does not constitute a fixed schematic to build a LPIT but a general one which could vary depending on the considered device.

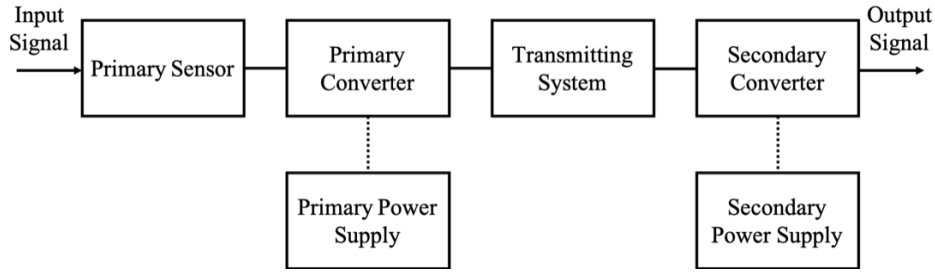


Fig. 1.11. General block diagram of a single-phase LPIT

Fig. 1.11 highlights that the basic principle of the LPITs is not common to all of them, but it varies depending on each technology for manufacturing them. The following section discusses two kinds of LPITs in detail, these are examined in the core of this thesis; the typical technologies adopted for LPITs are: resistive, capacitive, and resistive/capacitive dividers for Low-Power Voltage Transformers (LPVTs); and Rogowski coils, inductive transformers, shunts, for the Low-Power Current Transformers (LPCTs).

1.2.1.1 LPITs accuracy

The accuracy of the LPITs is just an extension of the concepts for the accuracy of inductive ITs. In fact, the definitions of ratio error ε and phase displacement $\Delta\varphi$ still apply:

$$\varepsilon = \frac{k_r Y_S - X_P}{X_P} * 100, \quad (1.17)$$

$$\Delta\varphi = \hat{Y}_S - \hat{X}_P. \quad (1.18)$$

The differences rely only on the notation of the expressions; in fact, for the LPITs it is not always true that the input quantity is the same as the output one. Hence, there is a new notation in (1.17) and (1.18): X_P and Y_S are the primary and secondary quantities, respectively; whereas \hat{X}_P and \hat{Y}_S are the phases related to these quantities.

1.2.2 Current Transformers: Rogowski Coils

1.2.2.1 Basic principles

The Rogowski coil [10, 11] is a measurement device used to measure alternating currents. It consists of an iron-free toroidal core, typically made of air or other insulating materials, on which a solenoid is wound. Then, the conductor carrying the current to be measured is inserted in the Rogowski as shown in Fig. 1.12; where S and R are cross-section and radius, respectively.

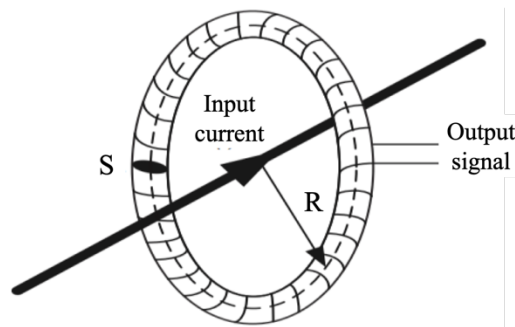


Fig. 1.12. Basic structure of a Rogowski coil

The working principle of a Rogowski coil is based on Ampere's law: the current $i_p(t)$ flowing through the primary conductor generates a varying magnetic field B , which induces a voltage $u_s(t)$

at the solenoidal terminals, proportional to the mutual inductance M between the primary and secondary conductors. Such phenomenon can be expressed as:

$$u_s(t) = -M \frac{di_p(t)}{dt}. \quad (1.19)$$

Equation (1.19) shows that the Rogowski output is not a current proportional to the primary one, but a voltage proportional to the derivative of $i_p(t)$. Therefore, in its basic configuration, the device cannot provide a current-to-current relation to be used to process the measurement performed with the Rogowski coil. To obtain such a relation, an integrating block is necessary in cascade to the device; however, for the sake of simplicity and to avoid any external components, typical off-the-shelf Rogowski coils do not include any integrator. In addition, the coils are provided to the end users with a current to voltage ratio (e.g. 10 A/ 100 mV) to be used during measurements.

Based on these principles, it is possible to obtain an equivalent circuit of the Rogowski coil, valid for low frequencies including the power frequencies, 50 and 60 Hz. See Fig. 1.13, which contains:

- An ideal transformer, which provides the nominal ratio of the device;
- an inductor L_S :

$$L_S = \frac{\mu_0 N^2 d_c}{2\pi} \log \frac{b}{a}, \quad (1.20)$$

- a resistor R_S :

$$R_S = \rho \frac{l_w}{\pi r^2}, \quad (1.21)$$

- a coupling capacitor C_S ,

$$C_S = \frac{4\pi^2 \varepsilon_0 (b+a)}{\log \frac{b+a}{a-a}}, \quad (1.22)$$

where ρ , ε_0 , and μ_0 are the wire electrical resistivity, vacuum permittivity and permeability, respectively. As for the geometrical parameters, N is the number of turns, b and a are the outer and inner diameters of the toroid, r is the wire radius, d_c is the single loop diameter and l_w is the length of the coil. For the sake of clarity, the meaning of the geometrical parameters is clarified in Fig. 1.14.

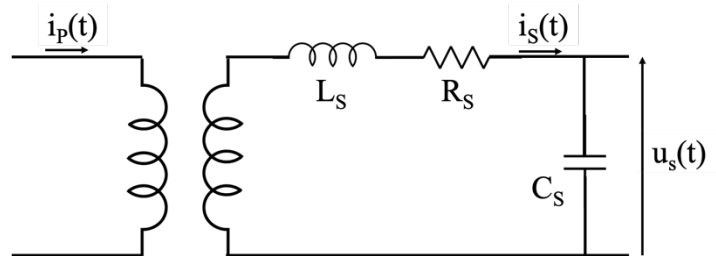


Fig. 1.13. Rogowski coil equivalent single-phase circuit

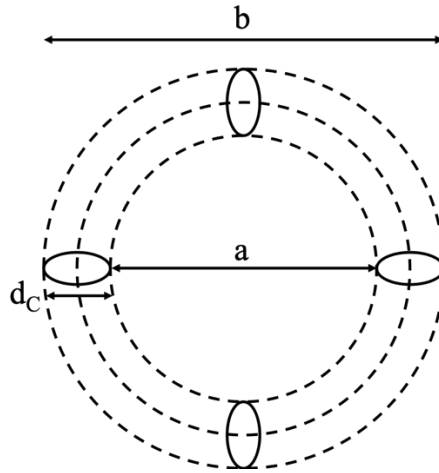


Fig. 1.14. Geometrical parameters clarification picture

Considering expressions (1.20) to (1.22) note that precise manufacturing information is required to obtain the Rogowski parameters; hence, obtaining such parameters is not straightforward for off-the-shelf devices.

1.2.2.2 Advantages and disadvantages

The previous subsection showed that the structure and the working principle of a Rogowski coil is quite simple. In addition, it has some features which can be compared briefly to legacy ITs.

The first feature derives from the core material, being iron-free, the Rogowski coil does not suffer from the nonlinearities of a typical IT; therefore, the Rogowski coil can be considered linear in its entire working range. Such a range is theoretically infinite, and significantly higher than the one of an IT, which is typically in the order of 10 times the rated current. Continuing with the geometrical features, a Rogowski coil is far smaller and more compact than an IT; hence it fits in all applications which do not have sufficient space for post-installation of instrumentation.

These coils also offer advantages regarding the measurements provided.: they work in a wide range of frequencies (from fractions of Hz to almost GHz) and they provide accurate answers to short transient input signals. In terms of safety, they guarantee the electrical insulation between the primary and the secondary circuits, considering that no active parts of the primary circuit are connected to the secondary windings.

However, Rogowski coils also have some drawbacks which make them unsuitable for certain applications. For example, the need of an integrating circuit in addition to the Rogowski coil makes it necessary to have power supply close to the Rogowski application, and that is not always possible for physical or safety reasons. Furthermore, Rogowski coils are very sensitive to the physical and electrical environment (i.e. primary conductor position, electric fields, temperature, etc.); hence a preliminary study on the location of the Rogowski coil is necessary to avoid collecting invalid measurements.

1.2.3 Voltage Transformers: Capacitive Dividers

1.2.3.1 Basic principles

Among the LPVTs, regulated by the IEC 61869-11 [12], the Capacitive Divider (CD) [13, 14] is one of the most common types. It is a passive LPVT and does not require any external power supply, which results in huge flexibility for in-field installation. As the name indicates, the CD consists of a series of two capacitors C_1 and C_2 as in Fig. 1.15; where V_p and V_s are the input and output voltages of the CD. In addition, the picture shows the terminal markings as A , a , and n for the high-voltage primary terminal, high-voltage secondary terminal and reference terminal, respectively as defined in [12].

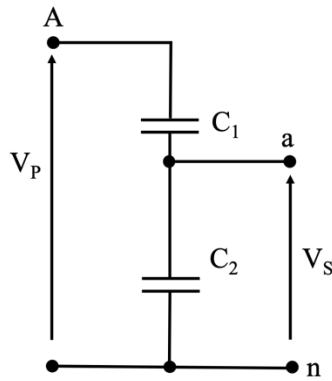


Fig. 1.15. Capacitive divider schematic

When the voltage V_p is applied, the two capacitors are subjected to the same charge Q but not to the same voltage. The relationship between the charge and the capacitor value C is described by the relation $V = Q/C$. Hence, the higher the value C , the lower the voltage at its terminals. Therefore, the input/output expression of the CD is summarized by:

$$V_S = V_P \frac{C_1}{C_1 + C_2} \quad (1.23)$$

In other words, to reduce the input voltage it is sufficient to have two capacitors with $C_1 < C_2$. Such a simple technology is spread, in alternating current applications, along all voltage levels, from the low to the extra-high voltage. Fig. 1.16 shows two CDs, one for medium voltage (left), and one for high voltage (right). Note that in many CDs one of the capacitors is obtained directly using the insulating material which establishes the cage of the overall CD. In fact, the key point is to reach the desired value of capacitance, hence several technologies like the one mentioned are adopted by manufacturers.



Fig. 1.16. Picture of a medium voltage (left) and a high voltage (right) CD

1.2.3.2 Advantages and disadvantages

The widespread deployment of CDs is sustained by their numerous advantages with respect to other technologies. For example, compared to a resistive divider, a CD does not suffer from the heat dissipation due to the resistors. Hence, the current flowing through the divider is not a limiting parameter of a CD. In terms of frequency, the CD is not subjected to any variation in its behavior because, even if the reactance is equal to $X_C = \frac{1}{2\pi fC}$, the frequency dependency affects both the capacitors of a CD, hence the overall effect is null. Therefore, CD has a linear behavior in a wide range of frequencies. There are two relevant disadvantages: first, CDs cannot be used in direct current

application, due to the nature of their capacitors. Second, as defined in 1.2.3.1 and concluded in (1.23) these properties are true when ideal (or highly accurate) capacitors are considered. In fact, a real capacitor can be represented as the series of a capacitor and a resistor R_c (also known as equivalent series resistor). The presence of the resistor gives rise to a series of side effects like the voltage drops and the dissipating heat, which can compromise the use of the capacitor and then of the application. To avoid such situations, a parameter used to quantify the capacitor “goodness” is the loss tangent $\tan\delta$, defined as the ratio between the equivalent resistance of the capacitor and the reactance of the capacitor itself:

$$\tan\delta = \frac{R_c}{X_C}. \quad (1.24)$$

The angle δ expresses the amount of nonideality from theoretically 90° between the capacitor’s voltage and current phasors angles.

Therefore, extending the description of a single capacitor to the capacitive divider in Fig. 1.15, the following Fig. 1.17 shows the real capacitor. Hence, (1.23) turns into:

$$V_S = V_P \frac{Z_1}{Z_1 + Z_2} \quad (1.25)$$

where $Z_1 = R_1 + jX_{C1}$ and $Z_2 = R_2 + jX_{C2}$. Highlighting $\tan\delta$, its effect on the final ratio of the divider can be assessed:

$$V_S = V_P \frac{R_2 + jX_{C2}}{R_1 + jX_{C1} + R_2 + jX_{C2}} = \frac{X_{C2}(\tan\delta_2 + j)}{X_{C1}(\tan\delta_1 + j) + X_{C2}(\tan\delta_2 + j)} = \frac{C_1(\tan\delta_2 + j)}{C_2(\tan\delta_1 + j) + C_1(\tan\delta_2 + j)} \quad (1.26)$$

In conclusion, the higher the $\tan\delta$ of the adopted capacitors, the higher the discrepancy between the nominal and the actual ratio of the capacitive divider.

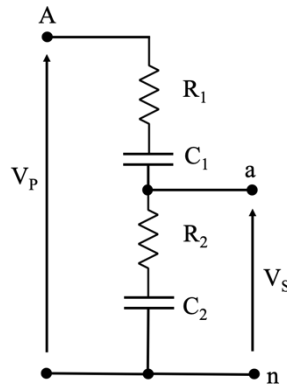


Fig. 1.17. Real capacitive divider schematic

Chapter 2

INTERNATIONAL STANDARDS

After the description of ITs, it is fundamental to complete their overview from the Standard perspective. The regulation of ITs started more than two decades ago and evolved over the years. In 1996, the first documents of Standard IEC 60044-1 were published, followed by the remaining ones (60044-2 to 8) in the next years. They contained the definitions, test criteria and specifications for all typical transformers. At the end of the first decade of the 2000s, a new Standard series has been studied and developed by the Technical Committee 38 (TC 38) of the IEC with the aim of replacing the old series. This Standard is IEC 61869, from 1 to 15. The following section briefly examines these Standards to understand what is regulated and what is not for the different types of instrument transformers. In particular, only the Standards related to the ITs described in the previous chapter are studied.

To complete the survey of the Standards, consider EN 50160 [15] when dealing with ITs. The Standard contains the voltage characteristics for the electricity supplied on all voltage levels of the power networks (i.e. from low to high voltage); hence, it describes quantities that ITs are built to measure.

2.1 IEC 61869

The Standard series is composed of 15 documents, each of which deals with a particular technology of instrument transformer or a general perspective on a group of them. To clarify this aspect, Fig. 2.1 lists a summary of the relevant documents along with the old Standards that they replace.

PRODUCT FAMILY STANDARDS		PRODUCT STANDARD	PRODUCTS	OLD STANDARD
61869-1 GENERAL REQUIREMENTS FOR INSTRUMENT TRANSFORMERS		61869-2	ADDITIONAL REQUIREMENTS FOR CURRENT TRANSFORMERS	60044-1 60044-6
		61869-3	ADDITIONAL REQUIREMENTS FOR INDUCTIVE VOLTAGE TRANSFORMERS	60044-2
		61869-4	ADDITIONAL REQUIREMENTS FOR COMBINED TRANSFORMERS	60044-3
		61869-5	ADDITIONAL REQUIREMENTS FOR CAPACITOR VOLTAGE TRANSFORMERS	60044-5
	61869-6 ADDITIONAL GENERAL REQUIREMENT FOR LOW POWER INSTRUMENT TRANSFORMERS	61869-7	ADDITIONAL REQUIREMENTS FOR ELECTRONIC VOLTAGE TRANSFORMERS	60044-7
		61869-8	ADDITIONAL REQUIREMENTS FOR ELECTRONIC CURRENT TRANSFORMERS	60044-8
		61869-9	DIGITAL INTERFACE FOR INSTRUMENT TRANSFORMERS	
		61869-10	ADDITIONAL REQUIREMENTS FOR LOW POWER PASSIVE CURRENT TRANSFORMERS	
		61869-11	ADDITIONAL REQUIREMENTS FOR LOW POWER VOLTAGE TRANSFORMERS	60044-7
		61869-12	ADDITIONAL REQUIREMENTS FOR COMBINED ELECTRONIC INSTRUMENT TRANSFORMERS AND COMBINED STAND ALONE INSTRUMENT TRANSFORMERS	
		61869-13	STAND ALONE MERGING UNIT	
		61869-14	ADDITIONAL REQUIREMENTS FOR DC CURRENT TRANSFORMERS	
		61869-15	ADDITIONAL REQUIREMENTS FOR DC VOLTAGE TRANSFORMERS	

Fig. 2.1. List of all the documents included in the Standard IEC 61869 series

The picture shows that 61869-1 and -6 provide general requirements on instrument transformers and low-power instrument transformers, respectively, whereas the other Standards detail the requirements for specific kinds of transformers.

2.1.1 IEC 61869-1 and 61869-6

All Standards of the 61869 series share a common structure which helps the reader to navigate through the documents. In particular, 61869-1 and [16, 9], representing “general requirements” Standards, have been structured in the same way:

- A first part is dedicated to terms and definitions that holds for the entire document; usually citing other Standards and references.
- A second part contains the operating conditions of the device which the standard is referring to. The conditions are either normal or for special services.
- A third part defines the rated conditions for the related tests.
- A fourth part briefly contains the design and constructions requirements. In it, both the electromagnetic and mechanical requirements can be found.
- A fifth and last part is more useful for users testing the devices. In fact, the last part contains a detailed description and relevant thresholds for the tests to be carried out on instrument transformers.

In addition to the presented structure, the documents of the Standard share the definitions and statements included in them. It is suggested to browse both Standards to gain complete knowledge of the topics. The following subsections collect important aspects from both documents.

2.1.1.1 Operating conditions and rated values

The environment conditions are vital information for many types of devices. For ITs, IEC 61869-1 defines three temperature categories, listed in Table 2.1, which refer to the air temperature affecting the IT.

Table 2.1. Temperature categories for Instrument Transformers

Category	Minimum Temperature [°C]	Maximum Temperature [°C]
-5/40	-5	40
-25/40	-25	40
-40/40	-40	40

In addition to those limits, the Standard allows to extend them to -50 °C and +50 °C if the instruments are installed in very cold or very hot places, respectively. Humidity is another essential environmental quantity, and 61869-1 simply specifies that it must not exceed 95 % in a measurement window of 24 h. For the purpose of this thesis, temperature and humidity are the most significant quantities having stricter limits defined by the Standard. However, it defines other environmental quantities such as altitude, vibrations, and pressure.

As for rated values, Standard 61869-1, a general document, only defines them for quantities valid for all kinds of ITs. This includes the highest voltage applicable, the possible insulation levels, and the usable frequency.

In Standard 61869-6, describing low-power instrument transformers, the list of rated values is increasing. In particular, it defines two specific quantities: the level of the voltage supply, needed by an active LPIT, and the burden connected to it during tests. This is an impedance composed by a 2 MΩ resistor in parallel with a 50 pF capacitance. In addition, the Standard adds limits to the rated frequency f_r :

- From 99 % to 101 % of f_r , for measuring purposes.
- From 96 % to 102 % of f_r , for protection purposes.

2.1.1.2 Tests on the ITs

Even for testing, both documents are coherent about their description. Standard 61869-1 defines four categories of tests:

- Routine test. Performed on each individual device to reveal possible manufacturing defects.
- Type test. Performed only on a limited sample of each product to reveal issues not considered in the routine tests.
- Special test. Specific tests defined in an agreement between customer and designer.
- Sample test. Special tests performed on one or more devices on particular aspects considered significant.

Such tests, listed in Table 2.2, are covered in all documents of the 61869 series. In particular, 61869-6 adds certain specific tests developed for the LPITs, and they are emphasized in italic in Table 2.2. Sample Tests, however, are not described in this table or in the Standards, because they are only developed when such requirements are established.

Table 2.2. List of tests, to be performed on ITs, defined in IEC 61869-1 and 6

TYPE TESTS	ROUTINE TESTS	SPECIAL TESTS
Temperature-rise test	Power-frequency voltage withstand tests on primary terminals	Chopped impulse voltage withstand test on primary terminals
Impulse voltage test on primary terminals	Partial discharge measurement	Multiple chopped impulse test on primary terminals
Wet test for outdoor type Transformers	Power-frequency voltage withstand tests between sections	Measurement of capacitance and dielectric dissipation factor
Electromagnetic compatibility tests	Power-frequency voltage withstand tests on secondary terminals	Transmitted overvoltage test
Test for accuracy	Test for accuracy	Mechanical tests
Verification of the degree of protection by enclosures	Verification of markings	Internal arc fault test
Enclosure tightness test at ambient temperature	Enclosure tightness test at ambient temperature	Enclosure tightness test at low and high temperatures
Pressure test for the enclosure	Pressure test for the enclosure	Gas dew point test
<i>Low-voltage component voltage withstand test</i>	<i>Power-frequency voltage withstand test for low-voltage components</i>	Corrosion test
		Fire hazard test
		<i>Vibration test</i>
		<i>Tests for accuracy versus harmonics and low frequency</i>

The table shows that Standards already provide a quite complete set of tests to verify the performance of the ITs. In addition, for several tests, they provide the test setup and the configuration of the ITs to help the user performing the required tests. However, considering the technology evolution and the development of power networks in recent years, new tests arise day-by-day. For evident reasons, Standards cannot be updated so frequently; hence, the industry and academic research are expected to provide contributions to the testing process. In the core of this research activity, the main tests (and the new developed ones) mainly focus on accuracy, electromagnetic compatibility and temperature.

2.1.2 IEC 61869-2 and 61869-3

Standards 2 and 3 [5, 7] deal with “Additional requirements for inductive voltage transformers” and “Additional requirements for inductive current transformers”, respectively. According to the structure of the documents for the 61869 Standard, this subsection focuses on significant definitions and thresholds valid for inductive voltage and current transformers used in this thesis.

Table 2.3 collects those quantities, distinguished by the Standard from which they are taken. The output value and the burden are typically used to check if the device under test is aligned with the standard. As for the burden, it is essential to provide the correct value before starting the tests. The accuracy classes are divided by levels of accuracy: the letter S, which follows the class (e.g. 0.5S)

means that the guaranteed accuracy of the IT is higher than a 0.5 class one. Other significant quantities are the primary and secondary currents/voltages: the Standard defines several values for the current transformers, while it refers to another Standard, the IEC 60038 [17] for voltage. In addition, the table provides the voltage values referred to phase-to-phase measurements in a three-phase condition. Such values have to be divided by $\sqrt{3}$ if a single-phase measurement performed.

Table 2.3. Rated quantities defined in the Standards for inductive current and voltage transformers

Rated Quantity	IEC 61869-2	IEC 61869-3
Output	2.5, 5, 10, 15, 30 VA	1, 2.5, 5, 10 VA
Burden	0.5, 1, 2, 5 Ω	-
Accuracy Class	0.1, 0.2, 0.2S, 0.5, 0.5S, 1, 3, 5	0.1, 0.2, 0.5, 1, 3
Primary Current/Voltage	10, 12.5, 15, 20, 25, 30, 40, 50, 60, 75 A	see IEC 60038
Secondary Current/Voltage	1, 5 A	Typically 100, 200 V

The description of the accuracy class requires further detailing due to its role in this thesis. In fact, the measurement accuracy is one of the backbones of the thesis, examined in the following chapters. The accuracy class limits defined in [5, 6] are listed in Tables 2.4 and 2.5, respectively.

Table 2.4. Limits of the ratio error and phase displacement for inductive current transformers

Acc. Class	Ratio Error $\pm\%$				Phase Displacement							
	At current (% of rated)				\pm Minutes				\pm Centiradians			
					At current (% of rated)				At current (% of rated)			
	5	20	100	120	5	20	100	120	5	20	100	120
0.1	0.4	0.2	0.1	0.1	15	8	5	5	0.45	0.24	0.15	0.15
0.2	0.75	0.35	0.2	0.2	30	15	10	10	0.45	0.24	0.15	0.15
0.2S	0.75	0.35	0.2	0.2	30	15	10	10	0.45	0.24	0.15	0.15
0.5	1.5	0.75	0.5	0.5	90	45	30	30	2.7	1.35	0.9	0.9
0.5S	1.5	0.75	0.5	0.5	90	45	30	30	2.7	1.35	0.9	0.9
1	3.0	1.5	1.0	1.0	180	90	60	60	5.4	2.7	1.8	1.8

Table 2.5. Limits of the ratio error and phase displacement for inductive voltage transformers

Acc. Class	Ratio Error $\pm\%$	Phase Displacement	
		\pm Minutes	\pm Centiradians
0.1	0.1	5	0.15
0.2	0.2	10	0.3
0.5	0.5	20	0.6
1	1.0	40	1.2
3	3.0	Not Specified	Not Specified

The data in Tables 2.4 and 2.5 holds for the measurement purpose ITs. In fact, the Standards distinguish the measurement ITs from the protective transformers. This thesis discusses measurement ITs only; however, for the sake of completeness, the following section briefly explains definitions related to protective ITs. In addition, there are accuracy tables for all transformers covered here.

Starting with the definition, a protective transformer is “a current transformer intended to transmit an information signal to protective and control devices” [5]. Such transformers can be identified by letters added to their accuracy class (e.g. P, PR, etc.). These new classes are defined as:

- Class P
“protective current transformer without remanent flux limit, for which the saturation behavior in the case of a symmetrical short-circuit is specified”.
- Class PR
“protective current transformer with remanent flux limit, for which the saturation behavior in the case of a symmetrical short-circuit is specified”.
- Class PX

“protective current transformer of low-leakage reactance without remanent flux limit for which knowledge of the excitation characteristic and of the secondary winding resistance, secondary burden resistance and turns ratio, is sufficient to assess its performance in relation to the protective relay system with which it is to be used”.

- Class PXR
“protective current transformer with remanent flux limit for which knowledge of the excitation characteristic and of the secondary winding resistance, secondary burden resistance and turns ratio, is sufficient to assess its performance in relation to the protective relay system with which it is to be used”.
- Class TPX
“protective current transformer without remanent flux limit, for which the saturation behavior in case of a transient short-circuit current is specified by the peak value of the instantaneous error”.
- Class TPY
“protective current transformer with remanent flux limit, for which the saturation behavior in case of a transient short-circuit current is specified by the peak value of the instantaneous error”.
- Class TPZ
“protective current transformer with a specified secondary time-constant, for which the saturation behavior in case of a transient short-circuit current is specified by the peak value of the alternating error component” [5].

These definitions all refer to current transformers, because the Standard introduces the protective instrument transformers in [5] and then only uses the information of Class P for VTs in [6].

For protective CTs, a new quantity has to be defined, the composite error:

$$\varepsilon_C = \frac{\sqrt{\frac{1}{T} \int_0^T (k_r i_s - i_p)^2 dt}}{I_P} \times 100 \%, \quad (2.1)$$

where i_p and i_s are the instantaneous values of the primary and secondary current, respectively. As for T , it represents the duration of one cycle, whereas k_r and I_P are the rated transformation ratio and the primary current rms value, respectively.

It is helpful to study the tables provided in [5, 6] for the accuracy specifications of the protective CTs and VTs (Table 2.6 and Table 2.7, respectively).

Table 2.6. Limits of the ratio error and phase displacement for protective inductive current transformers

Acc. Class	Ratio Error at rate current $\pm\%$	Phase Displacement		ε_C at rated current %
		Minutes	Centiradians	
5P and 5PR	1	± 60	1.8	5
10P and 10PR	3	-	-	10
TPX	0.5	± 30	± 0.9	-
TPY	1.0	± 60	± 1.8	-
TPZ	1.0	180 ± 18	5.3 ± 0.6	-

Table 2.7. Limits of the ratio error and phase displacement for protective inductive voltage transformers

Acc. Class	Ratio Error $\pm\%$	Phase Displacement	
		\pm Minutes	\pm Centiradians
3P	3.0	120	3.5
6P	6.0	240	7.0

2.1.3 IEC 61869-4 and 61869-12

The Standards 61869-4 and 12 [8, 18] deal with the combined (voltage and current) inductive transformers and the low-power version, respectively. As for document 12, it is still under development by the technical committee, so this thesis can only evaluate Standard 61869-4.

The document contains “Additional requirements for combined transformers”, which means “an instrument transformer consisting of a current and a voltage transformer in the same case” [1]. In this document, take particular note of the tests related to the combined presence of voltage and current sensors, aside from the other points in common with the other Standards. Such a set of tests has been developed to assess the performance of the IT in presence of this particular feature, and it can be briefly summarized below:

- First, the voltage ratio error and the phase displacement are determined with no current supplied to the IT (according to [7]).
- Second, the current is then applied to the IT and the accuracy parameters determined one more time.

The same procedure, substituting the voltage with the current, is applied to test the influence of the voltage transformer on the current one. Moreover, in the Standard, an annex is completely dedicated to further explain this physical phenomenon (not included in this thesis).

2.1.4 IEC 61869-10 and 61869-11

IEC 61869-10 and 11 [19, 11] provide “Additional requirements for low-power passive current transformers” and “Additional requirements for low-power passive voltage transformers”, respectively. They follow the structure used for documents 2 and 3 of the series; however, they cover the new LPIT (or sensors).

The rated values defined in [5] and [7] also apply to the LPITs with only minor changes when necessary; for instance, the new sensors have transmitting cables not included in inductive transformers. Primary and secondary values are different and are collected in Table 2.8.

Table 2.8. Rated quantities defined in the Standards for low-power current and voltage transformers

Rated Quantity	IEC 61869-10	IEC 61869-11
Primary Current/Voltage	5, 10, 20, 50, 100 A	See IEC 60038
Secondary Current/Voltage	22.5, 150, 225 mV	$3.25/\sqrt{3}$, $100/\sqrt{3}$ V

Conversely, the accuracy thresholds and specifications have been modified to include the new features of these devices. In particular, the values of Table 2.5 are still valid for the voltage sensors, except for the protective ones which limits are listed in Table 2.9.

Table 2.9. Limits of the ratio error and phase displacement for protective LPVTs

Acc. Class	Ratio Error $\pm\%$				Phase Displacement							
	At voltage (% of rated)				\pm Minutes				\pm Centiradians			
					At voltage (% of rated)				At voltage (% of rated)			
	2	20	80	100	2	20	80	100	2	20	80	100
0.1P	0.5	0.2	0.1	0.1	20	10	5	5	0.6	0.3	0.15	0.15
0.2P	1	0.4	0.2	0.2	40	20	10	10	1.2	0.6	0.3	0.3
0.5P	2	1	0.5	0.5	80	40	20	20	2.4	1.2	0.6	0.6
1P	4	2	1	1	160	80	40	40	4.8	2.4	1.2	1.2
3P	6	3	3	3	240	120	120	120	7	3.5	3.5	3.5
6P	12	6	6	6	480	240	240	240	14	7	7	7

The limits for the current sensors are listed in Table 2.10 and 2.11 for measuring and protective ITs, respectively. In the table, I_{pr} is the primary current and K_{pcr} is the rated extended primary current factor, which is a value definable by the user as the current sensors could work, with high linearity, in a wide range of primary currents.

Table 2.10. Limits of the ratio error and phase displacement for low-power current transformers

Acc. Class	Ratio Error $\pm\%$					Phase Displacement									
	At current (% of rated)					\pm Minutes					\pm Centiradians				
						At current (% of rated)					At current (% of rated)				
	0.01 I_{pr}	0.05 I_{pr}	0.2 I_{pr}	I_{pr}	K_{pcr}^* I_{pr}	0.01 I_{pr}	0.05 I_{pr}	0.2 I_{pr}	I_{pr}	K_{pcr}^* I_{pr}	0.01 I_{pr}	0.05 I_{pr}	0.2 I_{pr}	I_{pr}	K_{pcr}^* I_{pr}
0.1	-	0.4	0.2	0.1	0.1	-	15	8	5	5	-	0.45	0.24	0.15	0.15
0.2	-	0.75	0.35	0.2	0.2	-	30	15	10	10	-	0.9	0.45	0.3	0.3
0.2S	0.75	0.35	0.2	0.2	0.2	30	15	10	10	10	0.9	0.45	0.3	0.3	0.3
0.5	-	1.5	0.75	0.5	0.5	-	90	45	30	30	-	2.7	1.35	0.9	0.9
0.5S	1.5	0.75	0.5	0.5	0.5	90	45	30	30	30	2.7	1.35	0.9	0.9	0.9
1	-	3.0	1.5	1.0	1.0	-	180	90	60	60	-	5.4	2.7	1.8	1.8
3	-	-	4.5	3	3	-	-	-	-	-	-	-	-	-	-

Table 2.11. Limits of the ratio error and phase displacement for protective LPCTs

Acc. Class	Ratio Error at rate current $\pm\%$	Phase Displacement		ϵ_c at rated current %
		\pm Minutes	Centiradians	
5TPE	1	60	1.8	5
5P	1	60	1.8	5
10P	3	-	-	10

Note that Table 2.11 has defined a new class for protective LPCT: the TPE. “Class TPE low-power current transformers are designed for relay protection applications. The accuracy is defined by the highest permissible percentage composite error at the rated accuracy limit primary current prescribed for the accuracy class concerned. Class TPE designates transient protection electronic class CTs. Class TPE is defined by a maximum peak instantaneous error of 10 % at the accuracy limit condition, the rated primary circuit time constant, and the rated duty cycle. The peak instantaneous error includes direct and alternate current components. This is equivalent to the definition of TPY-class CTs” [9]. Comparing Tables 2.4 and 2.10, it can be concluded that the values at the rated current coincide, while Table 2.11 provides an extended set of accuracy limits for additional accuracy classes. Finally, the tables show the accuracy classes corresponding to the primary currents selected. The tests described in IEC 61869-10 and 11, are examined in Chapter 4.

2.2 EN 50160

The Standard EN 50160 is entitled “Voltage characteristics of electricity supplied by public electricity networks”. In 2010, the latest version has been published superseding the 2007 one. The document has an easy-to-read structure which includes, aside from basic terms and definitions, three main chapters dedicated to low, medium, and high voltage supply characteristics. This thesis does not discuss high voltage characteristics, but focuses on medium and low voltages.

2.2.1 Medium and Low Voltage supply characteristics

Defining the characteristics of all voltage levels available in power networks, the Standard starts from the rated values of the main quantities and then describes the possible phenomena which can occur during normal operation of a network. Such descriptions contain the limits for the major quantities in all relevant working conditions.

By starting with standardized values, the nominal low and medium voltages are 230 V and between 1 kV and 36 kV, respectively. The frequency is the second and last reference quantity, it is the same for both voltage levels:

- for systems with synchronous connection to an interconnected system
 - 50 Hz ± 1 %, during the 99.5 % of the year.
 - 50 Hz +4 %, -6 % during the 100 % of the year.
- for systems without synchronous connection to an interconnected system
 - 50 Hz ± 2 %, during the 95 % of the year.

- 50 Hz \pm 15 %, during the 100 % of the year.

These values show that the frequency limits are less strict for more delicate power networks with fewer connections.

The phenomena in voltage supply coincide for both low and medium voltages, and they are divided in two kinds of phenomena: continuous phenomena and voltage events. The former is a deviation from the nominal value that occurs continuously over time; the latter instead is a sudden and significant deviation from the nominal or desired wave shape. A complete list of phenomena and events is presented in Table 2.12.

Table 2.12. List of low/medium voltage phenomena and events

Continuous Phenomena	Voltage Events
Supply voltage variations	Interruptions of the supply voltage
Rapid voltage changes	Supply voltage dips/swells
Supply voltage unbalance	Transient overvoltages
Harmonic voltage	
Interharmonic voltage	
Mains signaling voltages	

Note the mentioning of harmonics and interharmonics. These are highly important as a power quality issue of the grid, and will be discussed in the following chapters. Hence, according to the Standards the presence of harmonics in voltage supply is limited to the values in Table 2.13; while for interharmonics the Standards do not yet include any limits.

Table 2.13. Percentage of the maximum value of each single harmonic allowed over the voltage supply

Odd harmonics				Even harmonics	
<i>Not multiple of 3</i>		<i>Multiple of 4</i>			
<i>Order h</i>	<i>Relative amplitude u_H</i>	<i>Order h</i>	<i>Relative amplitude u_H</i>	<i>Order h</i>	<i>Relative amplitude u_H</i>
5	6.0 %	3	5.0 %	2	2.0 %
7	5.0 %	9	1.5 %	4	1.0 %
11	3.5 %	15	0.5 %	6...24	0.5 %
13	3.0 %	21	0.5 %		
17	2.0 %				
19	1.5 %				
23	1.5 %				
25	1.5 %				

The table shows that each harmonic order has a peculiar limit depending on the severity and importance of such harmonic for the power network. In addition, the Standard limits the list to the 25th harmonic, because the higher order ones have very low impact on the network and are quite unpredictable.

In conclusion, the adoption of two Standards like the EN 50160 and the IEC 61869 series allows to have all necessary information when investigating ITs and how to test them. The Standards cover all existing kinds of ITs and the electricity they are supplied with, detailing the information required by the user before and after performing tests. However, the Standards do not include all possible tests, so they are subjected to periodical updates. Contributing to future updates of these regulatory documents, the main part of this thesis introduces new tests having the design based on these Standards.

Chapter 3

The Role of Uncertainty

This chapter introduces and discusses the role of metrology, the science of measurement, and the impact of uncertainty on the process and results of measurements. This includes essential principles and definitions that apply to scientific measurements in general, and an overview on basic and advanced aspects of uncertainty on metrology.

3.1 Basic Principles

What is Metrology? In [1], it is defined as “science of measurement and its application – it includes all theoretical and practical aspects of measurement, whatever the measurement uncertainty and field of application”. Consequently, measurements are the pillars of such a science, and they are defined, [1], as “process of experimentally obtaining one or more values that can reasonably be attributed to a quantity”.

It is common to apply this process on a daily basis, consciously or unconsciously, to obtain information and data from the surrounding world, such as understanding how much space is left in a shopping bag by looking inside of it, or sending shuttles to space by using instrumentation worth billions of euros.

When applying such a process, it concerns a property that is subjected to the measurement: the quantity. It is defined in [1] as “property of a phenomenon, body, or substance, where the property has a magnitude that can be expressed by means of a number and a reference”. Note that the concept of quantity can be also extended to vectors or tensors, whose components are quantities as well.

It is not possible to determine or obtain the "true value" of a quantity, instead a "reasonable" value for the measurand is estimated. The reasonable estimation in this definition indicates that the result of a measurement is not the true, actual value of the measurand; that value is unknown and it is only possible to estimate it.

So, the issue is the lack of knowledge about the real result of a measurement. This is known as uncertainty, and it is, [1], a “parameter, associated with the result of a measurement, that characterizes the dispersion of the values that could reasonably be attributed to the measurand”. So, uncertainty quantifies the level of lack of knowledge associated to a measurement, and there are three major types of the uncertainties [20]: definitional, interaction, and instrumental uncertainty.

The *definitional uncertainty* is directly related to the measurand, and it results from the imperfect definition of a measurand and its model. Before any measurement a preliminary model with various degrees of complexity is established, and this is never perfect.

The *interaction uncertainty* results from using a measurement instrument. When an instrument is connected to a measurand, the instrument is affecting and altering the quantity to be measured.

The *instrumental uncertainty* is another aspect resulting from the instrumentation. The instrument performing a measurement introduces such uncertainty due to its intrinsic imperfection, even if it is based on a standard reference.

These types of uncertainty affect the final measurement results, which can be grouped in two main categories [20]: systematic and random effects. Systematic effects occur continuously, they are highly difficult to detect but also easy to correct and remove if encountered. Random effects, on the other hand, are fully arbitrary and unpredictable phenomena, which cannot be compensated for. However, their effect on final results can be almost completely removed by repeating the same type of measurement. In this case, the statistical expectation of the random error on repeated measurements is zero.

Consider these examples. A systematic effect can be seen as a constant weight affecting a scale while measuring. In the measurement, a small amount of weight is subtracted or added to whatever

measurand, leading to an invalid result. A typical example for a random effect is the noise superimposed on a measurand which cannot be predicted as it manifests itself in an arbitrary way. Fig. 3.1 provides a graphic representation of these effects. The “actual” signal is depicted in blue, while red and yellow colors indicate the signals affected by systematic and random effects, respectively.

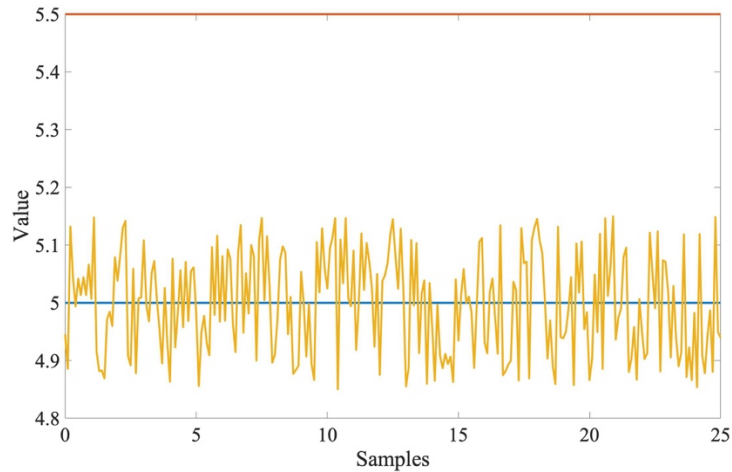


Fig. 3.1. Example of signal affected by random (yellow) and systematic (red) effects

In a conclusion, note it is not possible to obtain the true value of a quantity by measuring. There is no measurement without uncertainty. To be clear, providing a measurement without its uncertainty renders such measurement as ineffective and meaningless.

Note the particular aspects of the systematic error. As stated above, it is typically difficult to detect systematic errors, but what happens when it is not detectable at all or when the available information is not sufficient? An example is the error provided by the instrument’s manufacturer. It is typically the maximum value (positive) obtained from the series of instruments tested along with the one that is being used. During a measurement, this results in shifting of possible “true” value (A) to a new attributed value (B), as depicted in Fig. 3.2. Therefore, even if multiple measurements are performed, the result will be wrongly centered in a position different from the “true” value (case (a) Fig. 3.2). An adopted solution is the application of a probabilistic approach to treat the systematic errors. This way, both the random and the systematic effects are treated as a probability density function (PDF), which together compose the overall uncertainty (case (b) Fig. 3.2). One way to combine both effects in a PDF is by applying the Monte Carlo method, briefly described in 3.2.2.3.

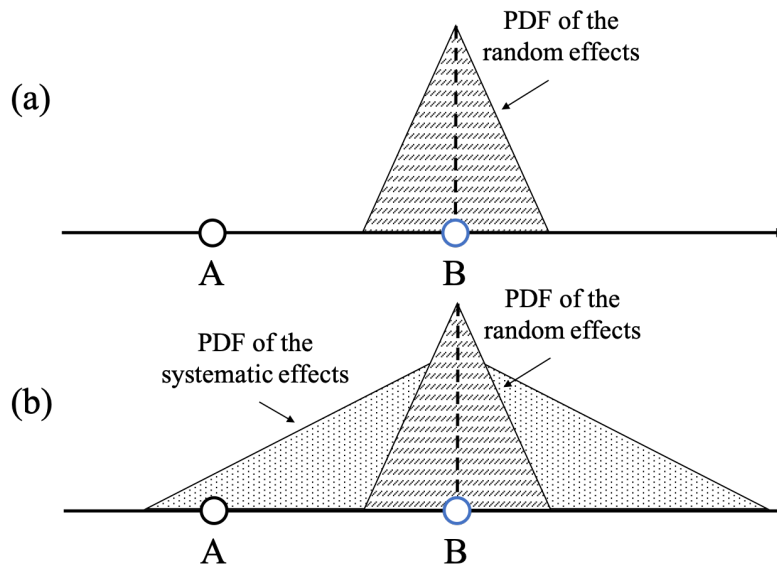


Fig. 3.2. Example of how to treat unknown systematic effects

3.2 Guide to the Expression of Uncertainty in Measurements

3.2.1 Introduction

The guide to the expression of uncertainty in measurements (GUM) [21] and its related documents [22, 23] have been developed by the Joint Committee for Guides in Metrology (JCGM) with a specific purpose: to spread the evaluation of measurement uncertainty by using the guidelines provided in the documents. These are aimed at helping experts, either in industry or in academia, increasing the role of uncertainty evaluation in their fields and research topics. Such documents, consist also of a useful tool for operators and non-experts with instructions how to process measurement results, and how to present them to an audience. Conversely, the GUM series may not be easy to comprehend for people with limited educational background. Therefore, experts are continuously trying to enhance the documents, including specific application examples extrapolated from the GUM.

The next subsection provides a general overview of the GUM core, to obtain multiple results: introducing and refreshing the concept of uncertainty evaluation, and clarifying some aspects useful in the later sections of the thesis.

3.2.2 The GUM

Following the introduction in the previous sections, it is fundamental to obtain a quantity that reflects the quality of a given measurement result. This should be done applying a universal method in order to compare measurements results either among a series of them or among results obtained from different Standards or datasheets. This quantity is the uncertainty, which is substituting the legacy error analysis, and as described in the following it is expressed as a coverage probability or level of confidence. This last parameter is defined as “the value $(1 - \alpha)$ of the probability associated with a confidence interval or a statistical coverage interval”, [21].

3.2.2.1 Basic definitions and concepts

Before discussing the uncertainty evaluation, it is essential to define some basic concepts:

- Standard uncertainty: uncertainty of the results of a measurement expressed as a standard deviation.
- Type A evaluation of uncertainty: method of evaluation of uncertainty by the statistical analysis of series of observations.

- Type B evaluation of uncertainty: method of evaluation of uncertainty by means other than the statistical analysis of series of observations.
- Combined standard uncertainty: standard uncertainty of the result of a measurement when that result is obtained from values of a number of other quantities, equal to the positive square root of a sum of terms, the terms being the variances or covariances of these other quantities weighted according to how the measurement result varies with changes in these quantities.
- Expanded uncertainty: quantity defining an interval about the result of a measurement that may be expected to encompass a large fraction of the distribution of values that could reasonably be attributed to the measurand.
- Coverage factor: numerical factor used as a multiplier of the combined standard uncertainty in order to obtain an expanded uncertainty. Typically referred to as k , it can assume as values 1, 2, or 3.

3.2.2.2 Evaluating standard uncertainty

Let's assume Y to be a measurand which depends on N quantities X_1, X_N through:

$$Y = f(X_1, X_2, \dots, X_N). \quad (3.1)$$

Denoting y as the estimated value of the measurand, the relation between it and the estimate of the input quantities x_i is:

$$y = f(x_1, x_2, \dots, x_N) \quad (3.2)$$

At this point, the type A and B methods can be described. Type A can be applied if n observations of a single quantity x_1 are available. Then, the best way to estimate the expected value of x is the arithmetic mean:

$$\bar{x} = \frac{1}{n} \sum_{i=1}^n x_i, \quad (3.3)$$

where (3.3) applies to all input quantities on which Y depends. After that, the discrepancies among the measured values, or in other words their dispersion from the mean, are quantified estimating the variance of the mean:

$$s^2(\bar{x}) = \frac{s^2(x_i)}{n} = \frac{\sum_{k=1}^n (x_k - \bar{x})^2}{n(n-1)}. \quad (3.4)$$

As for type B, the variance $u^2_{(x_i)}$ of an input quantity x_i is obtained from all available information on the quantity, including: old measurements, manufacturer's specification, experience, calibration certificates. From these sources, the standard uncertainty can be derived as a multiple of the standard deviation, as an interval having a defined level of confidence or even as limits of such an interval.

The reliability of type B method is not negligible compared to the type A one, in fact, the latter can become quite meaningless if the number of observations is limited.

Overall, the application of both methods allows to estimate the mean value of the measurand and to compute two standard uncertainties providing information of diverse measurement aspects. Hence, the final step is to combine the gathered information to compute the combined standard uncertainty. In its evaluation, two situations may occur: the input quantities x_i are uncorrelated, or two or more quantities are correlated with each other. In the former case, the combined variance $u^2_{c(y)}$ is given by:

$$u^2_{c(y)} = \sum_{i=1}^N \left(\frac{\partial f}{\partial x_i} \right)^2 u^2_{(x_i)}, \quad (3.5)$$

where f is the function defined in (3.1), and $u_{(x_i)}^2$ could be evaluated either with type A or type B method.

In the case of correlated input quantities, the computation becomes more complicated, and the combined uncertainty is:

$$u_c^2(y) = \sum_i^N \sum_j^N \frac{\partial f}{\partial x_i} \frac{\partial f}{\partial x_j} u(x_i, x_j), \quad (3.6)$$

where $u(x_i, x_j)$ is the estimated covariance associated to x_i and x_j .

Finally, a last step is required to complete the uncertainty evaluation process, obtaining a measurement result expressed as:

$$Y = y \pm U, \quad (3.7)$$

where U is the expanded uncertainty defined as $U = k u_c(y)$. As for k , it is the already defined coverage factor.

3.2.2.3 The Monte Carlo Method

The Monte Carlo method (MCM) is, [22], “method for the propagation of distributions by performing random sampling from probability distributions”. It is described in Supplement 1 of the GUM [22] and can be used to provide a representation of the PDF for the output quantity from which an estimate of the output quantity, the standard uncertainty associated with this estimate, and a coverage interval for that quantity, corresponding to a specified coverage probability, can be obtained.

The method is usually adopted when the guidelines suggested in the GUM [21] are difficult to apply. With the method, the available information is encoded in terms of PDFs for the input quantities. The approach operates with these PDFs to determine the PDF for the output quantity.

- Main stages of uncertainty evaluation
 - define the output quantity Y , the quantity intended to be measured (the measurand);
 - determine the input quantities $\mathbf{X} = X_1, X_2, \dots, X_N$ upon which Y depends;
 - develop a model relating Y and X ;
 - on the basis of available knowledge, assign PDFs to the X_i ;
 - propagate the PDFs for the X_i through the model to obtain the PDF for Y ;
 - from the PDF for Y , it can be calculated: its expectation, standard deviation and a coverage interval with a specified probability.

According to this procedure the key point is to propagate the distributions of the X_i . This can be done using (i) analytical methods (obtaining a mathematical representation), (ii) a first-order Taylor series instead of the model created for Y , (iii) as (ii) but including high-order element of the Taylor series, (iv) numerical methods.

The propagation approach can be summarized with Fig. 3.3 which explains that the output is one PDF associated to the measured quantity Y .

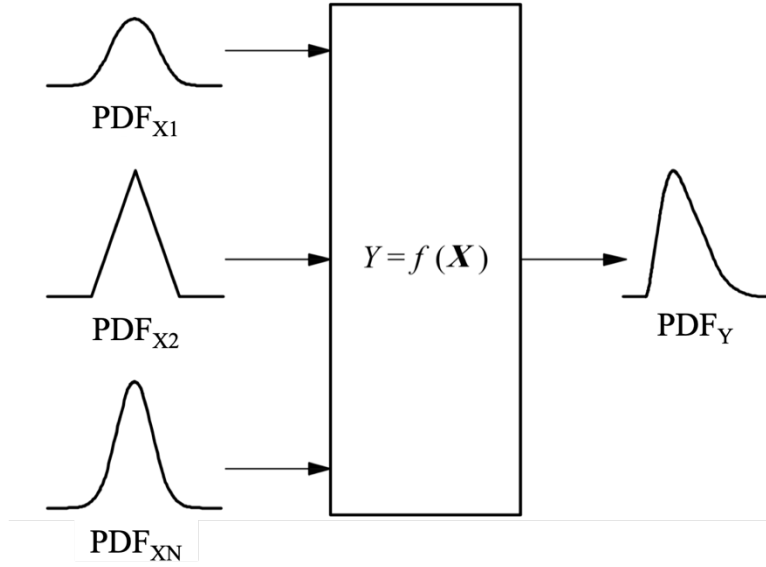


Fig. 3.3. Schematic representation of the PDF propagation

Note that the application of the PDF propagation with the MCM for example, compared to the GUM uncertainty framework (summarized in 3.2.2.2), never provides exact results but is more accurate for an extended set of cases. The GUM instead provides an exact result for a very limited set of simple cases.

The application of the MCM can be summarized as:

- a proper number M of Monte Carlo trials to be selected;
- generate M vectors, by sampling from the PDFs chosen for the X_i ;
- after the sampling, M models of Y are obtained;
- sort the M models into strictly increasing order and use them to compute the expected value, uncertainty and coverage interval of Y .

The application of the MCM is possible if the following conditions are met:

- the function f , expressing the relation between Y and the X_i , is continuous with respect to the X_i ;
- the distribution function for Y is continuous and strictly increasing;
- the PDF for Y is:
 - continuous over the interval for which this PDF is strictly positive;
 - unimodal;
 - strictly increasing to the left of the mode and strictly decreasing to the right of the mode;
- the expected value and the variance of Y exist;
- a sufficiently large M is used.

3.2.2.4 The central limit theorem

In addition to the suggestions of the GUM, it is recommended to add another essential theorem to deal with measurements and their uncertainty to the final users' tools: the Central Limit Theorem (CLT) [24]. It is of straightforward application in many use cases, and it states that: if the relationship between the measurand Y and its input quantities X_i is expressed as:

$$Y = c_1X_1 + c_2X_2 + \dots + c_NX_N = \sum_i^N c_iX_i, \quad (3.8)$$

where the c_i are the input quantities coefficients, then the distribution of Y will be normal whatever distribution the single input quantities have. More in detail, the distribution will be closer to normal as bigger as N is, up to an infinite value. The CLT specifies also that the expected value and the variance of Y are $E(Y) = \sum_i^N c_i E(X_i)$ and $\sigma^2(Y) = \sum_i^N c_i^2 \sigma^2(X_i)$, respectively. This applies, if the X_i are independent and no $c_i^2 \sigma^2(X_i)$ component prevails on the others.

Interesting results can be achieved by extending CLT and combining it with the GUM. The type A method to evaluate uncertainty has been described having the arithmetic mean as one of its pillars. Hence, by considering also that the mean is typically performed in most of the actual measurement campaigns, the CLT provides that:

let t be a random variable having whatever distribution with mean μ_t and standard deviation σ . Then, the probability distribution of the mean \bar{t} obtained from n observation t_i of t , tends to a normal distribution with mean value and standard deviation μ_t and σ/\sqrt{n} , respectively, as n increases. As it can be seen from the application of the CLT, if n is significantly high, a consequential reduction of the standard uncertainty can be achieved.

Chapter 4

Instrument Transformers & Smart Grids

This chapter collects the main results of the research conducted on the ITs. The following sections tackle different aspects of the IT. These can be distinguished in two main topics: the effect of influence quantities on the behavior of the ITs, and the use of ITs to improve the Smart Grid operations.

4.1 ITs vs. Influence Quantities

As discussed in Chapter 2, Standards related to ITs do not completely cover all issues arising when ITs work under the influence of one or more quantities. In this context, the three following case studies describe what happens when exposing inductive ITs to ambient temperatures different from the rated one and how passive LPCT behave when subjected to multiple influence quantities (including temperature).

4.1.1 Inductive VT, Verification of Accuracy Depending on Temperature

4.1.1.1 Introduction

Instrument transformers are widely used in primary and secondary substations for the measurement of electrical quantities as well as for the protection of power lines. In recent years, this kind of product has experienced a strong revolution from a technological perspective. With the event of electronic measuring and protective devices, which only require low energy input signals from voltage and current sensing elements (typically in the order of few volt, some milli-ampere and with input burdens of lower than 0.1 VA) the need for inductive voltage and current measuring transformers with traditional outputs (i.e. $110\sqrt{3}$ V or 1/5 A and powers of some or tens of Volt-Amperes) has decreased significantly.

However, the output value is not the only and first reason why inductive ITs are on the way to be replaced by sensors. The most important reasons are on the behavior and limits their feature in specific, and often typical, operating conditions of power networks. For instance, with the event of distributed generation, voltages and currents exhibit high harmonic contents (up to 100 kHz). Furthermore, protection relays are now requested to trip in a very fast time (in the order of 2-4 ms) and dips, sags and swells must be recorded with higher accuracy than in previous years. Inductive ITs do not feature characteristics suitable for the kind of required measurements mentioned above [25-28]. Just as an example, current transformers react in around 20ms at the occurrence of a fault.

However, there is still an application in power networks where inductive instrument transformers are still widely used and where LPIT do not find, for now, application: the legal metrology in energy and power measurements and, in particular, in metering for pricing. There is not a wide consensus among electric utilities and regulatory bodies to consider LPIT sufficiently reliable, stable and robust (in terms of metrological characteristics) to be taken into consideration also for this application. So, at present, potential and inductive current transformers are still largely used.

It is well known that they do not suffer from the weaknesses of LPIT (immunity, stability over time, over temperature, etc.), but they require to be calibrated before installation and their accuracy vs. frequency is verified in the range of $\pm 10\%$ of rated frequency. But in particular, both the old and the new Standards IEC 61869-2/3 [5, 7] do not specify the implementation of a test for verifying the accuracy vs. temperature of inductive instrument transformers. On the contrary, such a test is mandatory for LPITs. Even if the accuracy characteristics of inductive transformers are usually not affected by temperature variations, in some cases, and in particular when the production process is not fully under control, the ratio error and phase displacement can change in temperature to exceed the threshold limits of their specified accuracy class.

Considering this, recent research [29] has studied the metrological characteristics for the verification of the accuracy of inductive instrument transformers vs. temperature. Literature lacks references studying metrological performances of inductive transformers vs. temperature, while many papers

dealing with the behavior of power transformers vs. temperature are available. Examples include [30], where an equivalent thermal model of the transformer is created, and [31] evaluating an equivalent electrical circuit of the transformer. However, to the best knowledge of the authors, there are no studies investigating the temperature variations of ratio error and phase displacement of instrument transformers.

4.1.1.2 Experimental setup

Fig. 4.1 shows a schematic representation of the experimental setup used for evaluating the accuracy performance of VTs. It consists of the following main elements:

- a programmable power source Agilent 6813B, which features up to 300 V RMS, 1750 VA from DC to 1 kHz. It assures a proper stability of input sinusoidal voltage (in terms of both amplitude and frequency) to the transformer under test;
- a step-up voltage transformer, which features 0.1/15 kV, 20 VA. Its low voltage terminals are connected to the power source. It raises the output voltage of the power source to the rated voltage for the transformer under test;
- a resistive-capacitive voltage divider used as a reference. As a matter of fact, its transformation ratio is 5981:1 with a ratio error $< 0.1\%$ and a phase error 0.03 crad. At rated frequency of 50 Hz and a bandwidth (at 0.06 dB) up to 100 kHz;
- the voltage transformer under test; both voltage transformers had primary rated voltage of 10 kV;
- a thermostatic chamber, which hosted the voltage transformer under test in an environment whose temperature could be varied from $+5\text{ }^{\circ}\text{C}$ to $+55\text{ }^{\circ}\text{C}$;
- a differential resistive voltage divider with a rated ratio of 11.2:1. The used resistors feature temperature coefficients lower than 5 ppm/ $^{\circ}\text{C}$ and tolerance interval of $\pm 1/10000$. The divider has been used to reduce the output voltage of the transformers under test, which is $100/\sqrt{3}\text{ V}$ at rated voltage, to a value that can be sampled and digitized by the Data AcQuisition board (DAQ), which is $\pm 10\text{ V}_{pp}$;
- a 24-bit DAQ NI9239, which acquires the conditioned output voltages of the voltage transformer under test as well as of the reference;
- a personal computer, which stores the samples acquired by the DAQ and compute the desired parameters;
- 8 $\frac{1}{2}$ -digits multimeter HP3458A under metrological confirmation used to calibrate the equipment used for the tests;
- Wavetek Datron 4800 calibrator used to calibrate the equipment used for the tests.

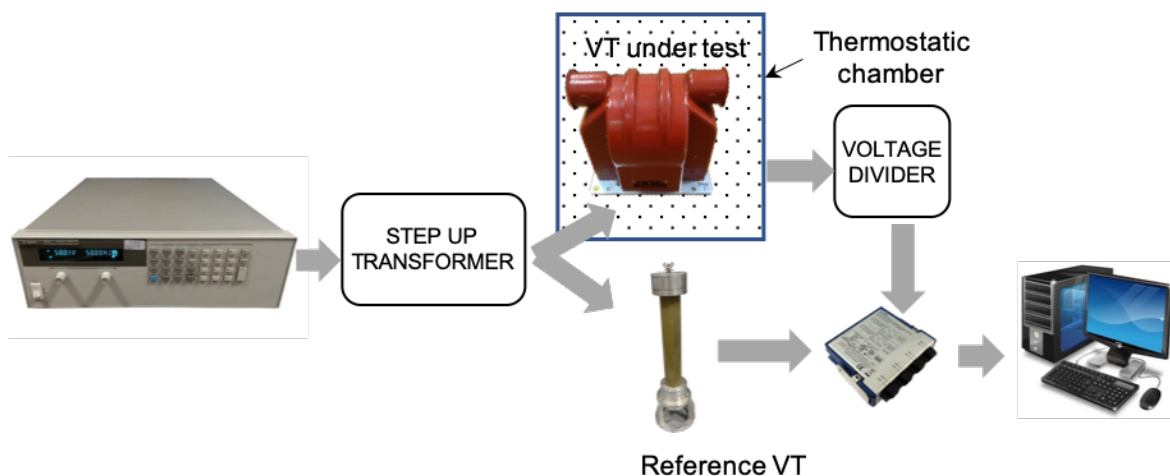


Fig. 4.1. Schematic representation of the experimental setup

Before detailing the performed tests, an in-depth analysis has been carried out in order to list all possible sources of uncertainty and their contribution to the overall uncertainty of the measuring system. Moreover, the accuracy characteristics of the devices used in the measurement chain have been considered for uncertainty evaluation.

The 8 ½-digits multimeter HP3458A has been used to perform accuracy tests on the voltage reference divider, on the voltage divider and on the DAQ.

Fig. 4.2 shows the setup used for the voltage reference divider: the divider is fed by the voltage provided by the Wavetek Datron 4800 calibrator and its RMS value is measured by the HP3458A multimeter, which is controlled via IEEE488 by a personal computer, not visible in the picture.

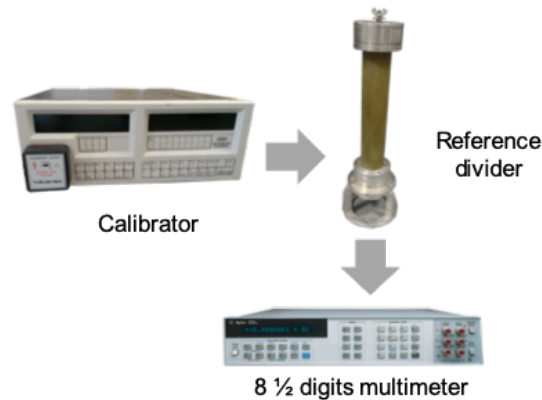


Fig. 4.2. Schematic representation of the setup for metrological characterization of the reference divider

Due to the voltage limitation of the calibrator, only 600 V RMS have been applied; however, according to the calibration certificate of the divider, it exhibits high linearity (non-linearity error lower than 10^{-4}) up to twice the rated voltage (10kV). The multimeter acquired 100 measurements, and the test was repeated twice a day for five days in order to confirm the repeatability of measurements. The results of this first test are shown in Table 4.1 proving the stability of the measurements with a standard deviation in the order of 10^{-6} , and a relative standard deviation of the mean value around $1.3 \cdot 10^{-5}$ for the 5 days of measurements.

Table 4.1. Repeated measurements of the 600 V output value provided by the Calibrator to the reference divider and measured with the multimeter 3458A

Day	Max Value [V]	Min Value [V]	Mean Value [V]	Std. Deviation [V]
1	0.100343	0.100338	0.100341	$1.28 \cdot 10^{-6}$
2	0.100313	0.100307	0.100310	$1.31 \cdot 10^{-6}$
3	0.100202	0.100196	0.100199	$1.30 \cdot 10^{-6}$
4	0.100229	0.100223	0.100227	$1.31 \cdot 10^{-6}$
5	0.100226	0.100219	0.100223	$1.43 \cdot 10^{-6}$

The second test aimed to verify the performance of the voltage divider. The setup used for the measurements is shown in Fig. 4.3 and it consists of the calibrator, the voltage divider and the multimeter.

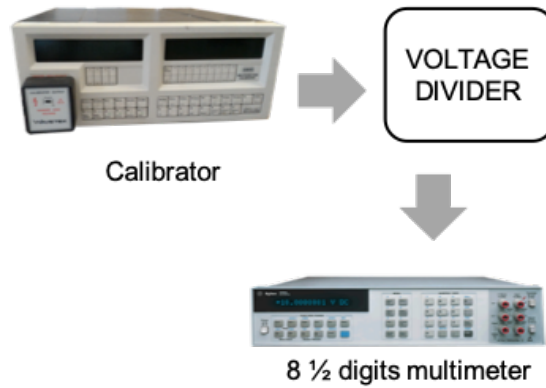


Fig. 4.3. Schematic representation of the setup for metrological characterization of the voltage divider

One hundred measurements have been performed twice a day for five consecutive days applying 57 V at the voltage divider terminals with the calibrator, which approximate the value at the output of the voltage transformer under test ($100/\sqrt{3}$ V) when the rated voltage at primary side is applied. The results of this second set of measurements are shown in Table 4.2. For the Table has been adopted the same structure of Table 4.1. What is not included in the table is the relative standard deviation which is in the order of $1.1 \cdot 10^{-5}$ for all the days of measurements.

Table 4.2. Repeated measurements of the 57V output value provided by the Calibrator to the resistance divider, measured with the multimeter 3458A

Day	Max Value [V]	Min Value [V]	Mean Value [V]	Std. Deviation [V]
1	5.08802	5.08779	5.08791	$5.51 \cdot 10^{-5}$
2	5.08793	5.08773	5.08782	$5.25 \cdot 10^{-5}$
3	5.08788	5.08765	5.08777	$5.73 \cdot 10^{-5}$
4	5.08795	5.08774	5.08784	$5.33 \cdot 10^{-5}$
5	5.08795	5.08772	5.08784	$5.41 \cdot 10^{-5}$

These two tests were performed using both the calibrator and the multimeter for a cross verification of measurements and the evaluation of their compatibility. The output of the calibrator was measured with the multimeter by applying two different voltage levels: 600 V and 57 V. These values were chosen in order to verify the instrument at the voltage levels requested by the other tests. In Fig. 4.4, the setup for the calibrator characterization is shown.

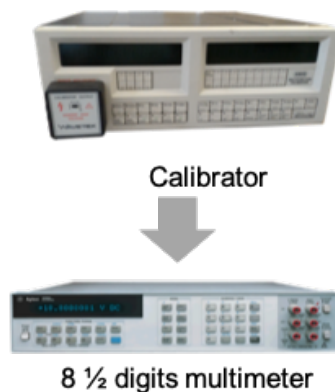


Fig. 4.4. Schematic representation of the setup for metrological characterization of the calibrator

Tables 4.3 and 4.4 show that the calibrator presents good stability too, with a standard deviation of 10^{-3} and 10^{-2} , for 57 V and 600 V, respectively.

Table 4.3. Repeated measurements of the 57V output value given from the Calibrator to the multimeter 3458A

Day	Max Value [V]	Min Value [V]	Mean Value [V]	Std. Deviation [V]
1	57.002	56.992	56.996	$1.55 \cdot 10^{-3}$
2	56.9906	56.9890	56.9898	$2.98 \cdot 10^{-4}$
3	56.9888	56.9868	56.9878	$3.12 \cdot 10^{-4}$
4	56.9898	56.9878	56.9881	$2.93 \cdot 10^{-4}$
5	56.9882	56.9843	56.9867	$8.34 \cdot 10^{-4}$

Table 4.4. Repeated measurements of the 600 V output value given from the Calibrator to the multimeter 3458A

Day	Max Value [V]	Min Value [V]	Mean Value [V]	Std. Deviation [V]
1	599.861	599.786	599.809	$9.20 \cdot 10^{-3}$
2	599.91	599.77	599.80	$4.36 \cdot 10^{-2}$
3	599.825	599.764	599.782	$8.28 \cdot 10^{-3}$
4	599.98	599.76	599.78	$1.85 \cdot 10^{-2}$
5	599.86	599.75	599.77	$1.93 \cdot 10^{-2}$

The third and last test consisted of the characterization of the DAQ used to acquire voltages from the other instruments. Fig. 4.5 illustrates the measurement setup for this objective. The test consisted of the application of different values of voltages ranging from $0.3 V_{pp}$ to $3.2 V_{pp}$ by using a function generator.

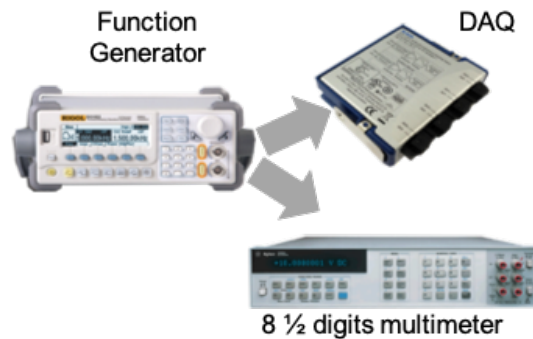


Fig. 4.5. Schematic representation of the setup for metrological characterization of the DAQ

The values were then measured with the DAQ and the HP3458A multimeter. Fig. 4.6 shows the results, the RMS values: note there is no difference between the best fit line and the bi-sector. However, an error of 10^{-5} V between the voltage measured with the 3458A and the one acquired with the DAQ has been measured.

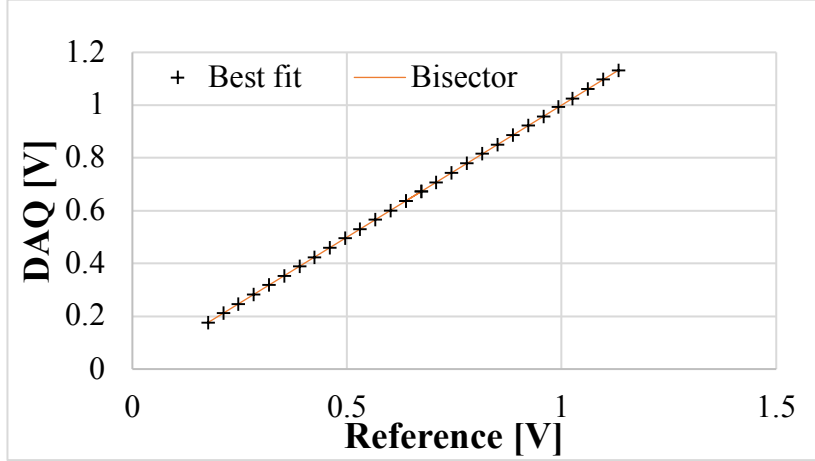


Fig. 4.6. Graph of the characterization of the DAQ compared to the HP 3458A multimeter

Twisted-pair and shielded cables connect all devices. The set up includes a ground star point, given that ground loops can generate, for this kind of measuring systems, variations in both phase and magnitude of quantities in the order of some part per ten thousand.

In addition, the testing covered the influence of the electric field effect generated by the high-voltage section on the low-voltage parts (voltage reference divider and reference divider, in particular). It has been observed that the influence on the measurement was in the order of 2 parts per ten thousand. Ensuring a suitable distance between the high and low voltage parts will make their contribution to uncertainty negligible.

4.1.1.3 Experimental tests & results

The main goal of the experimental activity has been to verify if the measurement setup described in the previous section is suitable for evaluating the accuracy performance of voltage transformers versus temperature.

As it is well known, in accordance with [7], the accuracy of a measuring voltage transformer is expressed by its accuracy class, which defines maximum values for ratio (or voltage) error ε and the phase displacement $\Delta\varphi$. According to [7] it is:

$$\varepsilon = \frac{k_r U_s - U_p}{U_p} \quad (4.1)$$

$$\Delta\varphi = \varphi_s - \varphi_p, \quad (4.2)$$

where k_r is the rated transformation ratio, U_s and U_p are the RMS of the secondary and primary voltages, respectively, φ_s and φ_p are the phase of secondary and primary voltage phasors, respectively. Standard [7] also specifies that the values of ε and $\Delta\varphi$ shall not exceed the limits of a given accuracy class for any voltage between 80 % and 120 % of the rated voltage and with burdens from 0 % and 100 % of the rated one with unit power factor (for burden lower than or equal to 10 VA) or from 25 % to 100 % of the rated one with power factor 0.8 (for burden greater than 10 VA).

Two measuring voltage transformers, which will be referred to as A and B in the following, and made by different manufacturers, were tested with the proposed setup. Table 4.5 lists the main characteristics of the two VTs. It can be noticed that both of them may be considered as belonging to accuracy class 0.2 or 0.5, depending on the burden. The lower burden corresponds to best accuracy class. For both transformers, a burden of 10 VA with unit power factor was chosen, which corresponds, for a rated secondary voltage of $100/\sqrt{3}$ V, to a 330 Ω resistor.

Table 4.5. Characteristics of the two transformers under test

Transformer	Voltage ratio [V/V]	Burden [VA]	Accuracy class
A	20000/100	10/25	0.2/0.5
B	20000/100	10/30	0.2/0.5

The manufacturer of transformer B states that its accuracy class holds for temperatures between -25 °C, +40 °C. No information on this is provided by the manufacturer of transformer A.

The above VTs, placed one at the time inside the thermostatic chamber, were tested at three different temperatures: 5 °C, 25 °C, and 45 °C in order to assess their accuracy performance on the whole range allowed by the chamber.

To ensure thermal steady state conditions as well as a uniform distribution of the heat (or of the cold) inside the chamber, the temperatures were maintained at least for 24 hours before running the test. Moreover, the transformers were turned on and fed with about 10 kV several hours before the test, thus allowing electromagnetic working conditions to be reached.

The measurement procedure is as follows. Once the above conditions are reached, the input voltage is adjusted to 10 kV and ten periods of the waveforms at the outputs of the resistive divider and of the reference divider are acquired at 10 kSa/s. Then, these waveform periods have been processed to compute the ratio error and phase error. Performing one hundred iterations allowed for determining ratio error and phase displacement for each VT under test and at each temperature, by a mean value and a standard deviation.

Tables 4.6 and 4.7 show for transformer A the minimum value, the maximum value, the mean value, and the standard deviation of the ratio error and the phase displacement, respectively.

Table 4.6. Ratio error for different temperatures for the transformer A

Temperature [°C]	Max Value [-]	Min Value [-]	Mean Value [-]	Std. Deviation [-]
5	$-7.461 \cdot 10^{-4}$	$-7.434 \cdot 10^{-4}$	$-7.448 \cdot 10^{-4}$	$6 \cdot 10^{-7}$
25	$-7.513 \cdot 10^{-4}$	$-7.484 \cdot 10^{-4}$	$-7.497 \cdot 10^{-4}$	$7 \cdot 10^{-7}$
45	$-7.853 \cdot 10^{-4}$	$-7.825 \cdot 10^{-4}$	$-7.837 \cdot 10^{-4}$	$6 \cdot 10^{-7}$

Table 4.7. Phase displacement for different ambient temperatures for the transformer A

Temperature [°C]	Max Value [rad]	Min Value [rad]	Mean Value [rad]	Std. Deviation [rad]
5	$-3.2646 \cdot 10^{-3}$	$-3.2614 \cdot 10^{-3}$	$-3.2629 \cdot 10^{-3}$	$7 \cdot 10^{-7}$
25	$-3.2605 \cdot 10^{-3}$	$-3.2573 \cdot 10^{-3}$	$-3.2589 \cdot 10^{-3}$	$6 \cdot 10^{-7}$
45	$-3.2412 \cdot 10^{-3}$	$-3.2372 \cdot 10^{-3}$	$-3.2396 \cdot 10^{-3}$	$1 \cdot 10^{-6}$

The first observation is that, for both quantities considered, the standard deviation is very low (about 10^{-7}). This allows to write ε and $\Delta\varphi$ with 4 significant digits, except for the value of ε at 45°C where such digits are 3. This way, even very low variations of the above quantities can be investigated/studied/examined. As a matter of fact, as all measurements are performed under the same working conditions, uncertainties on ε and $\Delta\varphi$ turn into systematic, even if unknown, contributions that can be considered negligible when only verifying variations. These observations from Tables 4.6 and 4.7 show that, for transformer A, ε increases with the increase of the temperature, whereas $\Delta\varphi$ exhibits the opposite behavior.

Tables 4.8 and 4.9 display for transformer B the minimum value, the maximum value, the mean value, and the standard deviation of the ratio and phase errors, respectively.

Table 4.8. Ratio error for different temperatures for the transformer B

Temperature [°C]	Max Value [-]	Min Value [-]	Mean Value [-]	Std. Deviation [-]
5	$-1.9479 \cdot 10^{-3}$	$-1.9443 \cdot 10^{-3}$	$-1.9463 \cdot 10^{-3}$	$8 \cdot 10^{-7}$
25	$-1.9725 \cdot 10^{-3}$	$-1.9699 \cdot 10^{-3}$	$-1.9710 \cdot 10^{-3}$	$6 \cdot 10^{-7}$
45	$-1.993 \cdot 10^{-3}$	$-1.984 \cdot 10^{-3}$	$-1.988 \cdot 10^{-3}$	$3 \cdot 10^{-6}$

Table 4.9. Phase displacement for different ambient temperatures for the transformer B

Temperature [°C]	Max Value [rad]	Min Value [rad]	Mean Value [rad]	Std. Deviation [rad]
5	$-2.1796 \cdot 10^{-3}$	$-2.1766 \cdot 10^{-3}$	$-2.1781 \cdot 10^{-3}$	$7 \cdot 10^{-7}$
25	$-2.150 \cdot 10^{-3}$	$-2.136 \cdot 10^{-3}$	$-2.143 \cdot 10^{-3}$	$6 \cdot 10^{-6}$
45	$-2.108 \cdot 10^{-3}$	$-2.103 \cdot 10^{-3}$	$-2.107 \cdot 10^{-3}$	$1 \cdot 10^{-6}$

Here, the standard deviation is generally a little bit higher than in the previous case, but still allows to write ε with 4 digits for 2 temperatures out of 3 and $\Delta\varphi$ with 4 digits for one case out of 3. In the other cases ε and $\Delta\varphi$ are expressed with 3 significant digits.

Nevertheless, the variations of the measured quantities are very low. Even for transformer B, Tables 4.8 and 4.9 allow to conclude that ε and $\Delta\varphi$ exhibit opposite behavior vs. temperature: when ε increases, $\Delta\varphi$ decreases.

Overall, the observed variations are small if compared with the limits of the relevant accuracy classes. This is due to phenomena that occur inside the transformers.

4.1.1.4 Conclusion

The proposed experimental setup has been used to evaluate the accuracy performance of two new measuring voltage transformers depending on the environment temperature. The results have shown that such a setup allows to determine ratio errors and phase displacements with a number of significant digits that is sufficient to appreciate very low variations of these quantities for voltage transformers with accuracy class 0.1.

4.1.2 Inductive CT, Verification of Accuracy Depending on Temperature

4.1.2.1 Introduction

This study [32] presents an in-depth experiment investigating the behavior of inductive ITs vs. temperature.

IEC Standard 61869-1 [16] classifies ITs in three different temperature categories according to minimum and maximum ambient air temperature: -5/40 °C, -25/40 °C, -40/40 °C. Unfortunately, IEC Standards 61869-2,3 [5, 7] concerning inductive current and voltage transformers, do not provide any specific test for verifying the accuracy class at different ambient temperatures. To my best knowledge, this topic has not been investigated and published yet. However, the issue deserves particular attention because, in case of metering for pricing, it can lead to energy measurement errors far outside the contractual limits typically agreed between supplier and customer.

This research started in [29] with developing a measurement setup for the accuracy vs. temperature analysis of the VTs. Therefore, the aim of this study is to complete the analysis of the inductive transformers' behavior under different working temperatures.

The analysis started in [29] has been completed by presenting an automatic measurement setup for the accuracy vs. temperature evaluation of inductive CTs. Two current transformers, made by two different manufacturers, have been tested in a thermostatic chamber in a temperature range between +5 and +55 °C. The automatic setup has been metrologically characterized representing a benchmark for the inductive CTs accuracy testing vs. temperature.

4.1.2.2 Automatic measurement setup

The accuracy investigation of inductive ITs vs. temperature focuses on developing a new setup shown in Fig. 4.7. It consists of:

- a calibrator Fluke 6105A (1000 V, 120 A, max values). It has an accuracy of 75 ppm for the current and the voltage amplitudes, while 10 μ rad for the phase. It has been used to ensure stability for the voltage and current inputs as well as a reference for the phase error measurements.
- current transformer under test, which are classified as:
 - transformer A, which has a 20/5 current ratio, a nominal burden of 6 VA, 0.5 accuracy class, manufactured in the 2015;
 - transformer B, which has a 100/5 current ratio, a nominal burden of 6 VA, 0.2 accuracy class, manufactured in the 2015.

Both transformers have a ferromagnetic core insulated with an epoxied surface. No further information about them is available from their nameplate.

- a thermostatic chamber featuring a temperature range between +5 and +55 °C. The transformer under test is placed inside the chamber as described below;
- a resistive shunt of 10 m Ω featuring a maximum current of 10 A. The output of the inductive CTs has been connected to it and to a 200 m Ω resistor used as burden, according to the specifications of the CT under test in terms of rated burden. The voltage at the shunt terminals is transferred to the acquisition system via BNC cable;
- an amplifier to adjust the voltage output of the shunt to a value consistent with the acquisition system range (0-10 V_{peak}). The amplifier gain can be selected among the following values: 1-5-10-50-100-500-1000;
- a 24-bit DAQ NI9239 which acquires the output voltage of the amplifier (proportional to the output current of the inductive CT) and the phase reference output provided by the calibrator;
- a laptop, used to analyze and compute the data acquired during the measurements, through the LabView software.

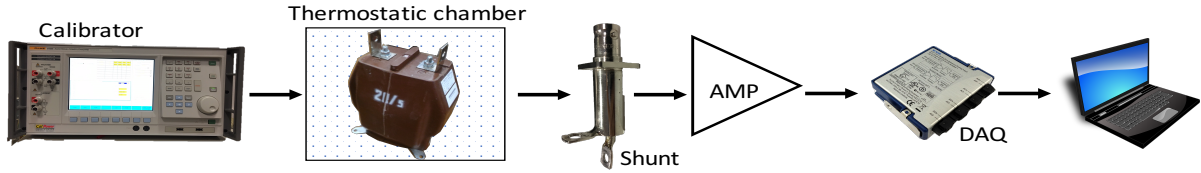


Fig. 4.7. Presented setup for the accuracy vs. temperature verification of current transformers

For developing a measurement setup that could represent a benchmark for the accuracy evaluation of the CTs, it has been mandatory to collect the uncertainty information of the items in the measurement chain. Therefore, the measurement system made by the shunt, the amplifier and the DAQ has been metrologically characterized by the setup depicted in Fig. 4.8. The characterization procedure provided correction terms φ_{SH} on the phase and k_{SH} on the RMS. Such values have been used to correct the output of the current transformers.

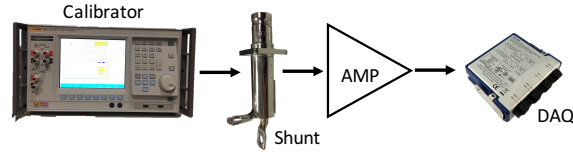


Fig. 4.8. Metrological characterization setup for the measurement chain shunt + amplifier + DAQ

The tests have been run as follows. The calibrator fed the shunt with values corresponding to 20 % and 100 % of the secondary rated current, which are test points defined in [5] for the accuracy class evaluation. These values resulted in 10 mV and 50 mV voltage drop on the shunt, respectively, since it has a $R_S = 10 \text{ m}\Omega$ resistance. Given that they are relatively small with respect to the full scale of the DAQ (10 V), a gain G of 500 and 100 have been chosen for the amplifier. Its output $v_S(t)$ has been acquired by the DAQ and used to compute k_{SH} :

$$k_{SH} = \frac{V_S}{R_S * G * I_{ref}} = \frac{I_S}{I_{ref}} \quad (4.3)$$

where V_S is the RMS value of $v_S(t)$, I_{ref} is the RMS value of the reference current provided by the calibrator, and $I_S = V_S / (R_S * G)$ is the RMS value of the secondary current measured by the shunt. The phase error φ_{SH} introduced by the measurement chain is defined as the difference between the phases \widehat{V}_S and \widehat{V}_{ref} of the phasors \vec{V}_S and \vec{V}_{ref} :

$$\varphi_{SH} = \widehat{V}_S - \widehat{V}_{ref} \quad (4.4)$$

where \vec{V}_S is the phasor of $v_S(t)$, and \vec{V}_{ref} is the phasor of the phase reference output, provided by the calibrator.

Then, one hundred measurements have been performed for each considered secondary rated current. Table 4.10 lists the mean values $E\{I_S\}$, $E\{\varphi_{SH}\}$ and $E\{k_{SH}\}$ of I_S , φ_{SH} and k_{SH} , along with their standard deviations s_I , s_k and s_φ .

Table 4.10. Results of the metrological characterization of the setup

I_{ref} (A)	$E\{I_S\}$ (A)	s_I (mA)	$E\{\varphi_{SH}\}$ (mrad)	s_φ (mrad)	$E\{k_{SH}\}$	s_k
1.0000	0.9978	0.4	0.0	0.3	0.9978	0.0004
5.0000	4.97992	0.5	0.00	0.08	0.9960	0.0005

Given that the contributions to uncertainty from the calibrator (75 ppm and 10 μ rad) are one order of magnitude lower than s_k and s_φ , those can be assumed to represent the uncertainty on the correction terms $E\{k_{SH}\}$ and $E\{\varphi_{SH}\}$.

4.1.2.3 Tests & results

The characteristics of the two inductive CTs, described in detail in the previous subsection, are summarized, for the sake of clarity, in Table 4.11. Observe that both current transformers feature the same 6 VA burden, which corresponds to a 240 m Ω resistor. Given that the standard [5] allows to use a load ranging from 25 % to 100 % of the rated burden, a 200 m Ω resistor was used considering the effect of the 10 m Ω shunt and the resistance of the wirings.

Table 4.11. Characteristics of the two transformers under test

Transformer	Current Ratio (A)	Burden (VA)	Accuracy Class
A	20/5	6	0.2
B	100/5	6	0.5

The test procedure adopted has been the same for both inductive CTs under test. The inductive CT under test has been placed inside the thermostatic chamber, while the other components of Fig. 4.7 have been connected outside the chamber, at ambient temperature. The inductive CT has been fed by the calibrator that provided a sinusoidal current with an RMS value equal to the rated primary current of the inductive CT under test (20 A and 100 A for the transformers A and B, respectively). Then, the temperature of the chamber has been set to different values. Before acquiring any data, the current transformers have been left running at these conditions for at least 24 hours. Such conditions guarantee that all its internal parts reached the thermal steady-state. After that, 100 measurements have been collected and, for each of them, the phase displacement $\Delta\vartheta$ and ratio error ε have been computed:

$$\varepsilon = \frac{\frac{k_r I_S}{E\{k_{SH}\}} - I_p}{I_p} \quad (4.5)$$

$$\Delta\vartheta = \vartheta_s + E\{\varphi_{SH}\} - \vartheta_p, \quad (4.6)$$

where, k_r is the transformer nominal ratio, I_S and I_p are the RMS values of the secondary and primary current, respectively, ϑ_s and ϑ_p are the secondary and primary current phasors phases. In particular, I_S has been obtained as previously described, I_p is the RMS value set with the calibrator, ϑ_s is equal to \widehat{V}_S and ϑ_p has been obtained from the phase reference output signal provided by the calibrator.

The procedure has been applied for different temperature values: +5, +25 and +45 $^{\circ}$ C.

Moreover, to further analyze the behavior of the inductive CTs accuracy vs. temperature, tests at the 20 % of the rated current have been performed for each of the three temperatures. Hence, the calibrator fed the transformers A and B with 4 and 20 A, respectively. This assessment is particularly

interesting, because at 20 % of the rated current, the accuracy class limits for the phase displacement and the ratio error differ from the rated ones shown in Table 4.12 [5].

Table 4.12. Thresholds of the ratio and phase errors for different percentages of the rated current

Accuracy Class	% of I_{ref}	ε (%)	$\Delta\vartheta$ (mrad)
0.2	20	0.35	4.5
	100	0.2	3
0.5	20	0.75	13.5
	100	0.5	9

The measurement results are presented in Tables 4.13 to 4.20. To clarify the notation, the tables present, for each temperature, the maximum, minimum and mean value of the phase displacement and the ratio error, along with their standard deviations. For the sake of clarity, the same results are also plotted in Figures 4.9 to 4.12, where also the relevant accuracy limits are shown.

For transformer A, when 100 % of the rated current is injected, ε and $\Delta\vartheta$ are shown in Tables 4.13 and 4.14, respectively.

Table 4.13. Ratio error for different temperatures for transformer A, at 100 % of the rated current

Temperature [°C]	Max Value [-]	Min Value [-]	Mean Value [-]	Std. Deviation [-]
5	$-16.18 \cdot 10^{-3}$	$-16.35 \cdot 10^{-3}$	$-16.28 \cdot 10^{-3}$	$3 \cdot 10^{-5}$
25	$-0.27 \cdot 10^{-3}$	$-0.57 \cdot 10^{-3}$	$-0.43 \cdot 10^{-3}$	$1 \cdot 10^{-4}$
45	$0.05 \cdot 10^{-3}$	$-0.12 \cdot 10^{-3}$	$-0.04 \cdot 10^{-3}$	$4 \cdot 10^{-5}$

Table 4.14. Phase displacement for different temperatures for transformer A, at 100 % of the rated current

Temperature [°C]	Max Value [rad]	Min Value [rad]	Mean Value [rad]	Std. Deviation [rad]
5	23.47	23.16	23.36	$6 \cdot 10^{-2}$
25	4.93	4.83	4.89	$2 \cdot 10^{-2}$
45	4.58	4.46	4.52	$2 \cdot 10^{-2}$

Observe that these parameters are strongly affected by the temperature, mainly when the transformer is working at +5 °C. In fact, referring to Table 4.12, ε and $\Delta\vartheta$ are considerably out of the accuracy limits defined by the standard [5]: -1.628 % for the ratio error (limit of the class equal to 0.5 %) and 23.36 mrad for the phase displacement (limit of the class equal to 9 mrad). At higher temperatures, the CT accuracy remains within the limits even if a significant variation of the ratio error occurs when moving from +25 °C to +45 °C. Tables 4.15 and 4.16 list ε and $\Delta\vartheta$, when the same transformer is fed with 20 % of the rated current. Similar comments to those of the previous case can be made.

Table 4.15. Ratio error for different temperatures for transformer A, at 20 % of the rated current

Temperature [°C]	Max Value [-]	Min Value [-]	Mean Value [-]	Std. Deviation [-]
5	$-22.914 \cdot 10^{-3}$	$-22.973 \cdot 10^{-3}$	$-22.931 \cdot 10^{-3}$	$6 \cdot 10^{-6}$
25	$-2.0 \cdot 10^{-3}$	$-3.2 \cdot 10^{-3}$	$-2.5 \cdot 10^{-3}$	$3 \cdot 10^{-4}$
45	$-3.42 \cdot 10^{-3}$	$-3.79 \cdot 10^{-3}$	$-3.70 \cdot 10^{-3}$	$5 \cdot 10^{-5}$

Table 4.16. Phase displacement for different temperatures for transformer A, at 20 % of the rated current

Temperature [°C]	Max Value [rad]	Min Value [rad]	Mean Value [rad]	Std. Deviation [rad]
5	37.85	37.71	37.74	$1 \cdot 10^{-2}$
25	9.6	8.6	9.0	0.3
45	9.73	9.27	9.62	$6 \cdot 10^{-2}$

Even in this case, at low temperature the transformer accuracy is out of its class, whereas this is not happening for higher temperatures. Figures 4.9 and 4.10 plot ε and $\Delta\theta$ results for transformer A.

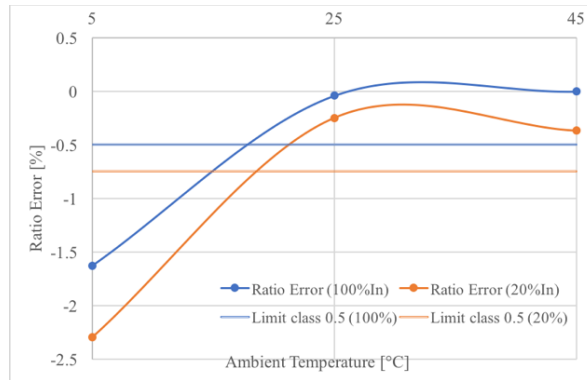


Fig. 4.9. Ratio Error vs. temperature of transformer A for 20 % and 100 % of the rated primary current

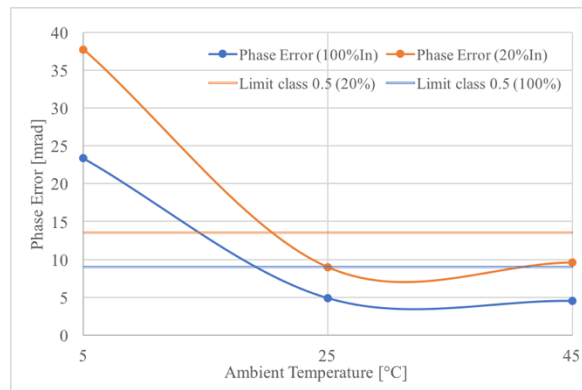


Fig. 4.10. Phase displacement vs. temperature of transformer A for 20 % and 100 % of the rated primary current

Measurements results for transformer B are presented in Tables 4.17 to 4.20.

Table 4.17. Ratio error for different temperatures for transformer B, at 100 % of the rated current

Temperature [°C]	Max Value [-]	Min Value [-]	Mean Value [-]	Std. Deviation [-]
5	$-2.56 \cdot 10^{-3}$	$-3.21 \cdot 10^{-3}$	$-2.91 \cdot 10^{-3}$	$1 \cdot 10^{-5}$
25	$-0.03 \cdot 10^{-3}$	$-0.46 \cdot 10^{-3}$	$-0.23 \cdot 10^{-3}$	$2 \cdot 10^{-5}$
45	$0.08 \cdot 10^{-3}$	$-0.37 \cdot 10^{-3}$	$-0.12 \cdot 10^{-3}$	$3 \cdot 10^{-5}$

Table 4.18. Phase displacement for different temperatures for transformer B, at 100 % of the rated current

Temperature [°C]	Max Value [rad]	Min Value [rad]	Mean Value [rad]	Std. Deviation [rad]
5	3.87	3.69	3.78	$1 \cdot 10^{-2}$
25	3.08	2.83	2.96	$2 \cdot 10^{-2}$
45	3.01	2.75	2.83	$3 \cdot 10^{-2}$

Table 4.19. Ratio error for different temperatures for transformer B, at 20 % of the rated current

Temperature [°C]	Max Value [-]	Min Value [-]	Mean Value [-]	Std. Deviation [-]
5	$-4.08 \cdot 10^{-3}$	$-4.19 \cdot 10^{-3}$	$-4.16 \cdot 10^{-3}$	$1 \cdot 10^{-5}$
25	$-2.70 \cdot 10^{-3}$	$-2.77 \cdot 10^{-3}$	$-2.75 \cdot 10^{-3}$	$2 \cdot 10^{-5}$
45	$-2.45 \cdot 10^{-3}$	$-2.66 \cdot 10^{-3}$	$-2.59 \cdot 10^{-3}$	$3 \cdot 10^{-5}$

Table 4.20. Phase displacement for different temperatures for transformer B, at 20 % of the rated current

Temperature [°C]	Max Value [rad]	Min Value [rad]	Mean Value [rad]	Std. Deviation [rad]
5	6.33	6.19	6.30	$1 \cdot 10^{-2}$
25	4.80	4.73	4.77	$2 \cdot 10^{-2}$
45	4.56	4.41	4.48	$3 \cdot 10^{-2}$

They highlight a behavior of transformer B quite similar to that of transformer A. When it operates at +5 °C, both ε and $\Delta\vartheta$ fall outside the accuracy class limits. This occurs at 20 % as well as at 100 % of the rated primary current. When the temperature increases, ε and $\Delta\vartheta$ take values within the limits defined by the standard [5]. Consider Figures 4.11 and 4.12 showing ε and $\Delta\vartheta$ results for transformer B.

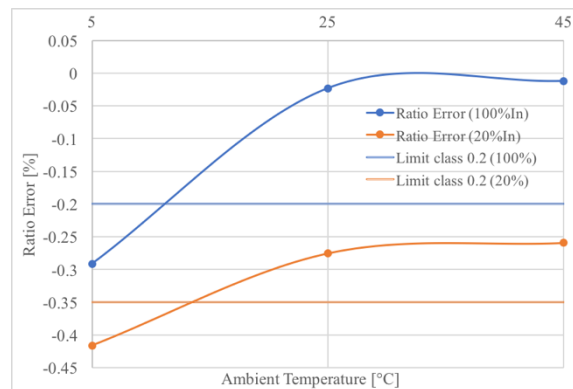


Fig. 4.11. Ratio Error vs. temperature of transformer B for 20 % and 100 % of the rated primary current

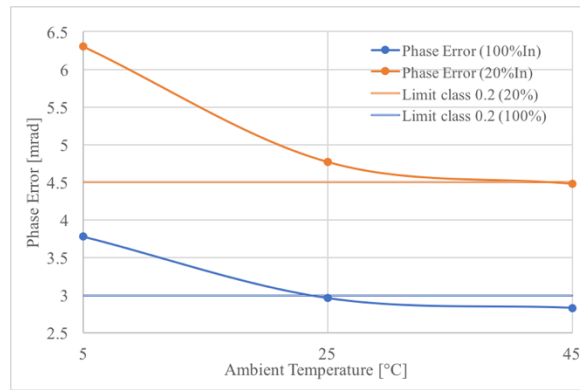


Fig. 4.12. Phase displacement vs. temperature of transformer B for 20 % and 100 % of the rated primary current

Overall, the main outcome consists of a significant variation of the accuracy of both tested CTs at low temperatures. This leads to two different issues:

- if the obtained results can be extended to several other CTs, an issue of fair billing arises;
- further investigations on the reasons that determine such behavior. For example, consider the piezo-magnetic phenomenon, which consists in a variation of the magnetic permeability when a ferromagnetic material is subjected to physical stress that turns into a geometrical modification. For the inductive CT, the lower temperature may cause a compression of the magnetic core resulting in different values of the parameters of the equivalent circuit of the CT.

4.1.2.4 Conclusion

Even if inductive instrument transformers are hardly used in new installations for smart grids anymore, they are still the preferred solution adopted for the metering for pricing. Here, the accuracy variation of inductive current transformer vs. temperature has been analyzed in depth and reported in this research. In this context, a new set-up has been designed and realized to evaluate the phase displacement and the ratio error variations of two inductive current transformers available on the market for tariff purposes at different ambient temperatures. The results of the tested inductive current transformers highlight that these transformers do not fulfill the accuracy class requirements when the temperature is below the conventional ambient temperature of 23°C, but higher than the minimum working temperature specified by the standards [16].

This behavior, not yet discussed in the literature, has been observed in multiple in-field measurement campaigns with different models of CT. It is expected that such a behavior is typical for many inductive current transformers on the market. Hence it may yield to measure currents and, mainly, energy or power with unexpected large errors, penalizing either the electric energy suppliers or the final users.

4.1.3 Accuracy vs. multiple influence quantities verification of passive LPCT

4.1.3.1 Introduction

This research presents a complete series of tests performed on LPITs, in particular on passive Rogowski-coil-type Low-Power Current Transformers, which could become benchmark-type tests in future Standards. As a matter of fact, Standards provide a variety of tests for each kind of instrument. For example, IEC Standard 61869-10 [19] defines accuracy tests for the LPCT vs. position, vs. frequency, and vs. temperature. Even literature contains several works on this critical topic, for example [33] assesses the mutual inductance of the Rogowski vs. primary conductor position. In [34] their performance is evaluated when the geometrical parameters are varying, whereas [35] studies the thermal expansion of the Rogowski as a principle cause of decreasing performance. Finally, the single effect of the primary conductor position and of the electromagnetic fields on the Rogowski measurements are analyzed in [36] and [37], respectively. Hence, in light of the aforementioned and by considering the growing importance of LPITs in smart grid operations, this research [38] made a further step towards a better knowledge of their behavior under the typical influence quantities. This has been done by assessing the effects of multiple influence quantities simultaneously affecting the LPCTs. To my knowledge, no accuracy performance has been tackled neither in the literature nor in the Standards to understand the effects a quantity could have on the Rogowski performance when combined with others. Hence, by considering the key role of the LPCTs accuracy analysis, this research presents a full set of tests combining three different quantities: primary conductor position, frequency, and ambient temperature. Tests have been performed according to [19] when possible, otherwise they have been designed by starting from it. The input signal for the tests is always a sinusoidal waveform at rated frequency (except for the frequency tests). This to understand the aforementioned quantity effects on an ideal signal, hence not consistent with the actual grid condition. Afterwards, results of the tests have been assessed in terms of the LPCTs accuracy parameters: ratio error and phase displacement. The results have confirmed the idea of using the proposed tests as benchmark for future Standards.

4.1.3.2 Automatic measurement system

This Section provides a description of the adopted measurement system. Its simple schematic representation is depicted in Fig. 4.13.

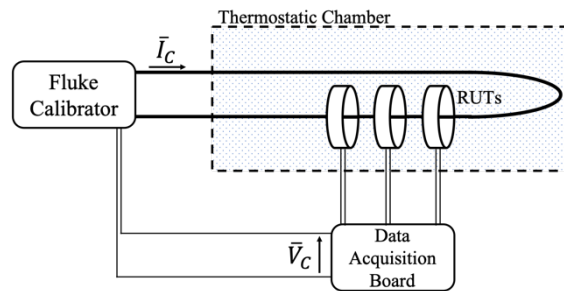


Fig. 4.13. Schematic representation of the developed automatic measurement setup

The picture consists of the following elements:

- Fluke Calibrator 6105A. It is used as a current and voltage reference source (\vec{I}_C and \vec{V}_C : current and voltage phasors) for all performed tests. Its main characteristics, including the accuracy ones, are listed in Table 4.21.

Table 4.21. Accuracy specification of the Calibrator Fluke 6105a

Range [V]	Accuracy (ppm + mV)
1 – 23	42 + 0.2
70 – 1008	60 + 10
Range [A]	Accuracy (% of output + % of range)
120	0.009 + 0.002
Frequency	Accuracy (ppm)
Full range	50

- Thermostatic chamber. It allows to vary its internal temperature in the range (5 – 70) °C. In addition, a Chauvin Arnoux 863 thermocouple-based temperature sensor has been used to verify the desired temperature in each performed test. It features a measurement range (-50 to +1300) °C, 0.1 °C resolution, and an accuracy of ± 0.3 % of the reading.
- A set of three Rogowski-coil-type current transformers. From here on they are referred to as X, Y, and Z for the sake of privacy, and made by three different manufacturers. X is a window-type Rogowski, whereas Y and Z are of the split-core-type. The Rogowski Under Test (RUT) characteristics are summarized in Table 4.22. In addition, the RUTs come from manufacturers which guarantee that their products are compliant with the most recent Standards. This way, one can assume that the sample choice would not affect the test results.

Table 4.22. Main Characteristics of the Rogowski coils under test

Feature	X	Y	Z
Type	Window	Split-core	Split-core
Ratio	100 A/ 31 mV	1000 A/ 100 mV	1000 A/ 100 mV
Inner Diameter	50 mm	115 mm	75 mm
Accuracy	Class 0.5	± 1 %	± 1 %

- A NI-9238 Data Acquisition board and its USB chassis NI-9171. The DAQ main features are summarized in Table 4.23. It has been used to collect the RUTs output and the voltage phasor of the calibrator, used as phase reference. Such a measurement set-up has been adopted to perform all tests described in the following sections.

Table 4.23. Main characteristics of the NI 9238

Architecture	24-bit	Max input signal	± 500 mV
Sample rate	50 kS/s/ch	Simultaneous channels	YES
ADC	Delta Sigma	Temperature range	-40 to 70 °C
Gain Error	± 0.07 %	Offset Error	± 0.005 %

4.1.3.3 Experimental tests

This Section describes tests to assess the effects of several quantities on the RUTs. With the same structure, results are presented in the next Section.

- Resistive burden characterization
Before performing the main tests, the resistive burden connected to each RUT has been characterized to estimate its value. To this purpose, 200 measurements have been performed with the HP Digital Multimeter 3458a on three 22 k Ω resistors.
- Accuracy vs. position tests
The first set of tests aimed to verify the effects of both the position of the internal and external conductors on the accuracy of the RUTs. To this purpose, according to [19], four different positions have been tested. As clarified by Fig. 4.14, they are referred to as A, B, C, and D.

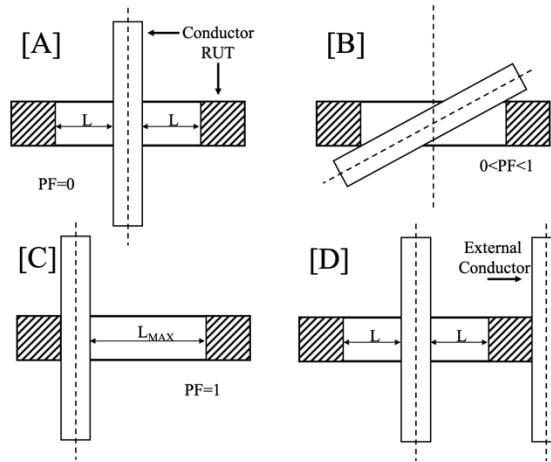


Fig. 4.14. Pictures of the 4 test configurations adopted. Each of them describes a different relative position between the LPCT and the internal and/or external conductor

For the first three positions, [19] defines the Position Factor (PF) as:

$$PF = \frac{d_{max} - d_{min}}{d_{max} + d_{min}}, \quad (4.7)$$

where d_{max} and d_{min} are the maximum and minimum distances between the primary conductor and the Rogowski window. The PF ranges between 0 and 1.

Position A is the rated one, where the internal conductor is centred with respect to the RUT, hence it has a Position Factor (PF) of 0. As for positions B and C they refer to not-null PF, $0 < PF < 1$ and 1, respectively. In particular, in B the conductor is completely bend over the RUT, whereas in C the conductor is perpendicular to the RUT but attached to it, hence not centred at all. Last position is D, where an external conductor is attached to the outer part of RUT. Moreover, as for D, [19] states that the transmitting cables of the LPCT must be 90° with respect to the external conductor. To better clarify this aspect, in Fig. 4.15 the correct positioning is depicted.

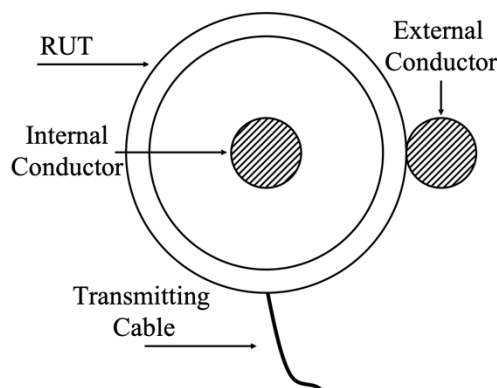


Fig. 4.15. Different perspective of the test D to highlight the relative position between the transmitting cable and the external conductor.

Afterwards, for the 4 test configurations, a primary current $\bar{I}_C = 100$ A (at 50 Hz and 22°C) has been injected with the calibrator through the primary conductor and measured with the 3 RUTs. Their outputs \bar{U}_S have been acquired without using any integrator in-between to avoid any interference with the RUT performance evaluation. Then, 100 measurements of \bar{U}_S have

been collected, and 100 values of ratio error and phase displacement (ε and φ) have been computed as:

$$\varepsilon = \frac{k|\bar{U}_S| - |\bar{I}_C|}{|\bar{I}_C|} \quad (4.8)$$

$$\varphi = \hat{U}_S - \hat{I}_C, \quad (4.9)$$

where, $|\bar{U}_S|$ and $|\bar{I}_C|$ are the modules of the Rogowski output voltage and the primary current phasors, respectively. As for k , it is the rated ratio of the RUTs, \hat{U}_S and \hat{V}_C instead, are the phases of the related abovementioned phasors. Afterwards the mean value, of the 100 measurement, of ratio error and phase displacement $\tilde{\varphi}$ have been computed (for all the performed tests).

Afterwards, all the described tests have been repeated at 48 Hz and 51 Hz. Such values have been adopted from [19] to tackle the harshest conditions, which refer to the use of the LPCTs for protective purposes. For the frequency tests, [19] states that the obtained ratio errors must be corrected as:

$$\varepsilon_{CF} = \frac{CF * k * |\bar{U}_S| - |\bar{I}_C|}{|\bar{I}_C|}, \quad (4.10)$$

where CF is the Correction Factor obtained as the ratio between the rated and the actual frequency, f_r and f_a , respectively:

$$CF = \frac{f_r}{f_a}. \quad (4.11)$$

- Accuracy vs. temperature tests

The second set of tests assessed the effects of the working temperature on the accuracy of the RUTs. To this purpose, the temperatures defined for the tests are 5, 22, and 40 °C. The upper limit has been defined according to [19], whereas the lower one is in accordance with a typical outdoor average ambient temperature in Italy during cold seasons. Therefore, each temperature has been set on the thermostatic chamber and kept for 8 hours. This, to ensure a proper thermal stability for both the chamber and all the RUTs. Once such a condition has been obtained, 100 measurements of \bar{U}_S have been acquired for the 4-test configurations and for the 3 frequencies (48, 50, and 51 Hz). Again, from the measurement results, ε and φ have been computed for each test configuration. In summary, an overall amount of 36 tests have been performed. For the sake of clarity, and for a better comprehension of the next Section, they have been numerated and listed in Table 4.24.

Table 4.24. List of all the performed test: 36 for each RUT

Position	5 °C			22 °C			40 °C		
	48 [Hz]	50 [Hz]	51 [Hz]	48 [Hz]	50 [Hz]	51 [Hz]	48 [Hz]	50 [Hz]	51 [Hz]
A	#30	#28	#29	#9	#1	#5	#15	#13	#14
B	#33	#31	#33	#10	#2	#6	#18	#16	#17
C	#36	#34	#35	#11	#3	#7	#21	#19	#20
D	#27	#25	#26	#12	#4	#8	#24	#22	#23

4.1.3.4 Experimental results

- Resistive burden characterization results

Table 4.25 collects all mean values \tilde{R} and related combined uncertainty u_c of the three resistors (R_X , R_Y , and R_Z). As for u_c , it has been calculated, according to the Guide to the expression of Uncertainty in Measurement [21], as:

$$u_c = \sqrt{(u_a)^2 + (u_b)^2}, \quad (4.12)$$

where u_a and u_b are the uncertainties evaluated with type A and type B methods, respectively. In particular, u_b has been computed by starting from the accuracy specification of the

multimeter 3458a used for the resistance measurements: $2 \cdot 10^{-6}$ error on the reading and $2 \cdot 10^{-7}$ error on the range. As for u_a , is computed by dividing the variance of the mean value measured by the number of measurements. From Table 4.25 it is possible to highlight the low uncertainty associated the resistors values.

Table 4.25. Resistive burden characterization results

Quantity	X	Y	Z
\tilde{R} [Ω]	21893.9	22032.5	21818.8
u_c [Ω]	0.4	0.5	0.3

- Results of the accuracy vs. position tests
By considering that no calibration coefficients were provided by the LPCT manufacturers, test #1 has been used as a reference test to determine the actual ratio of the 3 RUTs (K_X , K_Y , and K_Z). They are listed in Table 4.26 along with their associated combined uncertainty (computed according to (4.12)). In addition, all the ratio errors presented in the following have been computed by taking the ratios in Table 4.26 as the rated ones. Hence, for comparing purposes, test #1 ratio error is always set at value zero.

Table 4.26. Test #1 results. Used to determine the actual ratio of the Rogowski coils

Quantity	X	Y	Z
K [1/mV]	3720.26	10536.1	10162.7
u_c [1/mV]	0.09	0.2	0.2

Moving to the aim of the subsection, in Fig. 4.16 the results of the accuracy vs. position tests are shown at 50 Hz and at room temperature, 22 °C (#1, #2, #3, and #4). In the graph, and in all the following ones, the standard deviation of the ratio error (obtained from the mean of 100 measurements) is not presented for the sake of brevity.

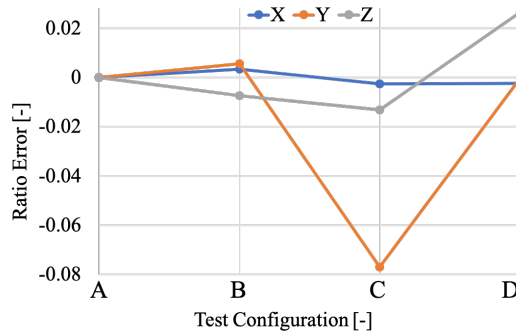


Fig. 4.16. Ratio Error results for tests #1 to #4. Accuracy vs. positions, 22 °C, 50 Hz

As a matter of fact, the standard deviation was always in the order of 10^{-5} for all performed tests.

Note that the window-type RUT (X) is hardly affected by the PF of the conductor, whereas Y and Z are sensitive to PF=1 (position C) and to the presence of an external conductor (position D), respectively. The phase displacement of these four sets of results has not been plotted for the sake of brevity because it has not been affected by the PF. Moreover, it was always in the order of fraction of milliradians for the three RUT.

In light of the position-tests results, it can be concluded that the conductor position is critical for the Rogowski performance. As confirmed in [33] the changes in the conductor position cause a variation of the mutual inductance M between conductors. Therefore, according to

$u_s(t) = -M \frac{di(t)}{dt}$, the result is a different output voltage $u_s(t)$ (by starting from the same input current $i(t)$). However, this issue is typically solved by using external accessories (usually of insulating material) aimed at keeping the conductor centered with respect to the Rogowski. However, as experienced in many in-field applications, this is not always possible, hence compensating solutions should be adopted.

By adding the contribution of another influence quantity, the frequency and the related results are depicted in Fig. 4.17 (dotted lines refer to 48 Hz whereas the solid ones to 51 Hz).

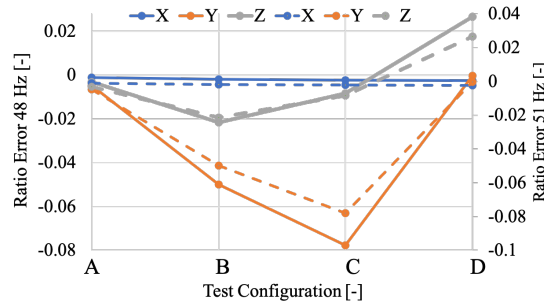


Fig. 4.17. Ratio Error results for tests #5 to #12. Accuracy vs. positions, 22 °C, 48 Hz (solid) and 51 Hz (dotted)

From it, a general comment is that the results confirm the overall trend (and absolute values) obtained from Fig. 4.16. However, aside for the case of X, which is not affected by frequency, all other RUTs suffer from its effect which is an increase of contribution to the overall uncertainty. As for φ , neither the frequency is affecting it, confirming what has already been obtained from the 50 Hz cases. As a final comment on this first set of results, it can be stated that at 50 Hz (rated frequency), positions C and D are critical for the split-core type Rogowski. As a matter of fact, ε significantly overcomes the limits declared by the manufacturers ($\pm 1\%$). Instead, for frequencies different from the rated one, even position B becomes critical. In particular, Y's accuracy is non-compliant for positions B and C, whereas Z's accuracy is non-compliant for positions B and D. Please note that in all frequency test results the proper CF has been applied.

- Results of the accuracy vs. temperature tests

In this subsection, the effects of a working temperature variation on the accuracy of the RUTs is assessed. To this purpose, let us start from the basic position A, where the LPCT is centred with respect to the internal conductor. Hence, Fig. 4.18 shows the results of the test #1, #13, and #28 (position A, at 50 Hz). From the picture, it can be concluded that X, the window-type Rogowski, is hardly affected by temperature when working at 50 Hz. Conversely, for Y and Z, the split-core coils/devices, temperature is significantly reducing their accuracy. In particular, at 40 °C the ratio error is increased up to one order of magnitude. However, for all RUTs, either at 5 °C or at 40 °C, ε remains within the accuracy limits provided by the manufacturers and listed in Table 4.22.

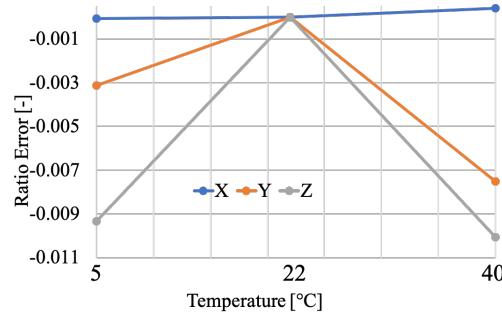


Fig. 4.18. Ratio Error results for tests #1, #13 and #28. Accuracy vs. temperature, 50 Hz

The computed phase displacements are listed in Table 4.27 with their associated combined uncertainty. From the Table it emerges that the temperature is not affecting φ for the studied RUTs and they always remain within the accuracy limits.

Table 4.27. Phase Error results for tests #1, #13, and #28

Test	X		Y		Z	
	$\tilde{\varphi}$ [mrad]	u_c [mrad]	$\tilde{\varphi}$ [mrad]	u_c [mrad]	$\tilde{\varphi}$ [mrad]	u_c [mrad]
#1	-0.17	0.09	-0.91	0.09	-0.65	0.09
#13	0.26	0.09	1.01	0.09	0.01	0.09
#28	0.27	0.09	1.35	0.09	0.01	0.09

In accordance with previous subsection B, the results mentioned above are now evaluated at frequencies different from the rated one. All the results are depicted in Fig. 4.19, where the dotted lines represent the 51 Hz tests (#5, #14, and #29) whereas the 48 Hz ones (#9, #15, and #30) are represented by a solid line. The first comment that arises from the graph is the overall confirmation of the trend observed in Fig. 4.16 for the tests at 50 Hz. Second, both 48 and 51 Hz tests provide almost the same results (in absolute value terms) for each tested temperature.

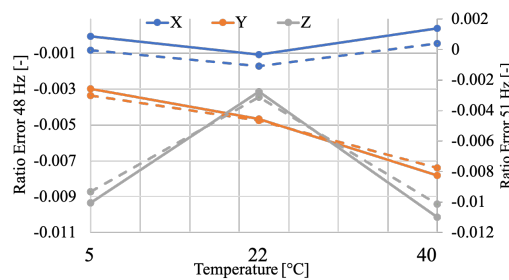


Fig. 4.19. Ratio Error results for tests #5, #9, #14, #15, #29 and #30. Accuracy vs. temperature, 48 Hz (solid) and 51 Hz (dotted)

As for the evaluation of the combined effects of temperature and frequency, Fig. 4.18 and Fig. 4.19 must be compared. From the comparison, the temperature provides the most significant contribution to the worsening accuracy. As a matter of fact, the frequency contribution is negligible and cannot be distinguished from the temperature one. Moving to the phase displacement evaluation, in the position A studied in this subsection, it can be concluded that φ is not affected neither by the temperature nor by the frequency. Hence, results are not reported for the sake of brevity.

Overall, the temperature seems to have a critical effect on the Rogowski performance. This can be associated to two phenomena affecting the RUT when the temperature varies: changes in its geometry and thermal expansion of the copper windings. Both are confirmed to have an

effect on the Rogowski performance [34, 35], hence two possible solutions to mitigate such effects might be: (i) using an external cage for the Rogowski with thermal properties aligned with the working temperatures; (ii) development of compensating (hardware or software) techniques to consider the effects of temperature on the Rogowski output.

- Evaluation of Temperature and Position combined effect on the RUTs accuracy
Among the novelties of this research, the evaluation of multiple influence quantities effects on the LPCTs performance is one of the most interesting. To this purpose, Figures 4.20 and 4.21 show the results of the position and temperature combined tests.

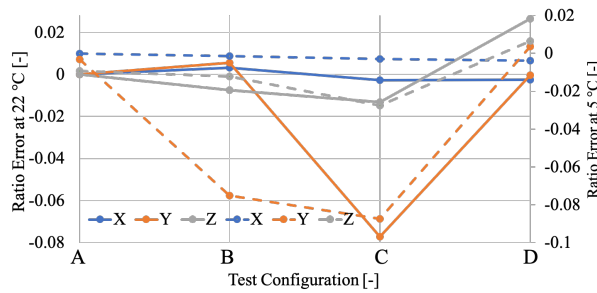


Fig. 4.20. Ratio Error results for tests at 50 Hz, for two different temperatures (22 °C, solid line; 5 °C, dotted line), for all the positions

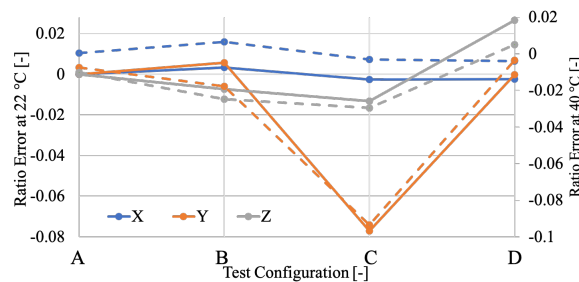


Fig. 4.21. Ratio Error results for tests at 50 Hz, for two different temperatures (22 °C, solid line; 40 °C, dotted line), for all the positions

Fig. 4.20 contains the comparison between the tests performed at 22 °C (solid lines) and the ones performed at 5 °C (dotted lines). From the graph analysis, it results that all the RUTs are affected by temperature even in rated position A. Therefore, the temperature makes X, Y, and Z exceed their accuracy limits. Such trend is then confirmed for the other positions tested and all RUTs. In addition, considering that the solid curves represent the computed ε obtained from the single effect of the conductor position, the graph allows to quantify the temperature contribution on the overall value of ε .

Similar comments can be drawn from Fig. 4.21, comparing the tests performed at 22 °C (solid lines) and the ones at 40 °C (dotted lines). However, compared to Fig. 4.20, a slight difference can be highlighted: a higher temperature seems to have less effect on the RUT' performance. This is true for all RUTs except for X, the window-type one, which is affected by both high and low temperatures. For the sake of completeness, the phase displacement results obtained by the above-mentioned test combinations are listed in Table 4.28. However, as in the previous tests, the phase error is not affected by the combination of temperature and conductor position.

Table 4.28. Phase displacement computation results for all the accuracy vs. temperature + position test combinations

Position	Quantity	X			Y			Z		
		5 °C	22 °C	40 °C	5 °C	22 °C	40 °C	5 °C	22 °C	40 °C
A	$\tilde{\varphi}$ [mrad]	-0.27	-0.17	-0.25	-1.35	-0.91	-1.01	0.01	-0.65	0.01
	u_c [mrad]	0.09	0.09	0.09	0.09	0.09	0.09	0.09	0.09	0.09
B	$\tilde{\varphi}$ [mrad]	-0.24	-0.18	-0.23	-1.22	-0.74	-0.44	-0.65	-0.91	-1.21
	u_c [mrad]	0.09	0.09	0.09	0.09	0.09	0.09	0.09	0.09	0.09
C	$\tilde{\varphi}$ [mrad]	-0.24	-0.08	-0.18	-1.27	-1.42	-1.25	-0.32	-0.45	0.02
	u_c [mrad]	0.09	0.09	0.09	0.09	0.09	0.09	0.09	0.09	0.09
D	$\tilde{\varphi}$ [mrad]	-0.21	-0.11	-0.17	-0.94	-0.92	-0.97	0.08	-0.15	0.02
	u_c [mrad]	0.09	0.09	0.09	0.09	0.09	0.09	0.09	0.09	0.09

- Evaluation of Temperature, Position, and Frequency combined effect on the RUTs' accuracy
 The final set of test results concerns the combination of three influence quantities applied to the RUTs in order to evaluate their performance. Results are presented in Figures 4.22, 4.23, and 4.24 for the LPCTs X, Y, and Z, respectively. They show the ratio errors of the possible test configurations, which include temperature, frequency, and position variations. In particular, each set of columns represents a position, while the colors refer to the temperatures: blue, green, and red, for 5, 22, and 40 °C, respectively. From the pictures it is possible to derive the ϵ trends based on the combined influences of the various quantities.

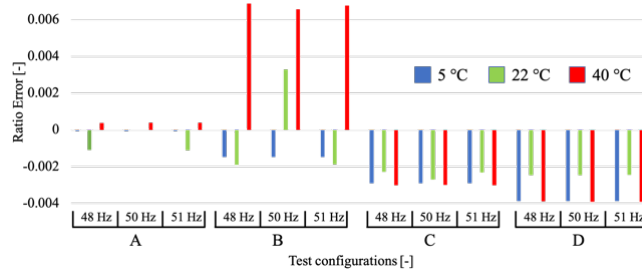


Fig. 4.22. Ratio Error results for tests concerning all the influence quantities acting on the RUT (X)

In Fig. 4.22, the negative effect of the temperature is superimposed on position B. In fact, the combination of these two influence quantities turns into a ratio around seven times greater than the allowed limit. On the contrary, working at frequencies different from the rated one does not result in any significant variation of the RUT performance accuracy. Similar comments on the frequency can also be stated for Fig. 4.23 and 4.24. The Y results in Fig. 4.23 show that positions B and C are particularly critical, whereas the presence of an external conductor (position D) is not affecting the performance of Y at all. Moreover, a low temperature seems to be more critical than high temperature in all performed tests.

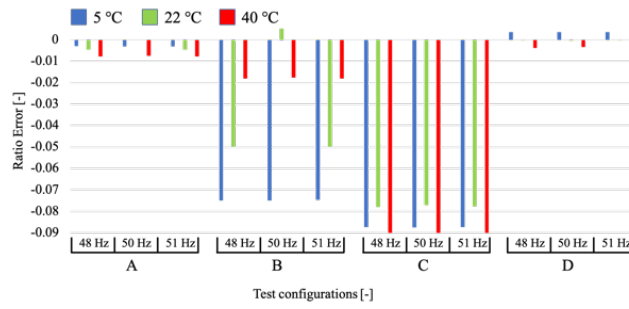


Fig. 4.23. Ratio Error results for tests concerning all the influence quantities acting on the RUT (Y)

Interesting results can be drawn also from Fig. 4.24: Z is sensitive to the presence of external cables. However, this sensitiveness seems to be reduced by a working temperature different from the rated one (22 °C). Again, the frequency does not influence the RUT operation, while temperature combined with position changes the results to critical values.

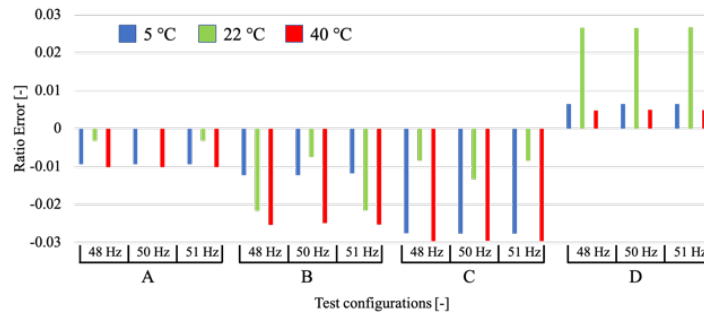


Fig. 4.24. Ratio Error results for tests concerning all the influence quantities acting on the RUT (Z)

From these results it can be concluded that, on the one hand the simultaneous presence of the influence quantities temperature and position causes a severe degradation of the LPCT performance. This is true for all RUTs studied in this work. In addition, such a degradation brings the ratio error out of its bounds, hence, not guaranteeing the manufacturers' stated accuracy anymore. On the other hand, φ seems not to be affected by any of the influence quantities tested in this work.

In addition, the interesting and satisfactory results presented support the idea of using the proposed tests as a benchmark for the Rogowski coil testing. Then, the study could be completed by assessing the Rogowski behavior with waveforms affected by all kinds of power quality issues (harmonics, interharmonics, dips, etc.).

4.1.3.5 Conclusion

This research describes a study on Low Power Passive Current Transformers, in particular the Rogowski type. Starting from their related Standards, new tests have been proposed to assess their accuracy performance under the simultaneous influence of multiple quantities: frequency, position and ambient temperature. Obtained results confirm the initial hypothesis: the passive transformers suffer from the multiple presence of such influence quantities. In particular, all tested devices exceeded their accuracy thresholds when temperature and position were different from the rated one. This holds for the ratio error, while the phase displacement is completely insensitive to the influence quantities applied. Along with the results, this section provided suggestions and comments on the possible technical solutions to be implemented in order to compensate the obtained results.

In conclusion, the research aims to be a first step towards the idea of testing the accuracy of the LPCTs, not just considering one influence quantity at the time, but multiple ones. In addition, it can be observed that the simultaneous presence of more than one influence quantity does not necessarily deteriorate the accuracy performance of the LPCT. Furthermore, the proposed tests and their results, might become a starting point for improving the existing Standards.

4.2 ITs Integration into Smart Grid Operation

The aim of this subsection is to present three case studies, developed in three different studies, which show the use and role of ITs among Smart Grids. More in detail, each study tackles a new application based on the measurements of the ITs for new features from the grid.

4.2.1 A novel approach for assessing the time reference in asynchronous measurements

4.2.1.1 Introduction

With the huge and fast development of Smart Grids and Distributed Generation, the need to perform measurements in several nodes of the power networks has become critically important for DSOs to effectively control their network operations. Furthermore, the possibility to synchronize the measurements from different nodes has allowed to improve the control performance: better control of the operation frequency, fault detection and location, higher network stability, islanding detection and restoration, improvement of the power flow in the network, and more.

The devices that perform synchronized measurements in the network are referred to as Phasor Measurements Units (PMUs) [39]. They ensure the measurement of the RMS values of voltages and currents but also of their phases with respect to a global time reference. This way, according to the definition of phasor given by Charles Proteus Steinmetz [40] in 1893, the *phasor* of a voltage or of a current is given by its RMS value and by its phase difference with respect to a defined time reference. The comparison between the phases of all voltages in a power network allows to evaluate the *state estimation* of the network, which, in turn, represents the gate for monitoring the entire network. Therefore, the added value of a PMU compared to a typical power meter is given by the possibility to evaluate the phase difference of all voltages in a network through the use of a global time reference. The use of PMUs in Transmission lines started around 1988 and its usefulness for a better network control and monitoring was well recognized. In Transmission lines, the error allowed in the evaluation of phases is not a critical parameter due to the very long distances and then to the large difference of the voltage phases (in the order of tens of mrad/km). So traditional VTs with 0.2 accuracy class, used for billing purposes, are well suitable for such an application.

However, in distribution networks this is not sufficient. Distribution lines are far shorter than transmission lines and the difference between the node voltage phases is typically very small, in the order of few mrad/km. Hence, VTs with common 0.5 accuracy class already installed for billing or measurement purposes are no longer suitable for PMU usage. In conclusion, beside the need to have an accurate time reference (with standard deviation in the order of 1 μ s or lower) also very accurate voltage transformers are required for assuring an accurate evaluation of the voltage phasors.

Nowadays the global time reference can be provided to all PMUs deployed in the network by means of wireless or wired communication protocols. The pulse-per-second (pps) information included in the Global Positioning System (GPS) signals represents the most common time reference information in the world. It can be easily and freely read by means of antennas and receivers for triggering all PMUs to a unique reference. Despite many advantages of this technique, it shows some critical issues: the most important one is represented by the need to install the antenna to receive satellite signals. But this is not always possible in certain environments such as urban areas, where many obstacles prevent reception, including trees, buildings, skyscrapers, underground secondary substations, roads and others.

In the last decade, wired time reference infrastructures have been developed too. Today their performance (in terms of delays and accuracy of the time reference) is getting closer to GPS. In particular, IEEE 1588 [41] and IEC 61850-5 [42] Standards are by far the most recommended and used practices for the transmission of reference times over wired communication infrastructures. However, these techniques show some limitations. In particular, if there is no suitable communications network, substantial investments are required for their implementation. Moreover, in rural areas the deployment of a wiring infrastructure can be almost impossible.

Therefore, this thesis proposes a novel analytical method for assessing the phase difference between the voltages at different nodes of a distribution power network. The main features of such a method

are that no global time reference is required for the units deployed in the field and that the accuracy in the measurement of the phase difference of the voltages at nodes is equivalent to that gauged by using existent technologies. It only requires that voltages and currents in each node of the network are simultaneously acquired with high accuracy. Nevertheless, the measurements at different nodes are performed asynchronously.

The very high accuracy required for the time stamp measurement in the present PMUs is turned into the requirement of having very high accuracy in the amplitude measurements. In other words, high accuracy requirements in the time domain have been moved into high accuracy requirements in the amplitude domain.

In scientific literature, only one application of unsynchronized measurement of phasors in power networks has been found [5]. In that paper, the authors iteratively determine the state of the network by means of the so-called augmented matrix approach. In contrast, several papers (see e.g. [44-51]) exploit unsynchronized measurements to tackle fault location issues.

The research [52] is structured as follows: in Section 4.2.1.2 the method is presented; in Section 4.2.1.3 provides a numerical example to show the performance of the proposed technique; Section 4.2.1.4 consists of comments and conclusion.

4.2.1.2 The approach

- Theoretical background: electric line modelling

Let us briefly recall how an electric line is modeled. As it is well known, an elementary portion of length dl of a single-wire line is usually represented as shown in Fig. 4.25, where r , l , c and g are the resistance, inductance, capacitance and conductance per unit length, respectively.

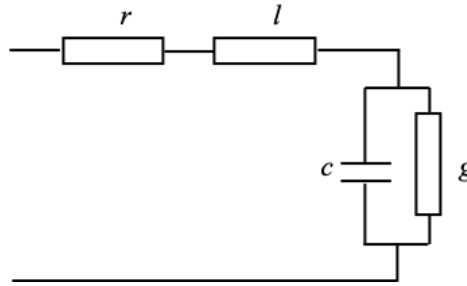


Fig. 4.25. Model of an elementary portion of a single-wire line

The line equations are:

$$\frac{d\bar{V}}{dx} = -\bar{z}\bar{I} \quad (4.13)$$

$$\frac{d\bar{I}}{dx} = -\bar{y}\bar{V} \quad (4.14)$$

where \bar{V} and \bar{I} are the phasor of voltage and current, respectively, x is the distance and:

$$\bar{z} = r + j\omega l \quad (4.15)$$

$$\bar{y} = g + j\omega c, \quad (4.16)$$

being ω the rated angular frequency.

For medium voltage cable lines, the effect of g is typically negligible.

By deriving (4.13) and (4.14) versus x , the following 2nd order differential equations are obtained:

$$\frac{d^2\bar{V}}{dx^2} = \bar{z}\bar{y}\bar{V} \quad (4.17)$$

$$\frac{d^2\bar{I}}{dx^2} = \bar{z}\bar{y}\bar{I} \quad (4.18)$$

By defining the propagation constant $\bar{\gamma}$, the characteristic impedance \bar{Z}_c and the characteristic admittance \bar{Y}_c as follows:

$$\bar{\gamma} = \sqrt{\bar{z}\bar{y}} \quad (4.19)$$

$$\bar{Z}_c = \sqrt{\frac{\bar{z}}{\bar{y}}} \quad (4.20)$$

$$\bar{Y}_c = \sqrt{\frac{\bar{y}}{\bar{z}}}, \quad (4.21)$$

the solutions of (4.17) and (4.18) can be written as:

$$\bar{V} = \bar{V}_1 \cosh(\bar{\gamma}x) - \bar{Z}_c \bar{I}_1 \sinh(\bar{\gamma}x) \quad (4.22)$$

$$\bar{I} = -\bar{Y}_c \bar{V}_1 \sinh(\bar{\gamma}x) + \bar{I}_1 \cosh(\bar{\gamma}x), \quad (4.23)$$

where \bar{V}_1 and \bar{I}_1 are the voltage and current phasors at the beginning of the line ($x=0$).

Equations (4.22) and (4.23) suggest that a distributed parameters single-wire line of given length ℓ can be represented by means of a two-port model defined by the following equation:

$$\begin{bmatrix} \bar{V}_2 \\ \bar{I}_2 \end{bmatrix} = \begin{bmatrix} \bar{A} & -\bar{B} \\ -\bar{C} & \bar{A} \end{bmatrix} \begin{bmatrix} \bar{V}_1 \\ \bar{I}_1 \end{bmatrix}, \quad (4.24)$$

where \bar{V}_2 and \bar{I}_2 are the voltage and current phasors at the end of the line ($x=\ell$) and:

$$\bar{A} = \cosh(\bar{\gamma}\ell) \quad (4.25)$$

$$\bar{B} = \bar{Z}_c \sinh(\bar{\gamma}\ell) \quad (4.26)$$

$$\bar{C} = \bar{Y}_c \sinh(\bar{\gamma}\ell) \quad (4.27)$$

Therefore, the line can be modeled by means of a T circuit (Fig. 4.26) as well as a Π one.

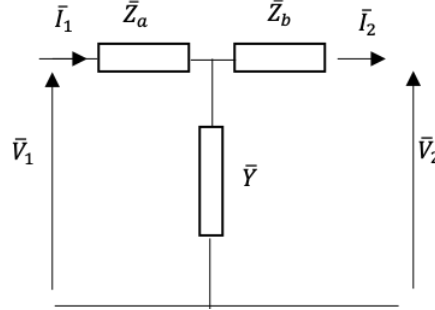


Fig. 4.26. T-circuit representation of a single-wire line

In the former case, which is the representation used in this study, the impedances depicted in Fig. 4.26 have the following expressions:

$$\bar{Z}_a = \bar{Z}_b = \frac{\bar{A}-1}{\bar{C}} \quad (4.28)$$

$$\bar{Y} = \bar{C} \quad (4.29)$$

- Procedure

As mentioned in the introduction, the main goal of this research is to estimate the phase difference between the voltage \bar{V}_1 at the beginning of the line, taken as reference and the voltage \bar{V}_2 at the end of the line without using synchronized measurements (Fig. 4.27).



Fig. 4.27. Single-wire line topology

Such phase difference is caused by the combined effect of both the line (according to its model shown in Fig. 4.26) and the equivalent impedance \bar{Z}_L of the load connected at the end of line. The lack of synchronization does not allow to write a sufficient number of independent equations to determine all three unknown parameters (\bar{Z}_L , $\bar{Z}_a = \bar{Z}_b$, \bar{Y}) of such a circuit. Therefore, the proposed method relies on a different model, shown in Fig. 4.28, whose parameters are computed in a such a way that line losses as well as the active powers at nodes 1 and 2 are the same as the actual ones.

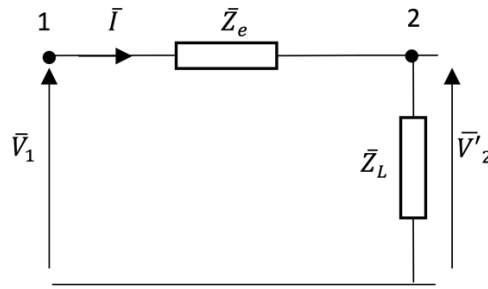


Fig. 4.28. Representation of a single-wire line and its load used in the proposed approach

As a matter of fact, active power is an integral quantity computed over one (or more) cycles and its value at such nodes is independent of the synchronization of its measurements. Of course, this holds only if the power system is in steady-state conditions for just one cycle in each node.

The following describes the procedure for estimating the searched phase difference. To this purpose, let us denote by $\Delta\varphi_a$ the actual value of such a phase difference and by $\Delta\varphi_e$ the related estimate provided by the approach.

First of all, the couples of phasors \bar{V}_1 and \bar{I}_1 , \bar{V}_2 and \bar{I}_2 must be measured. In each measurement node, voltage and current are simultaneously acquired, so that the relationship between the phasors of each couple is correct. Of course, due to the lack of synchronization, the phase difference between \bar{V}_1 and \bar{V}_2 is $\Delta\varphi_a + \delta$, where δ is a random angle depending on the random time difference between the acquisition of the two couples of phasors.

With reference to the circuit in Fig. 4.28, the following system of equations can be written:

$$\begin{cases} P'_2 = \text{Re} \left(\frac{|\bar{V}'_2|^2}{\bar{Z}'_L} \right) \\ \bar{V}'_2 = \bar{V}_1 \frac{\bar{Z}_L}{\bar{Z}_L + \bar{Z}_e} \end{cases}, \quad (4.30)$$

where P'_2 is the active power at the node 2 of such a circuit. The requirements about the equivalence in terms of active power between the circuit of Fig. 4.26 and Fig. 4.28 leads, as stated above, to $P'_2 = P_2$, which is known from the measurements of \bar{V}_2 and \bar{I}_2 . The above measurements allow also to determine the actual value of \bar{Z}_L :

$$\bar{Z}_L = \frac{\bar{V}_2}{\bar{I}_2} \quad (4.31)$$

Under the assumption of same line losses in the actual as well as in the proposed circuit, the resistive part R_e of the equivalent impedance \bar{Z}_e of Fig. 4.28 can be easily determined:

$$R_e = 2 \frac{P_1 - P_2}{I_1^2 + I_2^2}, \quad (4.32)$$

where P_1 and P_2 are the active powers measured at nodes 1 and 2, respectively and I_1 and I_2 are the RMS values of the above defined current phasors.

Now the system (4.30) can be solved to find the reactive part X_e of \bar{Z}_e . Some manipulations, reported in appendix, lead to the following 2nd order equation:

$$X_e^2 + 2X_e X_L + d = 0 \quad (4.33)$$

where X_L is the reactive part of \bar{Z}_L and:

$$d = |\bar{Z}_L|^2 - \frac{|\bar{V}_1|^2 |\bar{Z}_L|^2}{P_2} \operatorname{Re} \left\{ \frac{1}{\bar{Z}_L^*} \right\} + R_e \bar{Z}_L^* + R_e \bar{Z}_L + R_e^2 \quad (4.34)$$

One of the solutions of (4.33) is always negative if, as it is usual, the power factor of \bar{Z}_L is lagging.

Finally, \bar{V}_2' can be determined along with the phase difference $\Delta\varphi_e$, with respect to \bar{V}_1 by means of the second equation of (4.30). Fig. 4.29 summarizes the above described procedure.

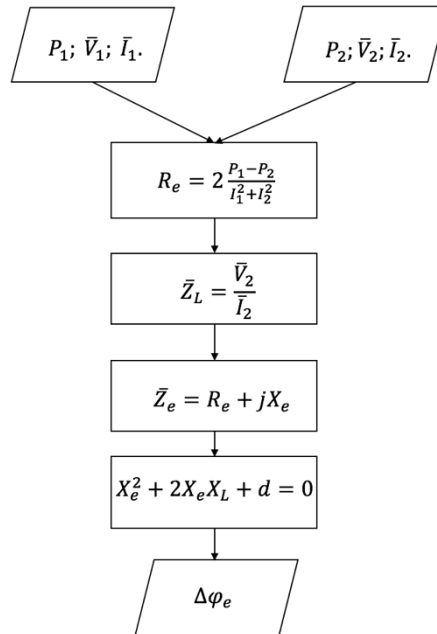


Fig. 4.29. Procedure for estimating the phase difference $\Delta\varphi_e$ between \bar{V}_1 and \bar{V}_2'

4.2.1.3 Numerical example

This section provides a numerical example of the proposed procedure. Three typical medium voltage single-wire cables with different cross-sections (50 mm², 95 mm², and 240 mm²) have been chosen. Each cable features the per-unit length parameters shown in Table 4.29, where r , c , and l have the same meaning as described in subsection 4.2.1.2.

Table 4.29. Per unit length parameters for the three types of cable.

S (mm ²)	r (mΩ/m)	l (uH/m)	c (nF/m)
50	0.587	0.4138	0.21
95	0.193	0.3694	0.26
240	0.0754	0.324	0.37

Different cable lengths, representative of typical distance between medium voltage nodes (5000 m, 7500 m, and 10000 m), have been considered.

For each combination of cable cross-section and length, the equivalent T-circuit of Fig. 4.26 has been solved by considering different loads. In particular, all loads have been given 0.8 power factor and apparent power S_L ranging from 500 kVA to 8 MVA. The specific values are reported in the following Tables. The solution of such a circuit provided the reference phase difference $\Delta\varphi_a$ between \bar{V}_1 and \bar{V}_2 .

The proposed procedure has been then applied to the data obtained from the above simulations to estimate the phase difference $\Delta\varphi_e$ between \bar{V}_1 and \bar{V}_2 .

Tables II, III and IV show the results for different lengths when the cable section is 50 mm². Table V, VI and VII refer to the 95 mm² case and, lastly, Table VIII, IX and X deal with the 240 mm² cable. As expected, the longer is the cables the larger is the phase difference between the phasors measured at the two nodes of the line. This fact is confirmed also by the results. In fact, shown for the 50 mm² cable in Tables 4.30, 4.31, and 4.32, $\Delta\varphi_a$ values with a 500 kVA load are 2.06, 2.85, 3.47 mrad, for a 5000, 7500, 10000 m cable, respectively.

Table 4.30. Actual and Estimated voltage phase difference for different loads in a 5000 m length, 50 mm² section cable

S_L (kVA)	$\Delta\varphi_a$ (mrad)	$\Delta\varphi_e$ (mrad)	$\Delta\varphi_a - \Delta\varphi_e$ (mrad)
500	2.06	2.53	0.46
1000	4.42	4.88	0.45
1500	6.74	7.20	0.45
2000	9.03	9.48	0.45
4000	17.86	18.32	0.45
8000	34.14	34.59	0.44

Table 4.31. Actual and Estimated voltage phase difference for different loads in a 7500 m length, 50 mm² section cable

S_L (kVA)	$\Delta\varphi_a$ (mrad)	$\Delta\varphi_e$ (mrad)	$\Delta\varphi_a - \Delta\varphi_e$ (mrad)
500	2.85	3.89	1.03
1000	6.35	7.38	1.03
1500	9.77	10.80	1.03
2000	13.12	14.15	1.03
4000	25.84	26.86	1.02
8000	48.44	49.44	1.00

Table 4.32. Actual and Estimated voltage phase difference for different loads in a 10000 m length, 50 mm² section cable

S_L (kVA)	$\Delta\varphi_a$ (mrad)	$\Delta\varphi_e$ (mrad)	$\Delta\varphi_a - \Delta\varphi_e$ (mrad)
500	3.47	5.31	1.84
1000	8.09	9.93	1.83
1500	12.58	14.41	1.83
2000	16.94	18.77	1.82
4000	33.26	35.07	1.81
8000	61.22	63.00	1.78

The same tables also present the estimated phase difference and the estimation error in the right-hand column. The absolute value of such an error is almost constant versus the load value. The larger the line length, the larger is the error. Same consideration applies for the other line cross sections. In case of 2 MVA load and 7500 m cable, for all three sections, Tables 4.31, 4.34, and 4.37 show that the

error decreases with the increase of the cable cross section. In particular, it is 1.03, 0.79, 0.67 mrad for a 50, 95, 240 mm² cable, respectively. It can be concluded that the proposed procedure features better performance in case of shorter lines (due to the smallest phase displacements involved), higher cross-section and in presence of high loaded lines. It must be highlighted that such errors are well acceptable for PMU applications. In fact, typical actual phase displacements in the DSMS systems are in the order of few mrad.

Table 4.33. Actual and Estimated voltage phase difference for different loads in a 5000 m length, 95 mm² section cable

S_L (kVA)	Δφ_a (mrad)	Δφ_e (mrad)	Δφ_a - Δφ_e (mrad)
500	0.23	0.58	0.35
1000	0.65	1.00	0.35
1500	1.08	1.43	0.35
2000	1.49	1.85	0.35
4000	3.13	3.48	0.34
8000	6.26	6.60	0.34

Table 4.34. Actual and Estimated voltage phase difference for different loads in a 7500 m length, 95 mm² section cable

S_L (kVA)	Δφ_a (mrad)	Δφ_e (mrad)	Δφ_a - Δφ_e (mrad)
500	0.20	0.99	0.79
1000	0.83	1.62	0.79
1500	1.46	2.25	0.79
2000	2.08	2.87	0.79
4000	4.48	5.27	0.78
8000	8.97	9.73	0.76

Table 4.35. Actual and Estimated voltage phase difference for different loads in a 10000 m length, 95 mm² section cable

S_L (kVA)	Δφ_a (mrad)	Δφ_e (mrad)	Δφ_a - Δφ_e (mrad)
500	0.69	1.485	1.415
1000	0.914	2.325	1.411
1500	1.744	3.151	1.406
2000	2.561	3.963	1.402
4000	5.700	7.084	1.384
8000	11.420	12.771	1.351

Table 4.36. Actual and Estimated voltage phase difference for different loads in a 5000 m length, 240 mm² section cable

S_L (kVA)	Δφ_a (mrad)	Δφ_e (mrad)	Δφ_a - Δφ_e (mrad)
500	-0.77	-0.46	0.30
1000	-1.43	-1.13	0.30
1500	-2.09	-1.43	0.30
2000	-2.75	-2.44	0.30
4000	-5.34	-5.04	0.29
8000	-10.39	-10.10	0.28

Table 4.37. Actual and Estimated voltage phase difference for different loads in a 7500 m length, 240 mm² section cable

S_L (kVA)	Δφ_a (mrad)	Δφ_e (mrad)	Δφ_a - Δφ_e (mrad)
500	-1.24	-0.55	0.68
1000	-2.23	-1.54	0.68
1500	-3.21	-2.53	0.67
2000	-4.18	-3.51	0.67
4000	-8.02	-7.35	0.67
8000	-15.40	-14.75	0.65

Table 4.38. Actual and Estimated voltage phase difference for different loads in a 10000 m length, 240 mm² section cable

S_L (kVA)	Δφ_a (mrad)	Δφ_e (mrad)	Δφ_a - Δφ_e (mrad)
500	-1.76	-0.54	1.21
1000	-3.07	-1.86	1.21
1500	-4.38	-3.17	1.20
2000	-5.67	-4.46	1.20
4000	-10.71	-9.54	1.17
8000	-20.30	-19.16	1.14

4.2.1.4 Final remarks

Numerical results have shown the effectiveness of the proposed approach for evaluating the phase difference between voltages at different nodes of a power network. Note that according to the presented approach the measurement of the voltage phasors can be accomplished by using power and energy meters. The major advantage of the proposed procedure and architecture is that measurements can be performed asynchronously and without using a global time reference. It leads to a simpler and less expensive measurement architecture. This way a larger deployment of instrumentation can be scheduled with benefits in terms of enhanced network observability (mainly in presence of DG), redundancy and, finally, more accurate measurements. The need for highly accurate measurements of time has been converted into the requirement of having very high accuracy in the amplitude measurements. High accuracy requirement in the time domain has been then moved into two main requirements: i) high accuracy in amplitude measurements and ii) narrow time-skew between voltage and current measurements of each energy meter. Hence, accuracy and uncertainty are now related to the measuring instrument; the latency in the time reference transmission will not lead to greater impact on the phase difference measurements.

One of main requirements of the presented approach is that during the period of time in which measurements at all nodes are performed, the system should be assumed under steady state conditions. This constraint is not particularly heavy for the method as the measurements at all nodes can, for instance, be performed starting from the zero crossing of the voltages. In this way all measurements will be performed in the same period of time at all nodes. The only difference in time is represented by the time delay due to the network topology (line impedances and loads). In particular, the method will not be affected by the actual phenomenon of changing network frequency over time, as all expressions would be evaluated for all nodes under the same operating conditions. Therefore, even one of the most useful parameters measured by PMU for the identification of the network stability, the Rate Of Change Of Frequency, can be measured by means of the presented approach.

However, keep in mind that accuracy in measurement of electrical quantities (voltages and currents) represents the most important requirements for this method for successful operations. As underlined in the introduction, the uncertainty in the measurements turns into an uncertainty in the phase difference between voltages.

4.2.1.5 Appendix

This Section shows the solution of the system (4.30) in Section II, below rewritten as (4.35):

$$\begin{cases} P'_2 = Re \left(\frac{|\bar{V}'_2|^2}{\bar{Z}_L^*} \right) \\ \bar{V}'_2 = \bar{V}_1 \frac{\bar{Z}_L}{\bar{Z}_L + \bar{Z}_e} \end{cases} \quad (4.35)$$

As described in the paper and according to Fig. 4.28, the estimated active power P'_2 must be equal to the actual active power P_2 measured at the second node of the line, hence:

$$P'_2 = Re \left(\frac{|\bar{V}'_2|^2}{\bar{Z}_L^*} \right) = P_2 \quad (4.36)$$

Remembering that the real part of the product between two complex numbers is:

$$Re(\bar{a}\bar{b}) = a_R b_R - a_I b_I \quad (4.37)$$

where the subscripts R and I indicate the real part and the imaginary coefficient of the complex numbers, respectively. By applying the (4.37) to the (4.36) and knowing that $|\bar{V}'_2|^2$ is real:

$$P_2 = Re \left(\frac{1}{\bar{Z}_L^*} \right) \cdot |\bar{V}'_2|^2 - 0 \quad (4.38)$$

By substituting the second of the (4.30) into the (4.38):

$$P_2 = Re \left(\frac{1}{\bar{Z}_L^*} \right) \cdot \left| \bar{V}_1 \frac{\bar{Z}_L}{\bar{Z}_L + \bar{Z}_e} \right|^2 = Re \left(\frac{1}{\bar{Z}_L^*} \right) \cdot \frac{|\bar{V}_1|^2 |\bar{Z}_L|^2}{|\bar{Z}_L + \bar{Z}_e|^2} \quad (4.39)$$

The variable X_e is contained into \bar{Z}_e and then it must be extracted from the (4.39):

$$|\bar{Z}_L + \bar{Z}_e|^2 = Re \left(\frac{1}{\bar{Z}_L^*} \right) \cdot \frac{|\bar{V}_1|^2 |\bar{Z}_L|^2}{P_2} \quad (4.40)$$

Given that all the terms in the right side of (4.40) are known, for sake of brevity they can be named as:

$$F = Re \left(\frac{1}{\bar{Z}_L^*} \right) \cdot \frac{|\bar{V}_1|^2 |\bar{Z}_L|^2}{P_2} \quad (4.41)$$

By arranging terms into (4.40) it holds:

$$\begin{aligned} |\bar{Z}_L + \bar{Z}_e|^2 &= (\bar{Z}_L + \bar{Z}_e)(\bar{Z}_L^* + \bar{Z}_e^*) = \\ &= |\bar{Z}_L|^2 + |\bar{Z}_e|^2 + \bar{Z}_L \bar{Z}_e^* + \bar{Z}_L^* \bar{Z}_e = F \end{aligned} \quad (4.42)$$

Equation (4.42) does not have a single solution because it contains two variables: R_e and X_e . However, as stated above, the equivalent resistance of the line is evaluated in a previous step; therefore in (4.41) it is a known term.

$$|R_e + jX_e|^2 + \bar{Z}_L(R_e - jX_e) + \bar{Z}_L^*(R_e + jX_e) + |\bar{Z}_L|^2 = F \quad (4.43)$$

After some arrangements:

$$R_e^2 + X_e^2 - jX_e(\bar{Z}_L - \bar{Z}_L^*) + H = 0 \quad (4.44)$$

where:

$$H = |\bar{Z}_L|^2 + \bar{Z}_L R_e + \bar{Z}_L^* R_e - F \quad (4.45)$$

Finally (4.44) leads to the expression (4.33) written in Section II:

$$X_e^2 + 2X_e X_L + d = 0 \quad (4.46)$$

Now, with the reduced quadratic equation expression the two solution of the (4.46) can be obtained:

$$X_{e1,2} = -X_L \pm \sqrt{X_L^2 - d} \quad (4.47)$$

$$X_{e1} = -X_L + \sqrt{X_L^2 - d} \quad (4.47a)$$

$$X_{e2} = -X_L - \sqrt{X_L^2 - d} \quad (4.47b)$$

From (4.47a) and (4.47b) it can be stated that, while the reactive part of a line is inductive, the (4.47b) is always negative and can be discarded. This way the solution of the quadratic equation (4.46) is unique.

4.2.2 Uncertainty analysis of an equivalent synchronization method for phasor measurements

4.2.2.1 Introduction

With the transition from traditional electric grids to Smart Grids, the distribution network is the portion of grids that sees the biggest number of changes, in the transmission and the low voltage networks. In accordance with the definition of Smart Grid [1], a power network is a grid where all nodes are connected to each other and communicate in order to establish, in real time, the state of the network. A major contribution to this modification is established by Distributed Generation, which has completely changed the traditional power flow: before DG, the power flowed only from power plants to end users, while now every user can become a minor energy supplier with his own electrical system (prosumer). As expected, such transformation of the distribution network has not spared the measurement instruments for the monitoring of the network. In Section 4.2.1 above, the role of the PMUs has been introduced for distribution and transmission networks. However, the intention to extend the usage of the PMUs also in the distribution network, already addressed in literature [53-55], presents some critical issues. These are the major concerns:

- in transition to Smart Grids, the power network has to be widely monitored, but the cost of PMUs does not allow their large-scale implementation;
- PMU accuracy in measuring the phase displacement is acceptable for the transmission network, but not suitable for the distribution network. Here, the grid lines are shorter and less loaded than in the transmission network, resulting in smaller phase displacements between the phase of the voltages;
- the time reference, required so a PMU can synchronize its measurements, often cannot be provided due to its location. For example, in urban areas, skyscrapers and trees prevent the GPS signal from reaching the antennas.

For these reasons, the study [52] presents a method to obtain an equivalent synchronization between the voltage phasors of two nodes of a MV distribution network (either made of cables or overhead lines), based on asynchronous measurements. In particular, the methods rely on a distributed measurement system where each remote unit is a simple power meter, which is much less expensive than a PMU and hence more affordable for Distribution System Operators (DSOs). Therefore, there is no need to provide a global time reference to all instruments.

Overall, the methods presented here and in [52] are not aimed at substituting PMUs, which are a key measuring device for transmission networks. Moreover, such methods work in specific grid sections, different from those where the PMUs are installed. However, it is not excluded that PMUs and the methods above can be used together with the aim of better monitoring the power networks.

In this research, the approach presented in [52] is firstly extended to a power network configuration made by any number of nodes. Following that, this thesis presents an equivalent synchronization monitoring only 75% of the nodes to reduce the number of the remote units.

To my best knowledge, this topic has been tackled for a different purpose in [43], where the authors iteratively determine the state of the network formulated by means of the so-called augmented matrix approach.

This chapter is organized as follows: Section 4.2.2.2 summarizes the line modeling and the procedure proposed in [52]; Section 4.2.2.3 recalls the proposed approaches for more complex power network configurations from [56]. Section 4.2.2.4 contains a summary of the results of the methods proposed in [56], while Section 4.2.2.5 describes a set-up that can be used for implementing these methods for synchronizing phasor measurements. Section 4.2.2.6 presents some numerical examples and discusses them in detail. Lastly, conclusion and final remarks are stated in Section 4.2.2.7.

4.2.2.2 Line modelling: PI-section line schematization

In this study, a PI-section line schematization has been adopted as done in the majority of the studies. Starting from the following line equations (4.48) and (4.49):

$$\frac{d\bar{v}}{dx} = -\bar{z}\bar{I} \quad (4.48)$$

$$\frac{d\bar{I}}{dx} = -\bar{y}\bar{V}, \quad (4.49)$$

where \bar{V} and \bar{I} are the voltage and current phasors respectively, x is the distance and \bar{z} and \bar{y} the impedance and the admittance per-unit length respectively, the two-port model matrix is obtained:

$$\begin{bmatrix} \bar{V}_2 \\ \bar{I}_2 \end{bmatrix} = \begin{bmatrix} \bar{A} & \bar{B} \\ \bar{C} & \bar{A} \end{bmatrix} \begin{bmatrix} \bar{V}_1 \\ \bar{I}_1 \end{bmatrix} \quad (4.50)$$

In (4.50):

$$\bar{A} = \cosh(\bar{y}l) \quad (4.51)$$

$$\bar{B} = \bar{Z}_c \sinh(\bar{y}l) \quad (4.52)$$

$$\bar{C} = \bar{Y}_c \sinh(\bar{y}l), \quad (4.53)$$

where \bar{y} is the propagation constant and l the length of the portion of the considered line.

Hence, the impedances \bar{Z}_1 and \bar{Z}_2 of the PI-section line can be derived from the parameters of the two-port model matrix:

$$\bar{Z}_1 = \bar{Z}_c \frac{\sinh(\bar{y}l)}{\cosh(\bar{y}l) - 1} \quad (4.54)$$

$$\bar{Z}_2 = \bar{Z}_c \sinh(\bar{y}l) \quad (4.55)$$

With such parameters, the PI-model of an electric line can be depicted as in Fig. 4.30.

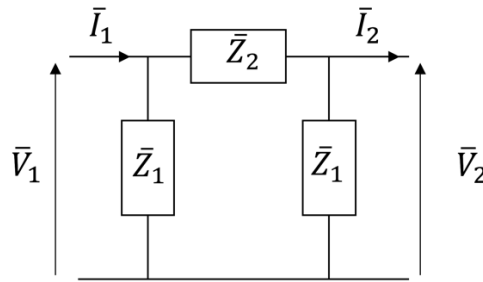


Fig. 4.30. PI-schematization of an electric line, resulting from the two-port model matrix

4.2.2.3 The proposed approaches

This Section recalls two proposed algorithms. The first one, referred to as method A, applies the algorithm presented in [52] - whose aim was to estimate the phase displacement between the voltages at the two terminals of a portion of cable - to a new power network. Given that any configuration can be divided into segments made by two nodes, such approach can be easily extended to power networks having any number of nodes. Consider the following simple, but generic example, a 4-nodes network in Fig. 4.31 below.

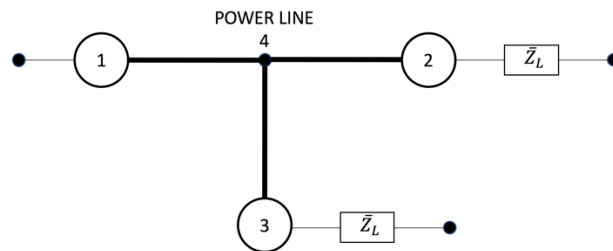


Fig. 4.31. 4-nodes power network configuration adopted for both the algorithms presented

Of course, even if a remote unit is not as expensive as a PMU, reducing the number of remote units without significantly decreasing the performance of the equivalent synchronization will be an important gain of the proposed approach. Therefore, a variant of the previous method which relies on information coming from 75 % of the network nodes has been presented and referred to as method B. This method will be subjected to the uncertainty analysis of this research.

- Method A

This subsection describes the application of method A to the power network configuration in Fig. 4.31. It is a 4-nodes network where 1 is the supply node taken as reference for phase displacement; 2 and 3 are load nodes where a typical R-L load is connected. Finally, 4 is simply a ramification node. Such a junction node, in the considered case, does not contain any kind of load. The method requires taking measurements at both terminals of all branches (as shown in Fig. 4.32). The following quantities are measured: currents phasors $\bar{I}_{14}, \bar{I}_{41}, \bar{I}_{42}, \bar{I}_{24}, \bar{I}_{43}, \bar{I}_{34}$, where the subscripts are defined as in Fig. 4.32, and the voltage phasors: $\bar{V}_1, \bar{V}_2, \bar{V}_3$ and \bar{V}_4 at the nodes 1, 2, 3 and 4, respectively.

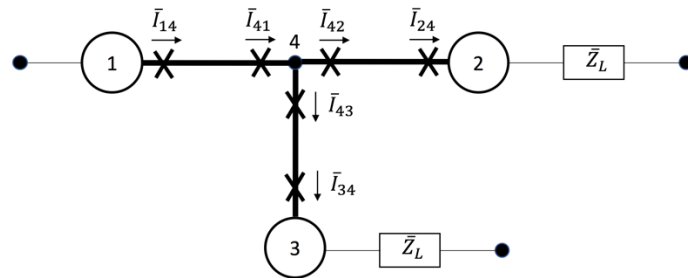


Fig. 4.32. Measurement points when applying the two terminals algorithm to the 4-nodes power network configuration

Each term of the couple of currents \bar{I}_{14} and \bar{I}_{41} , \bar{I}_{42} and \bar{I}_{24} , \bar{I}_{43} and \bar{I}_{34} , differs from its peer because of the capacitive effects of the line, and for their asynchronous acquisition. The former cause turns into a variation of both amplitude and phase of the current phasor, whereas the latter reason acts only on its phase.

According to [52], Fig. 4.33 shows the equivalent circuit for a generic branch of the network with terminals a and b , where \bar{V}_a is the phasor measured at the node a and \bar{V}_b' is the one obtained by solving such a circuit once \bar{Z}_e and \bar{Z}_L are known.

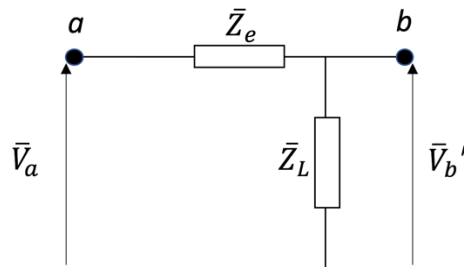


Fig. 4.33. Representation of a single-wire line and its load used in the proposed approach

The phase displacement φ_{ab}' between \bar{V}_a and \bar{V}_b' is the estimated value of the actual phase displacement φ_{ab} between \bar{V}_a and \bar{V}_b , where \bar{V}_b is the measured voltage phasor at node b . The impedance \bar{Z}_L is given by:

$$\bar{Z}_L = \frac{\bar{V}_b}{\bar{I}_{ba}} \quad (4.56)$$

where \bar{I}_{ba} is the phasor of the current measured in b and coming from a .
The real part R_e of \bar{Z}_e is:

$$R_e = 2 \frac{P_a - P_b}{I_{ab}^2 + I_{ba}^2} \quad (4.57)$$

where P_a and P_b are the active powers at nodes a and b computed from \bar{V}_a , \bar{I}_{ab} , and \bar{V}_b , \bar{I}_{ba} , respectively. The imaginary part X_e of \bar{Z}_e is obtained by solving the following system of equations:

$$\begin{cases} P'_b = Re \left(\frac{|\bar{V}_b'|^2}{\bar{Z}_L^*} \right) \\ \bar{V}_b' = \bar{V}_a \frac{\bar{Z}_L}{\bar{Z}_L + \bar{Z}_e} \end{cases}, \quad (4.58)$$

where $P'_b = P_b$.

Therefore:

$$\varphi_{ab}' = \widehat{\bar{V}}_b' - \widehat{\bar{V}}_a \quad (4.59)$$

where the symbol $\widehat{\bar{X}}$ refers to the phase of the generic phasor \bar{X} . These steps are applied to the 3 branches that form the power network, obtaining the phase displacements φ_{42}' , φ_{43}' , φ_{12}' and φ_{13}' :

$$\varphi_{42}' = \widehat{\bar{V}}_2' - \widehat{\bar{V}}_4 \quad (4.60)$$

$$\varphi_{43}' = \widehat{\bar{V}}_3' - \widehat{\bar{V}}_4 \quad (4.61)$$

so:

$$\varphi_{12}' = \varphi_{42} - \varphi_{14} \quad (4.62)$$

$$\varphi_{13}' = \varphi_{43} - \varphi_{14} \quad (4.63)$$

- **Method B**

As stated above, method B allows to determine the phase displacement among the voltage phasors of a power network:

- without any time reference;
- performing asynchronous measurements in the monitored nodes of the network;
- monitoring 75 % of the network nodes.

As in method A, this requires:

- in each monitored node, simultaneous acquisitions of voltage and current waveforms allow an easy determination of the corresponding voltage and current phasors;
- steady state condition for the time needed to acquire the above quantities (typically one cycle if waveforms are acquired at zero crossing of the voltage).

In addition, the following assumptions must be met:

- the lengths of the branches must be known;
- per-unit length reactance equal to a given value as explained in the following.

In contrast to expectations, assumptions c and d are not particularly strong. As a matter of fact, as for c , every utility has detailed maps reporting the length of all the branches of its distribution networks. For d , the variation of the reactance with the cable section is very limited, as shown in Fig. 4.34, where the values in Ω/km of the per-unit length resistance and the reactance are shown vs. the cross-section of the cable.

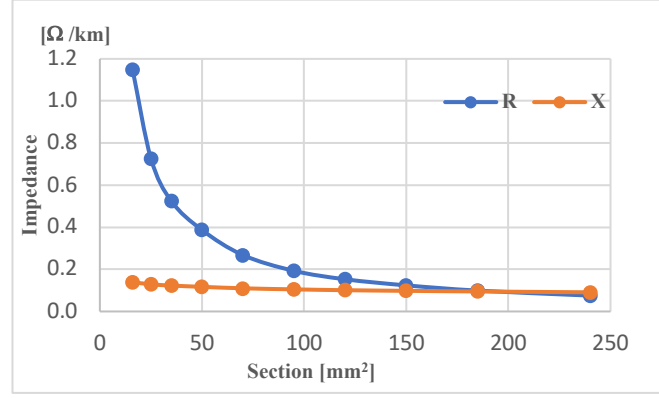


Fig. 4.34. Trend of the resistance and the reactance with respect to the cross section of a medium voltage cable (8.7-15 kV)

Data in Fig. 4.34 refers to a three-core medium voltage cable of a certain manufacturer. However, very similar values apply to cables of different producers. So, the per-unit length reactance x_{eq} of each branches of the considered network has been taken as equal to the average value of the once reported in Fig. 4.34.

In Fig. 4.31, it is assumed that nodes 1, 2 and 3 are the monitored nodes. Node 1 is also assumed as a reference for the phase displacement evaluation. For each monitored node, active powers can be computed as:

$$P_m = Re(\bar{V}_m \bar{I}_m^*) \quad (4.64)$$

where $m = 1, 2, 3$, \bar{V}_m and \bar{I}_m are the voltage and current phasors measured at node m , respectively, \bar{X}^* is the complex conjugate of the generic phasor \bar{X} .

The per-unit length line resistance of all branches is estimated as:

$$r_{eq} = \frac{\Delta P}{K_{14} I_1^2 + K_{42} I_2^2 + K_{43} I_3^2} \quad (4.65)$$

where:

$$\Delta P = P_1 - P_2 - P_3 \quad (4.66)$$

is the total amount of power losses in the network and K_{14} , K_{42} and K_{43} are the coefficients which express the length in kilometers of branches 1-4, 4-2 and 4-3, respectively.

Therefore, the per-unit length equivalent impedance \bar{z}_{eq} of all the branches of the considered network is:

$$\bar{z}_{eq} = r_{eq} + jx_{eq} \quad (4.67)$$

that leads to the following impedances \bar{Z}_{14} , \bar{Z}_{42} and \bar{Z}_{43} of branches 1-4, 4-2 and 4-3, respectively:

$$\bar{Z}_{14} = K_{14} \bar{z}_{eq} \quad (4.68)$$

$$\bar{Z}_{42} = K_{42} \bar{z}_{eq} \quad (4.69)$$

$$\bar{Z}_{43} = K_{43} \bar{z}_{eq} \quad (4.70)$$

The unknown voltage phasor \bar{V}_4' in node 4 is estimated as:

$$\bar{V}_4' = \bar{V}_1 - \bar{Z}_{14} \bar{I}_1 \quad (4.71)$$

This way, \bar{V}_2 and \bar{V}_3 can be resynchronized to \bar{V}_4' (and hence \bar{V}_1) by computing their estimate \bar{V}_2' and \bar{V}_3' :

$$\bar{V}_2' = \bar{V}_4' - \bar{Z}_{42} \bar{I}_2 \quad (4.72)$$

$$\bar{V}_3' = \bar{V}_4' - \bar{Z}_{43} \bar{I}_3 \quad (4.73)$$

Finally, the searched phase displacements φ_{12}' and φ_{13}' are:

$$\varphi_{12}' = \widehat{V}_2' - \widehat{V}_1 \quad (4.74)$$

$$\varphi_{13}' = \widehat{V}_3' - \widehat{V}_1 \quad (4.75)$$

4.2.2.4 Simulations results

The aim of this section is to recall and discuss the results presented in [56]. Several power network configurations have been simulated, by using the Simulink tool of Matlab 2017a, to evaluate and compare the performance of the models on which methods A and B rely on. Four examples with different lengths of branches and same cross section of 95 mm² have been studied. In each example, three different combinations of the loads connected to the nodes 2 and 3 have been considered. Table 4.39 lists the lengths K_{14} , K_{42} and K_{43} of the branches 1-4, 4-2 and 4-3, respectively, for cases #1, #2, #3 and #4. The performance of the methods has been evaluated by comparing the actual phase displacements (as obtained by the simulations) φ_{12} and φ_{13} with the values provided by the presented methods.

Table 4.39. Lengths of the branches in the different considered cases

Case	K_{14} [km]	K_{42} [km]	K_{43} [km]
#1	1	1	1
#2	3	2	1
#3	4	4	2
#4	8	5	4

Tables 4.40 and 4.41 compare methods A and B (results taken from [56]). Such tables show, for cases #1 and #4, the phase errors $\Delta\varphi_{12}$ and $\Delta\varphi_{13}$ with respect to φ_{12} and φ_{13} . In Tables 4.40 and 4.41, S_{L2} and S_{L3} refer to the apparent power of the loads connected to the nodes 2 and 3, respectively. that the results show, in addition to observations in [56], the equivalent performance of the two methods, although in the worst case, featuring the longest and highest loaded line, method B loads to a larger error than in method A.

Table 4.40. Actual phase displacements among the nodes φ_{ij} and phase errors $\Delta\varphi_{ij}$ introduced by the two methods, for the Case #1 and for different loads

		Actual phase displacements		Method A		Method B	
S_{L2} (MVA)	S_{L3} (MVA)	φ_{12} (mrad)	φ_{13} (mrad)	$\Delta\varphi_{12}$ (mrad)	$\Delta\varphi_{13}$ (mrad)	$\Delta\varphi_{12}$ (mrad)	$\Delta\varphi_{13}$ (mrad)
0.4	0.8	0.17	0.17	-0.07	-0.13	0.1	0.17
1	1	0.17	0.17	-0.16	-0.16	0.26	0.26
2	1.5	0.52	0.52	-0.47	-0.45	0.39	0.3

Table 4.41. Actual phase displacements among the nodes φ_{ij} and phase errors $\Delta\varphi_{ij}$ introduced by the two methods, for the Case #4 and for different loads

		Actual phase displacements		Method A		Method B	
S_{L2} (MVA)	S_{L3} (MVA)	φ_{12} (mrad)	φ_{13} (mrad)	$\Delta\varphi_{12}$ (mrad)	$\Delta\varphi_{13}$ (mrad)	$\Delta\varphi_{12}$ (mrad)	$\Delta\varphi_{13}$ (mrad)
0.4	0.8	0.17	0.17	0.53	0.36	0.85	0.88
1	1	0.17	0.17	-0.27	-0.33	1.48	1.28
2	1.5	0.52	0.52	-1.22	-1.12	3	2.6

These observations led authors to focus the uncertainty analysis on method B, since it provides the equivalent synchronization of the phasors with a network observability of 75 % (which corresponds to use only 75 % of the instruments required in method A). This leads to two different kinds of benefits: first, with the same number of instruments a larger area can be monitored; second, given the area, the measurement system will become less expensive than in method A.

The following Section only considers method B for the uncertainty analysis. Method B is recommended for future in-field implementations as it is less expensive than Method A, while offering the same performance.

4.2.2.5 Measurement setup

This section introduces a measurement set-up for applying method B. This set-up is just hypothetical example, but could be common in future in-field applications. The method relies on the measurements provided by a WAMS (Wide Area Monitoring System), as illustrated in Fig. 4.35.

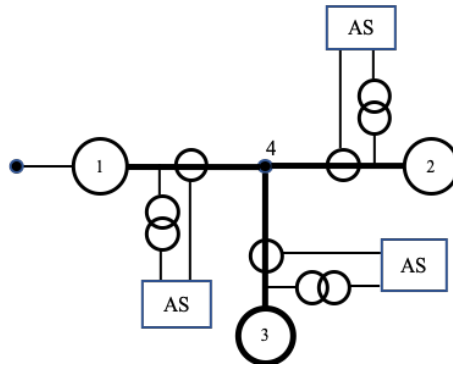


Fig. 4.35. Suggested measurement set-up and Acquisition System (AS) applied on the 4-nodes power network configuration

The common measurement instruments used for acquiring synchronized voltage and current phasors at the nodes of a power network are usually the PMUs, but the remote units of such a WAMS will not have any global time reference provided by typical communication protocols. Therefore, in order to reduce the costs, energy meters already installed in the network can be used in such a case. On this aspect, studies show several distributed measurements systems used for network monitoring and diagnostic: for instance, for fault location caused by internal or external sources [57-59], or for monitoring periodic disturbances [60, 61].

According to Fig. 4.35, a remote unit is placed in every measurement node (a set of ITs). Each unit consists of the following main elements:

- current and voltage transformers. The transformers could be both inductive transformers or low power instrument transformers. For the simulation activities, only the accuracy class is needed, otherwise there is no difference between the two;
- an acquisition system, which features simultaneous sampling (to reduce any additional phase error) as well as a Phase Locked Loop (PLL) system with the aim of neglecting the effects of the leakage phenomenon. For the acquisition system, an accuracy of $\pm 0.1\%$ is assumed, which considers all effects such as non-linearity, noise, gain, and quantization. An accuracy of 0.1% is about twice the value usually required in specifications for electrical utilities [62].

Current and voltage phasors are transmitted to a main unit via communication protocols (IEC 61850, DNP3, etc.), whose description is outside the scope of this research. Still, the latency of these protocols will not affect the method, because it does not require any synchronization and assuming the steady state condition of the network. The control unit, which collects all data coming from the different remote units, evaluates the phase displacement $\Delta\varphi_{1j}$ between the voltage phasors at nodes 1 and j , respectively. It is performed by applying the method B, as stated in previous Section. All phase displacements are computed with respect to node 1, that has been chosen as reference for the sake of simplicity without loss of generality.

4.2.2.6 Numerical examples

This section provides uncertainty analysis of method B along with presenting some numerical examples.

First of all, recall some information about the Monte Carlo method applied for uncertainty analysis. According to GUM and its Supplement 1 [21, 22], the result Y of a measurement is a random variable, being a function f of the input quantities X_i assumed as random variables. However, whenever the function f cannot be easily expressed, as in the case under study, an analytical approach would result in a very tough and complex task. Supplement I of GUM, which describes how to correctly apply MCM to a complex measurement function, is more suitable and effective. By following rules in this Standard, 100,000 iterations have been chosen for running MCM.

The effects of three main sources of uncertainty have been deeply analyzed:

- the accuracy of instrument transformers installed in the remote units;
- the lack of knowledge on the length of the branches K_{14}, K_{42}, K_{43} , which turns into an uncertainty on all the quantities $(\bar{Z}_{14}, \bar{Z}_{42}, \bar{Z}_{43})$, which depend on them;
- the lack of knowledge on the per-unit length reactance of line cables, which turn into an uncertainty on the assumed value x_{eq} .

These three effects together with the effects on uncertainty introduced by the acquisition system have been considered as random variables used to run a MCM trial. After that, an in-depth analysis has been carried out considering each time only one of the three sources of uncertainty, neglecting the others, to assess the single contribution to the overall uncertainty.

- Instrument Transformers

As expected, the contribution of the ITs in the combined uncertainty budget is generally predominant to other different sources. The first test out consists of the evaluation of uncertainty on $\Delta\varphi_{12}$ and $\Delta\varphi_{13}$, by considering only the contributions by the ITs. Such contributions have been assessed by considering typical accuracy classes for this type of instruments, 0.1-0.2-0.5. Each class defines a maximum value for the ratio error and the phase error for the ITs. Table 4.42 lists such values.

Table 4.42. Ratio errors and phase errors for CT and VT.

Accuracy Class	ϵ_{CT} (%)	ϵ_{VT} (%)	$\Delta\varphi_{CT}$ (crad)	$\Delta\varphi_{VT}$ (crad)
0.1	0.1	0.1	0.15	0.15
0.2	0.2	0.2	0.3	0.3
0.5	0.5	0.5	0.9	0.6

In Fig. 4.36, the amplitude of the 95 %-confidence interval of the phase displacement $\Delta\varphi_{12}$ is plotted vs. the accuracy class of the ITs.

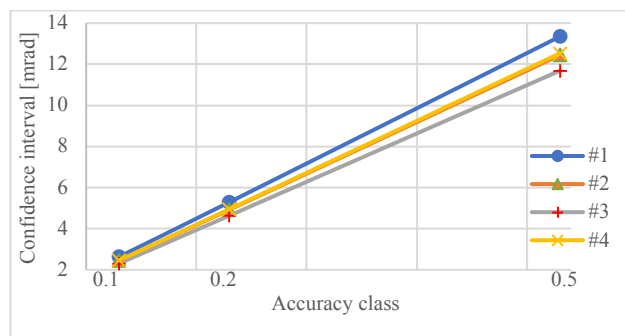


Fig. 4.36. Amplitude (mrad) of the 95% confidence interval of the phase displacement $\Delta\varphi_{12}$, considering only the effect of ITs with respect to the different accuracy classes, for the 4 analyzed cases

For the sake of simplicity, but without loss of generality, the same accuracy class has been used for both voltage and current transformers. Different markers refer to cases #1, #2, #3 and #4 as defined in Table 4.39. The plotted results are obtained when $S_{L2} = 2$ MVA and $S_{L3} = 1.5$ MVA.

However, similar graphs can be drawn also for other combinations of S_{L2} and S_{L3} . Similarly, 95 %-confidence interval for the phase displacement $\Delta\varphi_{13}$ is shown in Fig. 4.37.

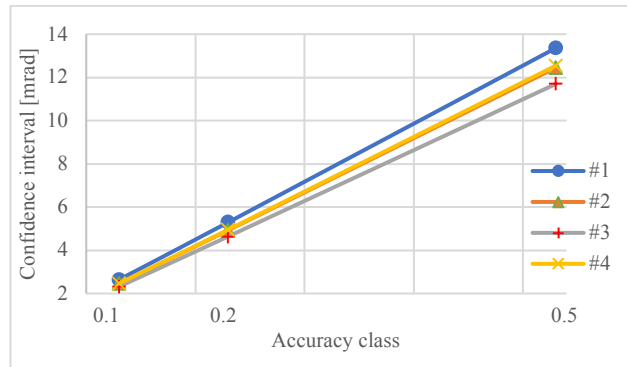


Fig. 4.37. Amplitude (mrad) of the 95% confidence interval of the phase displacement $\Delta\varphi_{13}$, considering only the effect of ITs with respect to the different accuracy classes, for the 4 analyzed cases

For both graphs the trend of the confidence interval is linearly increasing as the accuracy class gets poorer; moreover, it increases considerably in the case of the 0.5 accuracy class, where it becomes about 5 or 7 times larger than those relevant to 0.2 and 0.1 accuracy classes, respectively. This may lead to conclude that 0.5-accuracy class ITs are not particularly significant for the presented study. The plots also show that the impact of the ITs accuracy on phase displacement uncertainty does not change with the length of power network branches. In fact, all lines, which refer to different cases and hence to different branch lengths, are almost overlapping.

- **Branch Lengths**

A further important aspect to investigate is the inaccurate knowledge of the length of the branches effect on the uncertainty of the method results. While electrical utilities have very detailed power network maps, showing different features of the network in terms of cable types, joints, etc. Unfortunately, the length of the branches is often quite rough, as cable-laying activities turn into more or less significant discrepancies between the actual and the designed length. Starting from the cases of Table 4.39, which are taken as rated values, variations of 1 %, 2 %, 5 % and 10 % have been applied on the cable lengths. Then, the MCM has been applied and the 95 %-confidence interval of the phase error $\Delta\varphi_{12}$ has been obtained for two of the cases #1 and the #4, which are the ones featuring the shortest and the longest lengths, respectively. For the sake of brevity, the results of the study on $\Delta\varphi_{13}$ are not shown but they are very similar to the ones reported and discussed in the following. Fig. 4.38 contains the amplitudes of the 95%-confidence intervals of $\Delta\varphi_{12}$ with respect to the percentage of uncertainty on the length value.

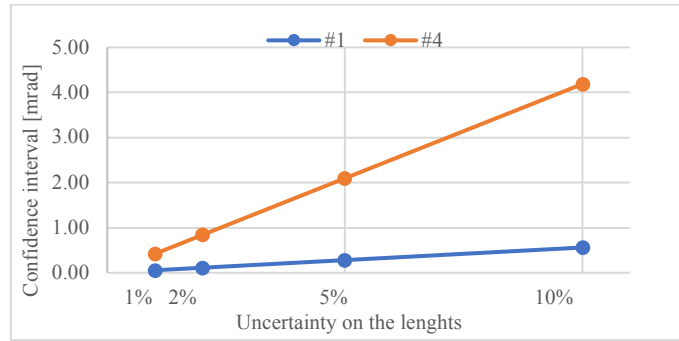


Fig. 4.38. Amplitude (mrad) of the 95%-confidence interval of the phase displacement $\Delta\phi_{12}$, when only the effect of the percentage variation of the branches length from the rated values are considered

Note that such an amplitude linearly increases with the increasing inaccuracy on the branch lengths. Moreover, the uncertainty on $\Delta\phi_{12}$ is higher for the case with the longest lines (case #4).

- **Per-unit Length Reactance**

Further analysis has been carried out by evaluating the contribution of the per-unit length reactance. In the proposed method B, the reactance of the cables is obtained by taking as constant the value of the per-unit length reactance. This, as explained in Section 4.2.2.3 and conversely to what happens for the resistance, is due to the very negligible variations of the reactance with respect to the cross-section of the cable. Hence, an average value for the per-unit length reactance has been chosen in the simulations; then, its influence on the overall uncertainty has been studied and the results are shown in what follows.

Different variations of the reactance have been applied to the selected average values, 5 %, 20 %, 30 % and 50 %. These large percentages have been selected by assuming that no information about the branch impedance is usually made available by utilities; moreover, the network topology is also constantly changing, resulting in the connection of different kind of cables with different values of per-unit length reactances. For the simulation analysis, 100,000 iterations of the MCM have been run. The results are shown in Fig. 4.39 for cases #1 and #4, which correspond to the shortest and the longest branch lengths, respectively.

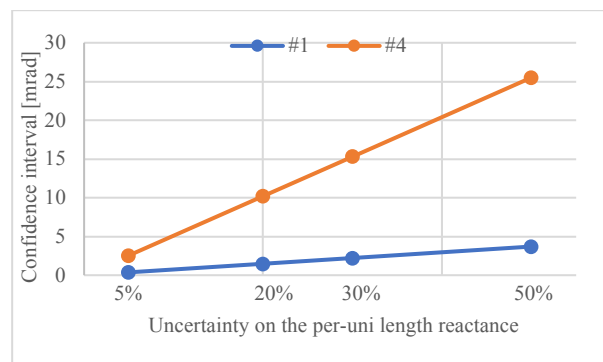


Fig. 4.39. Amplitude (mrad) of the 95%-confidence interval of the phase displacement $\Delta\phi_{13}$, when only the effect of the percentage variation of the per-unit length reactance from the rated values are considered

It can be noted that for both cases the trend of the confidence interval is linear; moreover, in case #4 (power network with long branches) the slope of the line is much higher than that in case #1 (very short lines). In conclusion, longer networks will be much more affected by higher

discrepancy between the actual and the selected value of the per-unit length reactance; resulting, in turn, in higher errors of the proposed method B.

- Overall Uncertainty Evaluation

Finally, the overall uncertainty of method B results can be evaluated considering all sources involved. This analysis considered the uncertainty introduced by the acquisition system, ITs accuracy classes, a 10 % variation for both the per-unit length reactance and the branch lengths. Then, the MCM has been applied and the results are listed in Tables 4.43 and 4.44 for the phase displacement errors $\Delta\varphi_{12}$ and $\Delta\varphi_{13}$, respectively.

Table 4.43. Amplitude (mrad) of the 95 %-confidence interval of the phase displacement $\Delta\varphi_{12}$, when all the sources of uncertainty are considered

Case	Accuracy classes		
	0.1	0.2	0.5
#1	3.093	5.933	14.812
#2	4.188	6.726	15.558
#3	5.317	7.550	16.091
#4	8.021	9.458	16.295

Table 4.44. Amplitude (mrad) of the 95 %-confidence interval of the phase displacement $\Delta\varphi_{13}$, when all the sources of uncertainty are considered

Case	Accuracy classes		
	0.1	0.2	0.5
#1	2.810	5.381	13.415
#2	3.427	5.494	12.720
#3	4.042	5.730	12.176
#4	7.106	8.361	14.336

Observe that longer lines result in larger confidence intervals while higher accuracy classes result in smaller intervals. It is also obvious from the Tables, that in case of accuracy class 0.5, things change significantly: the confidence interval are twice the amount of the 0.1 accuracy class.

4.2.2.7 Conclusion

This research addressed the problem of synchronizing phasor measurements in different nodes of the power network, with focus on the accuracy evaluation. The most common answer to this problem is to use a synchronization signal provided by wired or wireless communication infrastructure. The typical implementation of that solution is the PMU which relies on a time reference signal coming from the GPS system.

This work recalls and introduces two novel methods presented in a previous research. Then the study describes the measurement set-up in detail, in order to test one of the two methods presented (B). After that, the main uncertainty sources in the measurement chain have been considered, investigating their effects on the results by implementing the method B. To this purpose, MCM has been applied to evaluate the 95 %-confidence interval of the phase displacement errors $\Delta\varphi_{12}$ and $\Delta\varphi_{13}$. The results of the numerical examples have highlighted the effects of the main sources of uncertainty.

Concerning the ITs, the study has concluded that they provide the major source of uncertainty in the measurement chain, in particular using the 0.5 accuracy class. In consequence, this accuracy class cannot be considered suitable in the implementation of method B.

As far as the lack of knowledge on the branch length is concerned, there is a linear trend of the 95 %-confidence interval vs. the percentage of inaccuracy of the lengths. Moreover, by running the MC for different cable lengths, it arises that even for long lines the absolute value of the confidence interval is quite limited.

Regarding the third source of uncertainty, the lack of knowledge on the per-unit length reactance, different percentages have been considered for cases #1 and #4. Even in this case, the trend of the 95 %-confidence interval is linear and it can be concluded that it is acceptable also in the case of a 50 %-inaccuracy in the reactance value, provided that the length of the line is kept short in length.

4.2.3 A general expression for uncertainty evaluation in residual voltage measurement

4.2.3.1 Introduction

Most industrialized countries in the world decided to promote the decarbonisation of energy systems in recent years. European Commission's energy and climate policies, such as the SET-Plan, foresee that the context of future scenarios for electric power networks will ensure a stable and secure power supply as Renewable Energy Sources penetration increases up to 100 %.

Nevertheless, the wide-scale introduction of decentralized RES is causing significant and unprecedented changes in electrical power grids. Consequently, future electrical power grids will require real-time control and monitoring systems to ensure stability under increasingly complex and challenging conditions [63].

The generation of analogue measurement and control systems in power grid substations are approaching the end of their useful lifespan. More often their replacement is based on digital substation automation solutions according to IEC 61850-9 [64] and the use of new technologies to perform measurements and control operations more efficiently, eg with the massive use of Ring Main Units[65].

More specifically, Utilities and private customers dedicate special attention to ITs for various reasons. With the deployment of Smart Grids and Distributed Energy Resources new performance and features are required so the ITs can provide real-time network control with the best efficiency, speed and accuracy. For instance, the large use of power inverters for interconnecting large photovoltaic plants to the grid has led to the injection of high-order harmonics. These can interfere with industrial frequency components which may give rise to intermodulation. These demands include that such spectral components are correctly and accurately measured in order to let these systems run under real-time feedback control. Moreover, in case of off-nominal frequency, protection relays must now trip faster than before, in a few ms, instead of tens of ms as in the past. Furthermore, as energy is no more flowing in just one direction (multiple producers or prosumers are now connected to the same grid), very accurate energy and power measurements must be performed. This way it is possible to correctly split energy production revenues among prosumers and to accurately inject reactive energy into the grid. Again, the mass deployment of secondary substations and measurement nodes is limited by space and size constraints. Therefore, new requests for reduced dimensions of all electrical devices and systems have become a crucial parameter. Finally, the development and transmission of digital communications between the nodes of a power network have required that ITs include digital outputs [66], as stated before.

Still, one of the most important measurements for network stability and diagnostic remains the residual voltage. Its measurement is mandatory to coordinate protection including the implementation of differential protections to correctly classify ground faults, etc. At present, these measurements are performed by using inductive voltage transformers star-connected at the primary site and with open triangle at the secondary site. Typical accuracies required for the residual voltage measurements are in the order of some percent, while residual voltage values are in the order of few percent (4 %) of the rated [67].

In case the residual voltage is evaluated by using the line voltages (sum of the three ITs secondary voltages), reaching such a measurement accuracy gets very challenging. In particular, in the case of RES it is difficult as the power flow is bi-directional and the node voltages might suffer significant changes. Moreover, this is even worse if the ITs are not working at ambient temperatures, as demonstrated in literature [29]. This leads to requirements on the new devices used as voltage sensors, the LPVT.

This work [68] aims to present a novel study developed from the results of the related study [69] to correlate the uncertainty affecting the measurement of the residual voltage with the accuracy class of the LPVTs.

First, this study derives a new easy-to-use expression for estimating the uncertainty on the residual voltage for a generic 3-phase system. It will show that it provides accurate results without the use of

complex and long calculations as required by the application of analytical or numerical methods suggested by the GUM as well as its Supplement 1 [21, 22].

Such a study is requested by industry and might be used for completing two important Standards: the IEC 61869-11 [12] on LPVTs, and the future IEC 61869-105 [70] document dealing with uncertainty in calibration of ITs. Moreover, it will be useful to power network and system designers and operators for selecting suitable LPVTs according to the accuracy requested for the residual voltage measurement.

The validity of the proposed expression has been confirmed with both computer simulation and actual measurements. Tests are performed with a measurement set-up developed for the specific purpose of the residual voltage measurement.

The research is structured as follows: Section 4.2.3.2 describes the backbone concepts of [69] and presents the expression of the residual voltage in case of a generic (balanced or unbalanced) 3-phase system. Section 4.2.3.3 briefly summarizes the uncertainty results obtained in [69] and provides the residual voltage uncertainty for the aforementioned case-study. Section 4.2.3.4 details the set-up proposed for residual voltage measurement. Tests and results of the performed measurements are presented in Section 4.2.3.5. Finally, Section 4.2.3.6 summarizes the presented study along with conclusion.

4.2.3.2 Residual voltage

- Case-study definition

According to the International Electrotechnical Vocabulary, the residual voltage $v_r(t)$ is defined as “the sum of the instantaneous values of all three line-to-earth voltages, in a three-phase system” [1]:

$$v_r(t) = v_1(t) + v_2(t) + v_3(t) \quad (4.76)$$

where $v_1(t)$, $v_2(t)$ and $v_3(t)$ are the instantaneous line-to-earth voltages of lines 1, 2 and 3, respectively. In case of a sinusoidal steady-state condition, (4.76) turns into:

$$\bar{V}_R = \bar{V}_1 + \bar{V}_2 + \bar{V}_3 \quad (4.77)$$

where \bar{V}_i is the phasor of the generic quantity $v_i(t)$. If the residual voltage is a phasor (as in (4.77)) or a waveform (as in (4.76)), in practical application only the module is used.

Fig. 4.40 shows a typical set-up for the measurement of such a quantity, referred to as \bar{V}_R .

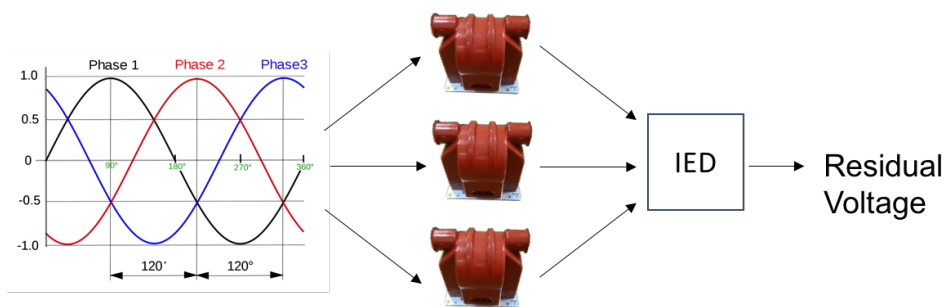


Fig. 4.40. Schematic of a typical set-up for the measurement of three-phase system of symmetric voltages

It consists of three LPVTs and an Intelligent Electronic Device, which acquires the LPVTs outputs and computes the residual voltage. Therefore, the value attributed to \bar{V}_R is affected by the effect of the uncertainty sources (gain and non-linearity error, offset, noise, ratio and phase error, etc.) located in the LPVTs as well as in the IED. Usually, the latter can be considered negligible compared to the uncertainty sources in the LPVT. [65, 71].

- Mathematic development

Consider three LPVTs featuring ratio errors ε_1 , ε_2 and ε_3 and phase errors $\Delta\varphi_1$, $\Delta\varphi_2$, and $\Delta\varphi_3$ as defined in [3]. Therefore, starting from (4.77), the residual voltage \bar{V}_R can be expressed as a function of such uncertainty contributions:

$$\bar{V}_R = [V_1(1 + \varepsilon_1)e^{j(\vartheta_1 + \Delta\varphi_1)} + V_2(1 + \varepsilon_2)e^{j(\vartheta_2 + \Delta\varphi_2)} + V_3(1 + \varepsilon_3)e^{j(\vartheta_3 + \Delta\varphi_3)}] \quad (4.78)$$

where V_i and ϑ_i are the generic RMS value and phase angle of the related phasor \bar{V}_i , respectively. Without loss of generality in [69], a balanced three-phase system condition has been assumed as a first scenario. This means that:

$$V_1 = V_2 = V_3 = V \quad (4.79)$$

and

$$\vartheta_1 = 0, \vartheta_2 = \frac{2}{3}\pi \text{ and } \vartheta_3 = -\frac{2}{3}\pi. \quad (4.80)$$

Such assumption has led to the following expression of the residual voltage module (see [69] for details):

$$|\bar{V}_R| = V \left[\left(\varepsilon_1 - \frac{\sqrt{3}}{2}\Delta\varphi_2 - \frac{1}{2}\varepsilon_2 + \frac{\sqrt{3}}{2}\Delta\varphi_3 - \frac{1}{2}\varepsilon_3 \right)^2 + \left(\Delta\varphi_1 - \frac{1}{2}\Delta\varphi_2 + \frac{\sqrt{3}}{2}\varepsilon_2 - \frac{1}{2}\Delta\varphi_3 - \frac{\sqrt{3}}{2}\varepsilon_3 \right)^2 \right]^{1/2}. \quad (4.81)$$

Note when all ε_i and $\Delta\varphi_i$ are zero, (4.81) provides $|\bar{V}_R| = 0$, according to the assumption of balanced voltages. Therefore, the expression in square brackets represents the error on \bar{V}_R for a balanced three-phase system of amplitude V . Of course, such error can be computed only if the values of the accuracy parameters ε and $\Delta\varphi$ are already known for each VT. Otherwise, (4.81) can be also used to evaluate the uncertainty on \bar{V}_R if ε_i and $\Delta\varphi_i$ are treated as random variables and one of these methods is applied, as suggested by GUM [21] and its supplement 1 [22].

In this research, a general expression of $|\bar{V}_R|$ is derived from (4.78), whether the system is balanced or unbalanced. Hence, by considering the Euler formulae, (4.78) turns into:

$$\bar{V}_R = \{V_1[(1 + \varepsilon_1)(\cos(\vartheta_1 + \Delta\varphi_1) + j\sin(\vartheta_1 + \Delta\varphi_1))] + V_2[(1 + \varepsilon_2)(\cos(\vartheta_2 + \Delta\varphi_2) + j\sin(\vartheta_2 + \Delta\varphi_2))] + V_3[(1 + \varepsilon_3)(\cos(\vartheta_3 + \Delta\varphi_3) + j\sin(\vartheta_3 + \Delta\varphi_3))]\} \quad (4.82)$$

Defining the following three parameters help to increase the reader comprehension:

$$\begin{aligned} L &= \cos(\vartheta_1 + \Delta\varphi_1) + j\sin(\vartheta_1 + \Delta\varphi_1) \\ M &= \cos(\vartheta_2 + \Delta\varphi_2) + j\sin(\vartheta_2 + \Delta\varphi_2) \\ N &= \cos(\vartheta_3 + \Delta\varphi_3) + j\sin(\vartheta_3 + \Delta\varphi_3) \end{aligned} \quad (4.83)$$

(4.82) can be re-written as:

$$\bar{V}_R = V_1L + \varepsilon_1V_1L + V_2M + \varepsilon_2V_2M + V_3N + \varepsilon_3V_3N, \quad (4.84)$$

which highlights the terms not affected by the ratio error of the LPVTs. Focusing on these terms (V_1L , V_2M and V_3N), in particular on the first, and by applying the addition sine formulae:

$$V_1L = V_1[\cos(\vartheta_1)\cos(\Delta\varphi_1) - \sin(\vartheta_1)\sin(\Delta\varphi_1)] + jV_1[\sin(\vartheta_1)\cos(\Delta\varphi_1) + \cos(\vartheta_1)\sin(\Delta\varphi_1)]. \quad (4.85)$$

Given that, in actual conditions, $\Delta\varphi_i$ is small, $\cos(\Delta\varphi_i) \cong 1$ and $\sin(\Delta\varphi_i) \cong \Delta\varphi_i$ are assumed; hence:

$$V_1L = \bar{V}_{R(1)} + V_1\Delta\varphi_1[j\cos(\vartheta_1) - \sin(\vartheta_1)] \quad (4.86)$$

where $\bar{V}_{R(1)}$ is the term of the residual voltage, included in (4.85), not affected by the ratio and phase error of the LPVTs:

$$\bar{V}_{R(1)} = V_1\cos(\vartheta_1) + jV_1\sin(\vartheta_1). \quad (4.87)$$

Therefore, by writing all terms of (4.84) as in (4.86) for the term V_1L , and by neglecting all second order terms (i.e. those which are a product of LPVT parameters ε_i and $\Delta\varphi_i$), (4.84) becomes:

$$\bar{V}_R = \bar{V}_{R(1)}(1 + \varepsilon_1) + \bar{V}_{R(2)}(1 + \varepsilon_2) + \bar{V}_{R(3)}(1 + \varepsilon_3) + V_1\Delta\varphi_1[j\cos(\vartheta_1) - \sin(\vartheta_1)] + V_2\Delta\varphi_2[j\cos(\vartheta_2) - \sin(\vartheta_2)] + V_3\Delta\varphi_3[j\cos(\vartheta_3) - \sin(\vartheta_3)], \quad (4.88)$$

which represents the residual voltage general expression in the case of an unbalanced 3-phase system. Eq. (4.88) can be expressed in terms of module (4.89), real (4.90) and imaginary part (4.91):

$$|\bar{V}_R| = \sqrt{(Re[\bar{V}_R])^2 + (Im[\bar{V}_R])^2} \quad (4.89)$$

$$Re[\bar{V}_R] = V_1\cos(\vartheta_1)(1 + \varepsilon_1) + V_2\cos(\vartheta_2)(1 + \varepsilon_2) + V_3\cos(\vartheta_3)(1 + \varepsilon_3) - V_1\sin(\vartheta_1)\Delta\varphi_1 - V_2\sin(\vartheta_2)\Delta\varphi_2 - V_3\sin(\vartheta_3)\Delta\varphi_3 \quad (4.90)$$

$$Im[\bar{V}_R] = V_1\sin(\vartheta_1)(1 + \varepsilon_1) + V_2\sin(\vartheta_2)(1 + \varepsilon_2) + V_3\sin(\vartheta_3)(1 + \varepsilon_3) + V_1\cos(\vartheta_1)\Delta\varphi_1 + V_2\cos(\vartheta_2)\Delta\varphi_2 + V_3\cos(\vartheta_3)\Delta\varphi_3. \quad (4.91)$$

Of course, if all parameters ε_i and $\Delta\varphi_i$ are equal to zero, (4.89) provides $|\bar{V}_R| = 0$ as for the case of a balanced 3-phase system.

In summary, (4.90) and (4.91) have been obtained by applying two simple and common assumptions: to consider $\Delta\varphi_i$ a small angle and to neglect terms which are the product of two LPVT parameters (for example $\Delta\varphi_i * \varepsilon_i$). As for the first assumption, errors of $2 \cdot 10^{-5}$ on the cosine value and $3 \mu\text{rad}$ on the angle one are made if $\Delta\varphi_i = 6 \text{ mrad}$ is taken (limit for the 0.5 accuracy class, worst case). For the latter assumption instead, this turns into considering zero in place of 10^{-5} (worst case for the 0.5 accuracy class).

4.2.3.3 Uncertainty evaluation

As mentioned in Section 4.2.3.2, the residual voltage error can be obtained only if the values of the accuracy parameters ε and $\Delta\varphi$ are already known for each VT. However, in practical situations, this is not possible and the uncertainty affecting $|\bar{V}_R|$ must be determined. In this context, parameters ε and $\Delta\varphi$ are treated as random variables. The GUM and its Supplement 1 provide detailed explanations on how to estimate this value, but the implementation of these methods may be quite complex and not easy for technicians who are not metrologists or university professors. For this reason, in light of the experience gained by the authors on the topic [71] and considering the existing literature [72], two simplified expressions for the uncertainty evaluation of the residual voltage measurement are presented. The first expression is based on [69] and can be applied to an (almost) balanced three-phase system. The second expression is a new formula developed by the authors to be used with any 3-phase system. The aim is to provide an easy-to-use formula directly applicable in the field, when only the accuracy class of the LPVTs is known.

- **Balanced 3-phase system**

In [69], (4.81) has been re-written in terms of 2 new random variables X and Y :

$$X = \varepsilon_1 - \frac{\sqrt{3}}{2}\Delta\varphi_2 - \frac{1}{2}\varepsilon_2 + \frac{\sqrt{3}}{2}\Delta\varphi_3 - \frac{1}{2}\varepsilon_3 \quad (4.92)$$

$$Y = \Delta\varphi_1 - \frac{1}{2}\Delta\varphi_2 + \frac{\sqrt{3}}{2}\varepsilon_2 - \frac{1}{2}\Delta\varphi_3 - \frac{\sqrt{3}}{2}\varepsilon_3, \quad (4.93)$$

whose variances σ_X^2 and σ_Y^2 , assuming that the three LPVTs have the same accuracy class, are:

$$\sigma_X^2 = \frac{3}{2}(\sigma_{\Delta\varphi}^2 + \sigma_\varepsilon^2) \quad (4.94)$$

$$\sigma_Y^2 = \frac{3}{2}(\sigma_{\Delta\varphi}^2 + \sigma_\varepsilon^2). \quad (4.95)$$

Then, it is:

$$\sigma_X^2 = \sigma_Y^2 \quad (4.96)$$

In (4.94) and (4.95), σ_ε^2 and $\sigma_{\Delta\varphi}^2$ are the variances of the random variables ε and $\Delta\varphi$ representing the chosen accuracy class for the LPVTs. Therefore, the probability distribution associated to the

random variable $|\bar{V}_R|$ defined by (4.81) is a well-known Rayleigh one [69]. Hence, the variance σ_R^2 of $|\bar{V}_R|$ is:

$$\sigma_R^2 = \left(2 - \frac{\pi}{2}\right) \sigma^2, \quad (4.97)$$

where $\sigma^2 = \sigma_X^2 = \sigma_Y^2$.

- Generic 3-phase system

The balanced 3-phase condition cannot always be met. Hence, an easy-to-use expression applicable in all cases is required. To this purpose, consider equations (4.90) and (4.91). Both are a linear combination of six zero-mean random variables $\varepsilon_1, \varepsilon_2, \varepsilon_3, \Delta\varphi_1, \Delta\varphi_2$ and $\Delta\varphi_3$. It is well-known that, given a random variable f defined as:

$$f = ag + bh, \quad (4.98)$$

where g and h are generic independent random variables and a and b are numerical coefficients, its variance σ_f^2 is given by:

$$\sigma_f^2 = a^2\sigma_g^2 + b^2\sigma_h^2, \quad (4.99)$$

where σ_g^2 and σ_h^2 are the variances of g and h , respectively.

Therefore, by applying (4.99) to (4.90) and (4.91):

$$\sigma_U^2 = V_1^2 \cos^2(\vartheta_1) \sigma_{\varepsilon_1}^2 + V_2^2 \cos^2(\vartheta_2) \sigma_{\varepsilon_2}^2 + V_3^2 \cos^2(\vartheta_3) \sigma_{\varepsilon_3}^2 + V_1^2 \sin^2(\vartheta_1) \sigma_{\Delta\varphi_1}^2 + V_2^2 \sin^2(\vartheta_2) \sigma_{\Delta\varphi_2}^2 + V_3^2 \sin^2(\vartheta_3) \sigma_{\Delta\varphi_3}^2 \quad (4.100)$$

$$\sigma_V^2 = V_1^2 \sin^2(\vartheta_1) \sigma_{\varepsilon_1}^2 + V_2^2 \sin^2(\vartheta_2) \sigma_{\varepsilon_2}^2 + V_3^2 \sin^2(\vartheta_3) \sigma_{\varepsilon_3}^2 + V_1^2 \cos^2(\vartheta_1) \sigma_{\Delta\varphi_1}^2 + V_2^2 \cos^2(\vartheta_2) \sigma_{\Delta\varphi_2}^2 + V_3^2 \cos^2(\vartheta_3) \sigma_{\Delta\varphi_3}^2. \quad (4.101)$$

Where:

$$U = \text{Re}[\bar{V}_R] \quad (4.102)$$

$$V = \text{Im}[\bar{V}_R] \quad (4.103)$$

In light of (4.102) and (4.103), (4.89) can be rewritten as:

$$|\bar{V}_R| = W = \sqrt{U^2 + V^2}. \quad (4.104)$$

If 3 LPVTs with the same accuracy class are assumed, hence $\sigma_{\varepsilon_1}^2 = \sigma_{\varepsilon_2}^2 = \sigma_{\varepsilon_3}^2 = \sigma_{\varepsilon}^2$ and $\sigma_{\Delta\varphi_1}^2 = \sigma_{\Delta\varphi_2}^2 = \sigma_{\Delta\varphi_3}^2 = \sigma_{\Delta\varphi}^2$, (4.100) and (4.101) turn into:

$$\sigma_U^2 = \sigma_{\varepsilon}^2 \left(V_1^2 \cos^2(\vartheta_1) + V_2^2 \cos^2(\vartheta_2) + V_3^2 \cos^2(\vartheta_3) \right) + \sigma_{\Delta\varphi}^2 \left(V_1^2 \sin^2(\vartheta_1) + V_2^2 \sin^2(\vartheta_2) + V_3^2 \sin^2(\vartheta_3) \right) \quad (4.105)$$

$$\sigma_V^2 = \sigma_{\varepsilon}^2 \left(V_1^2 \sin^2(\vartheta_1) + V_2^2 \sin^2(\vartheta_2) + V_3^2 \sin^2(\vartheta_3) \right) + \sigma_{\Delta\varphi}^2 \left(V_1^2 \cos^2(\vartheta_1) + V_2^2 \cos^2(\vartheta_2) + V_3^2 \cos^2(\vartheta_3) \right). \quad (4.106)$$

Hence:

$$\sigma_U^2 = a\sigma_{\varepsilon}^2 + b\sigma_{\Delta\varphi}^2 \quad (4.107)$$

$$\sigma_V^2 = b\sigma_{\varepsilon}^2 + a\sigma_{\Delta\varphi}^2, \quad (4.108)$$

where

$$a = V_1^2 \cos^2(\vartheta_1) + V_2^2 \cos^2(\vartheta_2) + V_3^2 \cos^2(\vartheta_3) \quad (4.109)$$

$$b = V_1^2 \sin^2(\vartheta_1) + V_2^2 \sin^2(\vartheta_2) + V_3^2 \sin^2(\vartheta_3) \quad (4.110)$$

are completely known to in-field operators.

In (4.107) and (4.108), the variances of U and V are different, so the Rayleigh distribution adopted in [69] cannot be applied. Consequently, a different strategy is to be applied.

In equations (4.90) and (4.91), U and V are the sum of several random variables. Therefore, according to the Central Limit Theorem, they are two normal random variables $U(\mu_U, \sigma_U^2)$ and $V(\mu_V, \sigma_V^2)$, respectively. It is:

$$\mu_U = V_1 \cos(\vartheta_1) + V_2 \cos(\vartheta_2) + V_3 \cos(\vartheta_3) \quad (4.111)$$

$$\mu_V = V_1 \sin(\vartheta_1) + V_2 \sin(\vartheta_2) + V_3 \sin(\vartheta_3). \quad (4.112)$$

The squares U^2 and V^2 of U and V have a chi-square distribution (χ^2) with one degree of freedom [73, 74]. Therefore, it is:

$$\sigma_{U^2}^2 = 2 \left(1 + 2 \left(\frac{\mu_U}{\sigma_U} \right)^2 \right) \sigma_U^4 \quad (4.113)$$

$$\sigma_{V^2}^2 = 2 \left(1 + 2 \left(\frac{\mu_V}{\sigma_V} \right)^2 \right) \sigma_V^4 \quad (4.114)$$

and

$$\mu_{U^2} = \sigma_U^2 + \mu_U^2 \quad (4.115)$$

$$\mu_{V^2} = \sigma_V^2 + \mu_V^2 \quad (4.116)$$

Where $\sigma_{U^2}^2$, μ_{U^2} and $\sigma_{V^2}^2$, μ_{V^2} are the variance and the mean value of the two random variables U^2 and V^2 , respectively.

Finally, $W^2 = U^2 + V^2$ is the sum of two generic random variables, which variance $\sigma_{W^2}^2$ is, according to (4.99):

$$\sigma_{W^2}^2 = \sigma_{U^2}^2 + \sigma_{V^2}^2 + 2cov(U^2, V^2). \quad (4.117)$$

and which mean μ_{W^2} is:

$$\mu_{W^2} = \mu_{U^2} + \mu_{V^2} \quad (4.118)$$

Eq. (4.117) is more general than (4.99). In fact, the covariance term $cov(U^2, V^2)$ has been added to consider also the case of dependents variables. In the present case, U^2 and V^2 are surely related. However, as confirmed in the result Section above, neglecting their covariance does not affect the overall results. Of course, further studies can be performed to analyze such a behavior in depth.

The distribution associated to W^2 is still a chi-square one, which is a special case of the gamma distribution [73, 74]. According to [75, 76] and in light of the aforementioned results, $W = \sqrt{W^2}$ follows a Nakagami distribution with the shape and the spread parameters m and Ω , respectively:

$$m = \frac{(\mu_{W^2})^2}{\sigma_{W^2}^2} \quad (4.119)$$

$$\Omega = \mu_{W^2} \quad (4.120)$$

Considering that terms inside (4.119) and (4.120) are well-known from the previous steps, μ_W and σ_W^2 can be computed as:

$$\mu_W = \frac{\Gamma(m+1/2)}{\Gamma(m)} \sqrt{\frac{\Omega}{m}} \quad (4.121)$$

$$\sigma_W^2 = \Omega \left[1 - \frac{1}{m} \left(\frac{\Gamma(m+1/2)}{\Gamma(m)} \right)^2 \right]. \quad (4.122)$$

$\Gamma(m)$ is the gamma function with m degrees of freedom. These two expressions allow, at a glance, to determine the mean value and the variance of the residual voltage module $|\bar{V}_R| = W$ (see (4.104)). As a further comment, the term $\frac{\Gamma(m+1/2)}{\Gamma(m)}$ in both (4.121) and (4.122) is also known as the Pochhammer function. Such a function can be used in software packages, instead of the Gamma one, to avoid computational issues that may occur when m takes high values.

Summarizing, (4.121) and (4.122) allow to determine the mean value and variance of the residual voltage module, by simply measuring the 3 voltage phasors by means of three LPVTs with given accuracy class. Note that the provided expression can also be used in the case of non-sinusoidal

waveforms. As a matter of fact, a Fourier transform is usually applied to extract the phasor component at power frequency (50 Hz), in the case of non-sinusoidal condition. Hence, the proposed expression application can be extended also to this case, by replacing the ratio and phase error of the LPVT with the corresponding ones derived by their propagation through the Fourier transform algorithm [77]. In particular, in presence of noise affecting the input voltage, applying the Fourier transform allows to neglect the effect of the noise on the phasor estimation in all the practical situations. In fact, [78] has already shown that, with a signal to noise ratio of 20, the error due to the noise on the estimate of the signal components is a fraction of percent. Hence, by considering that a typical signal-to-noise ratio in power system is below 1 %, it results that the noise contribution to the overall uncertainty can be considered negligible.

- Monte Carlo results

The Monte Carlo (MC) method is applied to validate (4.121) and (4.122). Usually, the LPVT manufacturers do not provide information regarding the probability distribution of ratio and phase errors. Therefore, in accordance with [21, 22], this lack of knowledge leads to assume the 6 random variables in (4.90) and (4.91) as uniformly distributed within the intervals whose limits are defined by the accuracy class specified by the LPVT manufacturers. To assess the proposed expressions in actual conditions, LPVTs featuring $20/\sqrt{3}$ kV – $3.25/\sqrt{3}$ V have been considered. In particular, three different sets of LPVTs have been simulated. In each set all the LPVTs use the same accuracy class: 0.1, 0.2 or 0.5. For the three above sets, 5 combinations of three voltage phasors of a three-phase system have been tested. The values have been chosen according to the voltage limits provided by the EN 50160 [15] and are listed in Table 4.45.

Table 4.45. List of the phasor values for the 15 tests

Test	Acc. class	V_1 [V]	V_2 [V]	V_3 [V]	ϑ_1 [°]	ϑ_2 [°]	ϑ_3 [°]
#1	0.1	11547	11547	11547	0	-120	120
#2	0.1	12124	12124	11547	0	-120	120
#3	0.1	12124	10392	11547	0	-120	120
#4	0.1	11547	11547	11547	0	-120	135
#5	0.1	12124	10392	11547	0	-110	130
#6	0.2	11547	11547	11547	0	-120	120
#7	0.2	12124	12124	11547	0	-120	120
#8	0.2	12124	10392	11547	0	-120	120
#9	0.2	11547	11547	11547	0	-120	135
#10	0.2	12124	10392	11547	0	-110	130
#11	0.5	11547	11547	11547	0	-120	120
#12	0.5	12124	12124	11547	0	-120	120
#13	0.5	12124	10392	11547	0	-120	120
#14	0.5	11547	11547	11547	0	-120	135
#15	0.5	12124	10392	11547	0	-110	130

Then, 1 million MCM trials are computed to estimate the probability density function (PDF), the mean and the variance of $|\vec{V}_R|$. As for $|\vec{V}_R|$, Fig. 4.41, 4.42 and 4.43 show their PDFs in the case of test #1 and accuracy classes 0.1, 0.2 and 0.5, respectively.

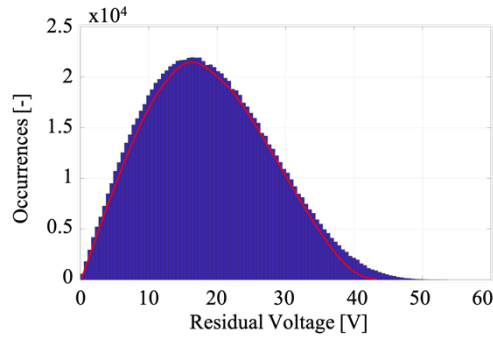


Fig. 4.41. PDF of $|\bar{V}_R|$ when three 0.1 class LPVTs are considered (case #1)

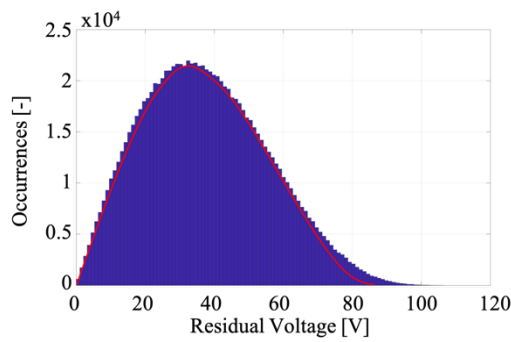


Fig. 4.42. PDF of $|\bar{V}_R|$ when three 0.2 class LPVTs are considered (case #6)

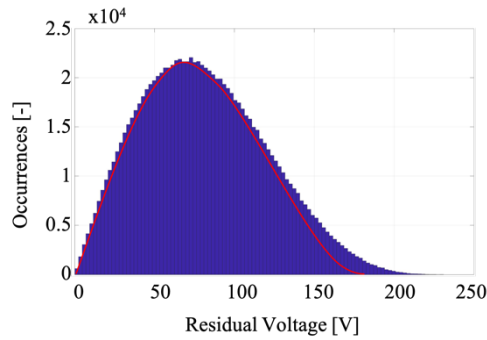


Fig. 4.43. PDF of $|\bar{V}_R|$ when three 0.5 class LPVTs are considered (case #11)

From these figures, it can be highlighted that the PDF shape is consistent with the Nakagami distribution (plotted in the graphs along with $|\bar{V}_R|$) adopted in the previous subsection to represent the $|\bar{V}_R|$. The same observation holds for all other cases, whose PDF values are not reported for the sake of brevity.

Afterwards, mean value and variance of $|\bar{V}_R|$ resulting from MC are compared with the ones obtained by applying (4.121) and (4.122). Table 4.46 shows the test results, where the subscripts MC and N refer to the Monte Carlo and the analytical expressions based on the Nakagami distribution, respectively.

Table 4.46. Mean value and variance of $|\bar{V}_R|$ for the #15 tests applying the MC method and the proposed expression

Test	Acc. Class	μ_{MC} [V]	σ_{MC}^2 [V ²]	μ_N [V]	σ_N^2 [V ²]
#1	0.1	19	82	18	93
#2	0.1	577	234	577	232
#3	0.1	1528	214	1528	210
#4	0.1	3014	217	3014	213
#5	0.1	1471	196	1471	208
#6	0.2	38	328	37	372
#7	0.2	578	936	578	925
#8	0.2	1528	857	1528	838
#9	0.2	3015	867	3015	852
#10	0.2	1471	783	1471	833
#11	0.5	81	1561	80	1745
#12	0.5	581	4338	581	4268
#13	0.5	1529	3983	1529	3931
#14	0.5	3015	4072	3015	4032
#15	0.5	1472	3804	1472	3921

The comparison shows that, for each accuracy class, mean values and variances provided by (4.121) and (4.122) are fully consistent and substantially equal to the ones obtained by the MC trials. This holds for all performed tests (range 19 – 3000 V, which contains all MV residual voltage values). In other words, the developed expression may be conveniently adopted in any power network condition and for any absolute value of the residual voltage. It only requires the knowledge of the measured voltages and the accuracy classes of the LPVTs installed in the network. In addition, the variance significantly increases with the accuracy class, as expected. Moreover, aside from case #1, #6 and #11 (where the residual voltage is not greater than 0.7 % of the rated voltage), the variance is substantially independent of the residual voltage value.

4.2.3.4 Experimental setup

An experimental set-up has been designed for a programmable (in amplitude and phase) low-voltage 3-phase system and to evaluate the residual voltage module $|\bar{V}_R|$. The choice of a low-voltage (LV) system, instead of a medium-voltage (MV) one, is due to the availability of programmable LV sources. This does not affect the evaluation of the proposed expressions, which can be applied irrespective of the input voltage. The system, depicted in Fig. 4.44, consists of:

- Agilent 6834B AC programmable Power source, featuring maximum values of 300 Vrms and 4500 VA, a frequency range 45 to 5000 Hz.
- Yokogawa WT3000 Wattmeter featuring 0.01 % of reading (%R) + 0.03 % of range accuracy (%FS) on the voltage measurement and one digit on the phase measurement. The Wattmeter acts as a reference for $|\bar{V}_R|$ measurements.
- 3 VT LEM CV-3-1000, featuring conversion ratio 10000 V / 10 V, rated voltage of 700 V and 0.2 accuracy class. It introduces a negligible phase delay according to its datasheet. As for the noise introduced by the VT, the datasheet does not report any value, and it has been considered negligible in terms of uncertainty computation.
- A 24-bit NI 9239 Data Acquisition board (DAQ), and a Personal Computer (PC). The NI DAQ related uncertainty has been neglected in the measurement chain due to its very small contribution compared to other components in the measurement chain (0.03 % of reading, 0.008 % of range). In particular, the NI DAQ accuracy parameters are at least one order of magnitude lower than the LPVTs ones. Furthermore, the DAQ has an input noise of 70 μ V, which is approximately lower by a factor of 10^{-4} than the secondary outputs obtained (about 1 V) as detailed in the following Sections. Such effect is negligible compared to the contribution of the LPVT, which is greater by at least one order of magnitude.

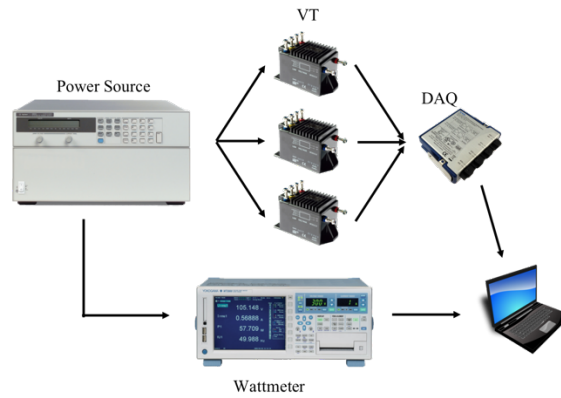


Fig. 4.44. Schematic of the measurement set-up adopted for the residual voltage measurement

In a nutshell, the 3-phase Power Source feeds both the Wattmeter and the 3 LPVTs. Then, the voltages needed for the residual voltage computation are acquired via LabView from the Wattmeter and via DAQ from the 3 VTs. Afterwards, data are collected and processed through a PC.

4.2.3.5 Experimental tests & results

This Section presents tests and results of the residual voltage measurements in actual/real conditions. Twenty different tests have been performed, with varying values for amplitude and phase of the 3 phasors in the limits defined by Standard EN 50160 [15]. Hence, the resulting 20 test conditions, that have been used has input quantities, are listed in Table 4.47 whereas Table 4.48 reports the corresponding results.

Table 4.47. List of the phasor values for each of the 20 tests performed

Test	V_1 [V]	V_2 [V]	V_3 [V]	ϑ_1 [°]	ϑ_2 [°]	ϑ_3 [°]
#1	230	230	230	0	-120	120
#2	207	230	230	0	-120	120
#3	218.5	230	230	0	-120	120
#4	253	230	230	0	-120	120
#5	241.5	230	230	0	-120	120
#6	207	218.5	230	0	-120	120
#7	207	207	230	0	-120	120
#8	207	241.5	230	0	-120	120
#9	207	253	230	0	-120	120
#10	218.5	218.5	230	0	-120	120
#11	218.5	241.5	230	0	-120	120
#12	218.5	253	230	0	-120	120
#13	230	230	0	0	-120	0
#14	230	230	230	0	-120	130
#15	230	230	230	0	-120	125
#16	230	230	230	0	-120	115
#17	230	230	230	0	-120	110
#18	230	230	230	0	-120	121
#19	230	230	230	0	-121	121
#20	230	230	218.5	0	-120	121

For each test, the absolute value of the residual voltage $|\bar{V}_R|$ has been measured 100 times by both Wattmeter and DAQ. These measurements have been used to compute $|\bar{V}_R|$ mean value and standard deviation of the mean.

Table 4.48. Residual voltage measurement results comparison between simulations and actual tests

Test	$ \bar{V}_R _W$ [V]	u_W [V]	$ \bar{V}_R _{DAQ}$ [V]	σ_{DAQ} [V]	$ \bar{V}_R _N$ [V]	u_N [V]
#1	0.22	$5 \cdot 10^{-2}$	0.6542	$3 \cdot 10^{-4}$	1.0	0.5
#2	22.78	$8 \cdot 10^{-2}$	22.6130	$1 \cdot 10^{-4}$	22.6	0.6
#3	11.23	$7 \cdot 10^{-2}$	11.15434	$4 \cdot 10^{-5}$	11.2	0.6
#4	23.22	$7 \cdot 10^{-2}$	23.43270	$3 \cdot 10^{-5}$	23.4	0.6
#5	11.78	$7 \cdot 10^{-2}$	11.85376	$4 \cdot 10^{-5}$	11.9	0.6
#6	19.54	$8 \cdot 10^{-2}$	19.31514	$3 \cdot 10^{-5}$	19.3	0.6
#7	22.59	$7 \cdot 10^{-2}$	22.33561	$4 \cdot 10^{-5}$	22.3	0.5
#8	30.29	$7 \cdot 10^{-2}$	30.26731	$3 \cdot 10^{-5}$	30.3	0.6
#9	39.75	$6 \cdot 10^{-2}$	39.80380	$4 \cdot 10^{-5}$	39.8	0.6
#10	11.07	$7 \cdot 10^{-2}$	10.8727	$3 \cdot 10^{-4}$	10.9	0.6
#11	19.80	$6 \cdot 10^{-2}$	19.91989	$4 \cdot 10^{-5}$	19.9	0.6
#12	30.48	$6 \cdot 10^{-2}$	30.54182	$5 \cdot 10^{-5}$	30.5	0.6
#13	230.21	$8 \cdot 10^{-2}$	230.23121	$3 \cdot 10^{-5}$	230.2	0.5
#14	39.99	$6 \cdot 10^{-2}$	40.02377	$5 \cdot 10^{-5}$	40.0	0.6
#15	20.04	$6 \cdot 10^{-2}$	20.0049	$1 \cdot 10^{-4}$	20.0	0.6
#16	20.19	$6 \cdot 10^{-2}$	20.09044	$5 \cdot 10^{-5}$	20.1	0.6
#17	40.19	$6 \cdot 10^{-2}$	40.15524	$5 \cdot 10^{-5}$	40.2	0.6
#18	3.93	$6 \cdot 10^{-2}$	4.03867	$5 \cdot 10^{-5}$	4.1	0.6
#19	6.65	$7 \cdot 10^{-2}$	6.6032	$1 \cdot 10^{-4}$	6.6	0.6
#20	12.61	$7 \cdot 10^{-2}$	12.69038	$4 \cdot 10^{-5}$	12.7	0.6

Table 4.48 contains:

- $|\bar{V}_R|$ mean value $|\bar{V}_R|_W$ and its combined uncertainty u_W for the measurements performed with the Wattmeter. The uncertainty has been computed as:

$$u_W = \sqrt{\sigma_{W_a}^2 + \sigma_{W_b}^2} \quad (4.123)$$

where σ_{W_a} is the standard deviation of the mean and σ_{W_b} is the standard uncertainty evaluated with type B method as explained in [21, 22], starting from the wattmeter nominal accuracy specifications reported in Section 4.2.3.4;

- a $|\bar{V}_R|$ mean value $|\bar{V}_R|_{DAQ}$ and standard deviation of the mean σ_{DAQ} for the measurements performed with the 3 LPVTs and acquired by the DAQ. Such test aims to represent an actual condition where typical LPVTs are adopted. In σ_{DAQ} evaluation, the contribution by the data acquisition system has been neglected as explained before.
- $|\bar{V}_R|$ mean value $|\bar{V}_R|_N$ and combined uncertainty u_N obtained starting from (4.121) and (4.122). The test set-up consisted of three voltage phasors, measured with the LPVTs, as input for the proposed expression along with their accuracy class parameters. The u_N has been computed as:

$$u_N = \sqrt{\sigma_{DAQ}^2 + \sigma_N^2} \quad (49)$$

where σ_N^2 is the variance obtained from (4.122).

From Table 4.48, several comments arise. Comparing the results from the wattmeter measurements with the data obtained from the proposed expression confirms the efficiency of the algorithm. The obtained results have been compared with the reference data obtained with the wattmeter for evaluation, and limits ($\pm L$) of 95 %-confidence interval have been calculated for $|\bar{V}_R|_W$ and $|\bar{V}_R|_N$ mean values. Table 4.49 lists these interval limits for all tests. Both intervals have been computed by considering a coverage factor $k = 2$. Such assumption is justified also for the Nakagami distribution as explained at the end of this Section.

Table 4.49. 95 %-confidence interval limits for the mean values $|\bar{V}_R|_W$ and $|\bar{V}_R|_N$

Test	$ \bar{V}_R _W$		$ \bar{V}_R _N$	
	-L [V]	+L [V]	-L [V]	+L [V]
#1	0.11	0.31	0.0	1.9
#2	22.63	22.93	21.5	23.8
#3	11.08	11.37	10.0	12.3
#4	23.07	23.37	22.2	24.6
#5	11.63	11.93	10.7	13.1
#6	19.39	19.69	18.2	20.4
#7	22.45	22.73	21.3	23.4
#8	30.16	30.43	29.1	31.4
#9	39.62	39.87	38.6	41.0
#10	10.92	11.21	9.8	12.0
#11	19.67	19.93	18.8	21.1
#12	30.35	30.61	29.4	31.7
#13	230.04	230.38	229.3	231.2
#14	39.86	40.11	38.9	41.2
#15	19.92	20.17	18.8	21.2
#16	20.07	20.32	18.9	21.3
#17	40.06	40.31	39.0	41.3
#18	3.82	4.05	2.9	5.2
#19	6.51	6.80	5.5	7.8
#20	12.47	12.75	11.5	13.9

Table 4.49 confirms the relevance and applicability of the simple method presented for each test the two different intervals superimpose one each other. Fig. 4.45 shows a graphical representation of the mean values along with their confidence intervals for cases #2, #3 and #4. For these cases, the two intervals, referred to as N and W to be consistent with Table 4.49, have been plotted next to each other to better highlight the superimposition.

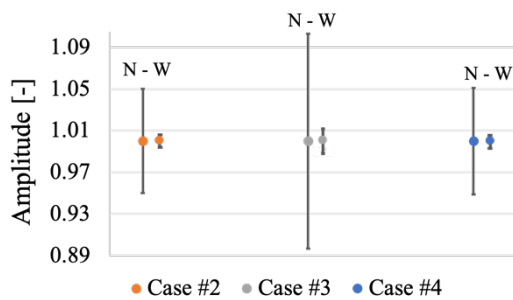


Fig. 4.45. Graphical representation of the measurements and their 95 % confidence intervals, in the case of tests #2, #3 and #4

The high non-linearity of the residual voltage module expression (4.104) leads to a non-symmetrical probability density function associated to the $|\bar{V}_R|$ random variable. In fact, the Nakagami distribution may exhibit a non-symmetrical shape for particular values of its parameters. The asymmetry is caused by the module which converts positive and negative real and imaginary terms of \bar{V}_R into always positive terms. This results in a shift of the $|\bar{V}_R|$ mean value from the measured value of $|\bar{V}_R|$. Moreover, this effect is considerable when the latter is close to zero (case #1), while it becomes negligible when this variable increases. This conclusion can be verified with two examples. They both deal with case #1 for a balanced three-phase system. Hence, the $|\bar{V}_R|$ is ideally zero. The first example refers to Table 4.46, comparing the proposed expression to the MC method. As it emerges from the μ_{MC} and μ_N values, they largely differ from the theoretical null value. The reason is

explainable by the effect of the ratio and phase errors, treated as random variables with zero mean. This correctly leads to the shift of $|\bar{V}_R|$ mean value as detailed before. The second example refers to case #1 in Table 4.48. A minor discrepancy can be noted between $|\bar{V}_R|_{DAQ}$ and $|\bar{V}_R|_N$, although they are computed starting from the same voltage phasors. The only difference from the previous example is that it refers to an actual measurement and not to a simulation. The $|\bar{V}_R|_N$ distribution tends to follow a normal distribution (Fig. 4.46 shows the case #2 PDF of $|\bar{V}_R|_N$). This holds for all tests whose means are far greater than zero. This applies to all of them except for case #1 (as confirmed by Fig. 4.41, 4.42 and 4.43).

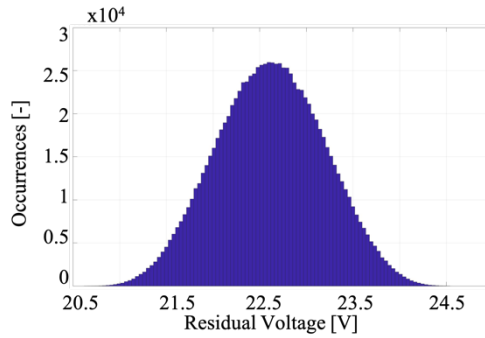


Fig. 4.46. PDF of $|\bar{V}_R|_N$ for case #2

In fact, high mean values turn into an $m > 1$ parameter in (4.121) and (4.122). Therefore, in a balanced three-phase system, which features $m = 1$, the effect is a probability density function far from being a normal distribution. Fig. 4.47 confirms the previous statement showing the Nakagami distribution for several m values. In this context, the 95 %-confidence intervals, described above, have been computed assuming a symmetric distribution.

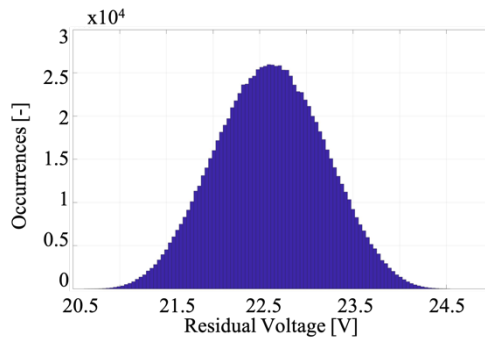


Fig. 4.47. PDF of a generic Nakagami distribution for several m and ω (o) parameters

4.2.3.6 Conclusion

The introduction of the LPVT technology has allowed to implement many new operating and measurement functions due to their better performance with respect to inductive ITs (bandwidth, accuracy, linearity, etc.). However, one critical value requires that LPVTs feature higher accuracies compared to values of ITs with open triangle. Such a value, the residual voltage, is still widely used for monitoring and controlling the operation of power networks. The correlation of the accuracy class of LPVTs to the uncertainty affecting the residual voltage is not straightforward. However, this relationship is strongly demanded by practitioners and all people involved in network design and operation.

To this end, the presented research extended a study which began in a companion paper presenting an expression for the correlation between the LPIT accuracy class and the residual voltage

uncertainty. In that work a symmetrical 3-phase system was studied. In this paper instead, an expression for a general 3-phase system has been proposed by authors.

The aim of this study has been to put all operators in a condition to simply evaluate and determine the expected uncertainty affecting the residual voltage when employing LPVTs with a given accuracy class.

To this purpose, this study derived a simplified expression based on the Nakagami distribution. Test and simulation results demonstrated the effectiveness of this assumption in any power network condition. Simulation results have been also confirmed by the measurements performed in an actual 3-phase system deployed in the laboratory. In conclusion, the proposed expression can become a simple and common way to predict the uncertainty related to the residual voltage measurement in all actual situations with a high accuracy.

Conclusion

This thesis work aims to introduce the reader into the field of Instrument Transformers, from a metrological point of view. In the beginning, an essential background is included. Therefore, Chapter 1 introduces the Instrument Transformer topic along with a detailed description of the main relevant technologies. Then, to align with their international state of the art, Chapter 2 describes and analyses all standards related to ITs. In addition, the mandatory requirements in terms of supplied electricity are included to understand which power networks quantities the ITs are subjected to.

This introduction to the work has been completed with its second “core”, the metrology. To this purpose, the basis of metrology and the concept of uncertainty have been introduced in chapter 3. These aspects have been a backbone for the entire Ph.D. duration and the research included here.

In this context, it has then been possible to address the main research, presented in chapter 4. It is divided in two main parts; firstly, the effects of external influence quantities on the IT’s behaviour have been presented. Secondly, some new application integrating the ITs in the Smart Grid operation have been proposed and described in the chapter.

These are the main conclusions and comments from the research in the previous chapters: as far as the effects of the external quantities on ITs are concerned, it has been demonstrated that the current knowledge and Standards do not always include all possible conditions. In particular, during the normal operation of ITs, several influence quantities act on them, changing their working point. Furthermore, some of these quantities have critical effects on ITs, and compromise their correct behaviour. To this purpose, in chapter 4, several tests have been described and verified in order to be considered for inclusion in future Standards.

Moving to the ITs’ integration in Smart Grid, some interesting applications have been presented in the second half of chapter 4. As the investigation shows, many applications can be designed by using ITs (although they are a consolidated technology, used and installed in-field for almost three decades). This can be explained by two main reasons. First of all, with the increasing need of knowledge from the grid (i.e. measurement points/nodes), the ITs are the link between the measuring devices and the grid, hence their role is and will be always fundamental. Second, there is no straightforward answer on the question of how accurate the collected measurements are. The reason is that available tools to evaluate uncertainty are typically used/applied by experts and metrologists. For this purpose, providing new tools and easy-to-use expressions could help to increase the uncertainty awareness and evaluation among non-experts and in-field operators.

In conclusion, this work takes a further step towards the full integration of ITs and Smart Grids. Of course, the possible number of applications are almost infinite; however, new inputs and starting points have been suggested to help researchers in this evolution process.

REFERENCES

- [1] IEC 60050, International Electrotechnical Vocabulary (IEV), 2019.
- [2] Kothari, D.P. Nagrath, I.J. (2010). *Electric Machines* (4th ed.). Tata McGraw-Hill.
- [3] Daniels, A. R. (1985). *Introduction to Electrical Machines*. Macmillan.
- [4] Harris, F. K. (1975). *Electrical Measurements*. Krieger.
- [5] IEC 61869-2:2014, “Instrument transformers - Part 2: Additional requirements for current transformers”, International Standardization Organization, Geneva, Switzerland, 2014.
- [6] S. B. McGrayne, F. N. H. Robinson et al, “Electricity”, *Encyclopaedia Britannica*, 2019.
- [7] IEC 61869-3:2014, “Instrument transformers - Part 3: Additional requirements for voltage transformers”, International Standardization Organization, Geneva, Switzerland, 2014.
- [8] IEC 61869-4:2014, “Instrument transformers - Part 4: Additional requirements for combined transformers”, International Standardization Organization, Geneva, Switzerland, 2014.
- [9] IEC 61869-6:2016, “Instrument transformers - Part 6: Additional general requirements for low-power instrument transformers”, International Standardization Organization, Geneva, Switzerland, 2016.
- [10] M. H. Samimi, A. Mahari, M. A. Farahnakian, H. Mohseni, “The Rogowski Coil Principles and Applications: A Review”, *IEEE Sensors Journal*, vol. 15, no. 2, pp. 651-658, 2015.
- [11] J. Lehr, P. Ron, *Foundations of Pulsed Power Technology*, IEEE Press Wiley, 445 Hoes Lane, Piscataway, NJ, 2017.
- [12] IEC 61869-11:2017, “Instrument transformers - Part 11: Additional requirements for low-power passive voltage transformers”, International Standardization Organization, Geneva, Switzerland, 2017.
- [13] K. Stankovic, U. Kovacevic, “Combined Measuring Uncertainty of Capacitive Divider With Concentrated Capacitance on High-Voltage Scale”, *IEEE Transaction on Plasma Science*, vol. 46, no. 8, pp. 2972-2978, 2018.
- [14] T. Hobejogi, J. Biela, “Coaxial capacitive voltage divider with high division ratio for high voltage pulses with very fast rise times”, *IEEE Pulsed Power Conference*, Chicago, IL, June 2011.
- [15] EN 50160:2011, “Voltage characteristics of electricity supplied by public electricity networks”, European committee for standardization, Brussels, 2017.
- [16] IEC 61869-1:2007, “Instrument transformers - Part 1: General requirements”, International Standardization Organization, Geneva, Switzerland, 2007.
- [17] IEC 60038:2002, “IEC Standard Voltages”, International Standardization Organization, Geneva, Switzerland, 2002.
- [18] IEC 61869-12, “Instrument transformers - Part 12: Additional requirements for combined electronic instrument transformer or combined stand alone sensors”, International Standardization Organization, Geneva, Switzerland, Draft 2018.
- [19] IEC 61869-10:2017, “Instrument transformers - Part 10: Specific requirements for low power passive current transformers”, International Standardization Organization, Geneva, Switzerland, 2017.
- [20] A. Ferrero, D. Petri, P. Carbone, M. Catelani, *Modern Measurements*, IEEE Press Wiley, 445 Hoes Lane, Piscataway, NJ, 2015.
- [21] BIPM JCGM 100:2008. Evaluation of measurement data – Guide to the expression of uncertainty in measurement (GUM), GUM 1995 with minor corrections (2008). Available at BIPM <http://www.bipm.org/en/publications/guides/gum.html>
- [22] BIPM JCGM 101:2008. Evaluation of measurement data – Supplement 1 to the Guide to the expression of uncertainty in measurement – Propagation of distributions using a Monte Carlo method. Available at BIPM <http://www.bipm.org/en/publications/guides/gum.html>

- [23] BIPM JCGM 104:2009. Evaluation of measurement data – An introduction to the “Guide to the expression of uncertainty in measurements” and related documents.
- [24] R. Mathieu, *Probability, Statistics and Estimation*, Creative commons attribution-noncommercial, 2013.
- [25] M. Asprou, E. Kyriakides, M. Albu, “Bad data detection considering the accuracy of instrument transformers” IEEE Power and Energy Society General Meeting, pp. 1-5, 2016.
- [26] R. Stiegler, J. Meyer, J. Kilter, S. Konzelman, “Assessment of voltage instrument transformers accuracy for harmonic measurements in transmission systems”, 17th international conference on harmonics and quality power, pp. 152-157, 2016.
- [27] M. Kaczmarek, S. Jama, “Accuracy of inductive voltage transformer in the presence of voltage high harmonics”, International Conference on High Voltage Engineering and Application, pp. 1-4, 2014.
- [28] Y. Tong, B. Liu, X. Deng, Y. Wang, “The experimental study on the electronic instrument transformer harmonic accuracy”, China international conference on electricity distribution, pp. 1136-1139, 2014.
- [29] A. Mingotti, L. Peretto, R. Tinarelli, “Assessment of Metrological Characteristics of Calibration Systems for Accuracy vs. Temperature Verification of Voltage Transformer”, Proc. of IEEE Workshop on Applied Measurements for Power Systems, Liverpool, September 2017.
- [30] W. H. Tang, Q. H. Wu, Z. J. Richardson, “Equivalent heat circuit based power transformer thermal model”, IEEE proceedings – electric power applications, vol. 149, no. 2, pp. 87-92, 2002.
- [31] F. Della Torre, M. Faifer, A. P. Morando, R. Ottoboni, C. Cherbaucich, M. Gentili, P. Mazza, “Instrument transformers: a different approach to their modeling”, IEEE international workshop on applied measurement for power systems, pp. 37-42, 2011.
- [32] A. Mingotti, G. Pasini, L. Peretto, R. Tinarelli, “Effect of temperature on the accuracy of inductive current transformers”, *IEEE International Instrumentation and Measurement Technology Conference*, Houston, TX, USA, 2018.
- [33] L. Ferkovic, D. Ilic, R. Malaric, “Mutual inductance of a precise Rogowski coil in dependence of the position of primary conductor”, *IEEE Transactions on Instrumentation and Measurement*, vol. 58, no. 1, pp. 122-128, 2009.
- [34] P. Fubin, G. Lei, Y. Yubo, B. Qiangsheng, J. Jianfei, “Effects of geometrical parameters on the performance of Rogowski coil for current measuring”, IEEE PES Asia-Pacific Power and Energy Engineering Conference, Xi’an, Oct. 2016.
- [35] H.M. Wang, F. Liu, H.L. Zhang, S.X. Zheng, “Analysis of the thermal expansion effect on measurement precision of Rogowski coils”, *International Conference on Power Electronics and Drives Systems*, Kuala Lumpur, Dec. 2005.
- [36] W. Teppan, P. Turpin, M. Beguin, “IEC 61869 compliant Rogowski coil for volume production”, IEEE International Workshop on Applied Measurements for Power Systems, Aachen, Sep. 2016.
- [37] L. Peretto, L. Sandrolini, R. Tinarelli, “Effects of radiated electromagnetic fields on measurements performed by air-core passive LPCTs”, IEEE International Workshop on Applied Measurements for Power Systems, Aachen, Sep. 2015.
- [38] A. Mingotti, L. Peretto, R. Tinarelli, “Effects of Multiple Influence Quantities on Rogowski-Coil-Type Current Transformers”, *submitted to IEEE Transaction on Instrumentation and Measurement*, April 2019.
- [39] A. Monti, C. Muscas, F. Ponci, “Phasor Measurement Units and Wide Area Monitoring Systems, From the sensor to the systems”, Elsevier, 2016.
- [40] Steinmetz CP. Complex quantities and their use in electrical engineering. In: Proceedings of the international electrical congress. AIEE; 1893. p. 33–74.

- [41] IEEE, IEEE standard for a precision clock synchronization protocol for networked measurement and control systems, IEEE Std 1588-2008 (Revision of IEEE Std 1588-2002), July 2008.
- [42] IEC, "Communication networks and systems for power utility automation — Part 5: Communication requirements for functions and device models", IEC Standard IEC 61850-5:2013; 2013.
- [43] P. Janssen, T. Sezi, J.C. Maun, "Distribution system state estimation using unsynchronized phasor measurements", *Proc. of IEEE 2012 ISGT Europe*, pp. 1-6, 2012.
- [44] A.L. Dalcastagne, S. Noceti Filho, H.H. Zurn, R. Seara, "An Iterative Two-Terminal Fault-Location Method Based on Unsynchronized Phasors", *IEEE Transactions on Power Delivery*, vol. 23, no. 4, pp. 2318-2329, Oct. 2008.
- [45] D. Novosel, D. G. Hart, E. Udren and J. Garitty, "Unsynchronized two-terminal fault location estimation", *IEEE Trans. Power Del.*, vol. 11, no. 1, pp. 130-138, 1996.
- [46] A.A. Girgis, D.G. Hart, W.L. Peterson, "Unsynchronized two-terminal fault location estimation", *IEEE Transactions on Power Delivery*, vol. 7, no.1, Jan 1996.
- [47] Chi-Shan Yu; Li-Ren Chang; Jr-Ru Cho, "New Fault Impedance Computations for Unsynchronized Two-Terminal Fault-Location Computations", *IEEE Transactions on Power Delivery*, vol. 26, no. 4, pp. 2879-2881, Oct. 2011.
- [48] J. Izykowski, R. Molag, E. Rosolowski, M.M. Saha, "Accurate location of faults on power transmission lines with use of two-end unsynchronized measurements", *IEEE Transactions on Power Delivery*, vol. 21, no.2, April 2006.
- [49] M. Fulczyk, P. Balcerek, J. Izykowski, E. Rosolowski, M. M. Saha, "Two-end unsynchronized fault location algorithm for double-circuit series compensated lines", *Proc. of IEEE Power and Energy Society General Meeting*, 2008.
- [50] B. Mahamedi, J.G. Zhu, "Unsynchronized Fault Location Based on the Negative-Sequence Voltage Magnitude for Double-Circuit Transmission Lines", *IEEE Transactions on Power Delivery*, vol. 29, no.4, Aug. 2014.
- [51] L. Yuansheng, W. Gang, L. Haifeng, "Time-Domain Fault-Location Method on HVDC Transmission Lines Under Unsynchronized Two-End Measurement and Uncertain Line Parameters", *IEEE Transactions on Power Delivery*, vol. 30, no.3, June 2015.
- [52] A. Mingotti, L. Peretto, R. Tinarelli, "A Novel Equivalent Power Network Impedance Approach for Assessing the Time Reference in Asynchronous Measurements", *proc of 2017 IEEE I2MTC*, may 2017, Turin, Italy.
- [53] P. Castello; J. Liu; C. Muscas; P. A. Pegoraro; F. Ponci; A. Monti, "A Fast and Accurate PMU Algorithm for P+M Class Measurement of Synchrophasor and Frequency", *IEEE Transactions on Instrumentation and Measurements*, vol. 63, no. 12, pp 2837-2845, 2014.
- [54] A. Carta; N. Locci; C. Muscas, "A PMU for the Measurement of Synchronized Harmonic Phasors in Three-Phase Distribution Networks", *IEEE Transactions on Instrumentation and Measurement*, vol 58, no. 10, 2009.
- [55] P. A. Pegoraro, A. Meloni, L. Atzori, P. Castello, "PMU-Based Distribution System State Estimation with Adaptive Accuracy Exploiting Local Decision Metrics and IoT Paradigm", vol 66, no.4, 2017.
- [56] A. Mingotti, L. Peretto, R. Tinarelli, "An Equivalent Synchronization for Phasor Measurements in Power Networks", *Proc. of IEEE 2017 AMPS*, pp 101-105, 2017.
- [57] L. Peretto; R. Sasdelli; E. Scala; R. Tinarelli, "Performance Characterization of a Measurement System for Locating Transient Voltage Sources in Power Distribution Networks", *IEEE Transactions on Instrumentation and Measurements*, vol. 58, no. 2, pp 450-456, 2009.
- [58] L. Peretto; R. Sasdelli; E. Scala; R. Tinarelli, "Metrological Characterization of a Distributed Measurement System to Locate Faults in Power Networks", *IEEE Instrumentation and Measurement Technology Conference*, pp 95-100, 2008.

- [59] M. Paolone; L. Peretto; R. Sasdelli; R. Tinarelli; M. Bernardi, C. A. Nucci, "On the use of data from distributed measurement systems for correlating voltage transients to lightning", *IEEE Transactions on Instrumentation and Measurements*, vol. 53, no. 4, pp 1202-1208, 2004.
- [60] C. Muscas; L. Peretto; S. Sulis; R. Tinarelli, "Investigation on Multipoint Measurement techniques for PQ Monitoring", *IEEE Transactions on Instrumentation and Measurements*, vol 55, no. 5, pp 1684-1690, 2006.
- [61] C. Muscas, "Power quality monitoring in modern electric distribution systems", *IEEE Instrumentation and Measurement Magazine*, vol. 13, no. 5, pp 19-27, 2010.
- [62] e-distribuzione DV7070, "Fault detection and power meter – Specifications and test methods", November 2016 (in italian).
- [63] A. Angioni, J. Shang, F. Ponci, A. Monti, "Real-time monitoring of distribution systems based on state estimation", *IEEE Transaction on Instrumentation and Measurements*, vol. 65, no. 10, pp. 2234-2243, 2016.
- [64] IEC 61850-9-2:2011, "Communication networks and systems for power utility automation - Part 9-2: Specific communication service mapping (SCSM) - Sampled values over ISO/IEC 8802-3", International Standardization Organization, Geneva, Switzerland, 2008
- [65] A. Mingotti, L. Peretto, R. Tinarelli, A. Angioni, A. Monti and F. Ponci, "Calibration of Synchronized Measurement System: from the Instrument Transformer to the PMU", IEEE workshop on Applied Measurements for Power Systems, AMPS, Bologna, Sep. 2018.
- [66] IEC 61869-13:2016, "Instrument transformers - Part 13: Stand Alone Mergin Unit", International Standardization Organization, Geneva, Switzerland.
- [67] Sepam Series 80 – Protective Relays, Instruction Bulletin 63230-216-230B1, Schneider Electric, 2007.
- [68] A. Mingotti, A. Baldi, L. Peretto, R. Tinarelli, "A General Easy-to-use Expression for Uncertainty Evaluation in Residual Voltage Measurement", *IEEE Transactions on Instrumentation and Measurement* (Early Access), May 2019.
- [69] A. Mingotti, L. Peretto, R. Tinarelli, "Low Power Voltage Transformer Accuracy Class Effects on the Residual Voltage Measurement", Proc. of IEEE I2MTC, Houston, May 2018.
- [70] IEC 61869-105, "Uncertainty in the calibration of Instrument Transformers", under preparation by IEC TC38/WG55.
- [71] A. Mingotti, L. Peretto, R. Tinarelli, K. Yigit, "Simplified Approach to Evaluate the Combined Uncertainty in Measurement Instruments for Power Systems", *IEEE Transactions on Instrumentation and Measurement*, vol. 66, n. 9, pp 2258-2265, 2017.
- [72] M. Asprou; E. Kyriakides; M. Albu, "The Effect of Variable Weights in a WLS State Estimator Considering Instrument Transformer Uncertainties" *IEEE Transactions on Instrumentation and Measurement*, vol. 66, n. 9, pp 2258-2265, 2017.
- [73] M. Evans, N. Hastings, B. Peacock, "Chi Distribution." §8.3 in *Statistical Distributions*, 3rd ed. New York: Wiley, p. 57, 2000.
- [74] N. Johnson, S. Kotz, Balakrishnan, N. *Continuous Univariate Distributions*, Vol. 1, 2nd ed. Boston, MA: Houghton Mifflin, 1994.
- [75] Laurenson, Dave (1994). "Nakagami Distribution". *Indoor Radio Channel Propagation Modelling by Ray Tracing Techniques*. Retrieved 2007-08-04.
- [76] J. F. Paris, "Nakagami-q (Hoyt) distribution function with applications", *IEEE Electronic Letters*, vol. 45, no. 4, pp. 210-211, Feb. 2009.
- [77] G. Betta, C. Liguori, A. Pietrosanto, "Propagation of uncertainty in a discrete Fourier transform algorithm", *Measurement*, vol. 27, Issue 4, pp 231-239, 2000.
- [78] J. F. Prewitt, "Amplitude bias in the Fourier transforms of noisy signals", *IEEE Transactions on Antennas and Propagation*, vol. 26, no. 5, pp 730-731, Sep. 1978

LIST OF FIGURES

- Fig. 1.1. Main components of a generic transformer
- Fig. 1.2. Transformer equivalent circuit, referred to the primary windings
- Fig. 1.3. Connection of the CT in series to the main circuit
- Fig. 1.4. Vector diagram of the CT
- Fig. 1.5. From left to right: wound-type, bar-type, toroidal-type CT
- Fig. 1.6. Connection of the VT in parallel to the main circuit
- Fig. 1.7. Vector diagram of the VT
- Fig. 1.8. From left to right: wound-type, capacitive-type VT
- Fig. 1.9. Schematic of a capacitive voltage transformer
- Fig. 1.10. Picture (left) and simple schematic (right) of a combined transformer
- Fig. 1.11. General block diagram of a single-phase LPIT
- Fig. 1.12. Basic structure of a Rogowski coil
- Fig. 1.13. Rogowski coil equivalent single-phase circuit
- Fig. 1.14. Geometrical parameters clarification picture
- Fig. 1.15. Capacitive divider schematic
- Fig. 1.16. Picture of a medium voltage (left) and a high voltage (right) CD
- Fig. 1.17. Real capacitive divider schematic
- Fig. 2.1. List of all the documents included in the Standard IEC 61869 series
- Fig. 3.1. Example of signal affected by random (yellow) and systematic (red) effects
- Fig. 3.2. Example of how to treat unknown systematic effects
- Fig. 3.3. Schematic representation of the PDF propagation
- Fig. 4.1. Schematic representation of the experimental setup
- Fig. 4.2. Schematic representation of the setup for metrological characterization of the reference divider
- Fig. 4.3. Schematic representation of the setup for metrological characterization of the voltage divider
- Fig. 4.4. Schematic representation of the setup for metrological characterization of the calibrator
- Fig. 4.5. Schematic representation of the setup for metrological characterization of the DAQ
- Fig. 4.6. Graph of the characterization of the DAQ compared to the HP 3458A multimeter
- Fig. 4.7. Presented setup for the accuracy vs. temperature verification of current transformers
- Fig. 4.8. Metrological characterization setup for the measurement chain shunt + amplifier + DAQ
- Fig. 4.9. Ratio Error vs. temperature of transformer A for 20 % and 100 % of the rated primary current
- Fig. 4.10. Phase displacement vs. temperature of transformer A for 20 % and 100 % of the rated primary current
- Fig. 4.11. Ratio Error vs. temperature of transformer B for 20 % and 100 % of the rated primary current
- Fig. 4.12. Phase displacement vs. temperature of transformer B for 20 % and 100 % of the rated primary current
- Fig. 4.13. Schematic representation of the developed automatic measurement setup
- Fig. 4.14. Pictures of the 4 test configurations adopted. Each of them describes a different relative position between the LPCT and the internal and/or external conductor
- Fig. 4.15. Different perspective of the test D to highlight the relative position between the transmitting cable and the external conductor.
- Fig. 4.16. Ratio Error results for tests #1 to #4. Accuracy vs. positions, 22 °C, 50 Hz
- Fig. 4.17. Ratio Error results for tests #5 to #12. Accuracy vs. positions, 22 °C, 48 Hz (solid) and 51 Hz (dotted)

- Fig. 4.18. Ratio Error results for tests #1, #13 and #28. Accuracy vs. temperature, 50 Hz
- Fig. 4.19. Ratio Error results for tests #5, #9, #14, #15, #29 and #30. Accuracy vs. temperature, 48 Hz (solid) and 51 Hz (dotted)
- Fig. 4.20. Ratio Error results for tests at 50 Hz, for two different temperatures (22 °C, solid line; 5 °C, dotted line), for all the positions
- Fig. 4.21. Ratio Error results for tests at 50 Hz, for two different temperatures (22 °C, solid line; 40 °C, dotted line), for all the positions
- Fig. 4.22. Ratio Error results for tests concerning all the influence quantities acting on the RUT (X)
- Fig. 4.23. Ratio Error results for tests concerning all the influence quantities acting on the RUT (Y)
- Fig. 4.24. Ratio Error results for tests concerning all the influence quantities acting on the RUT (Z)
- Fig. 4.25. Model of an elementary portion of a single-wire line
- Fig. 4.26. T-circuit representation of a single-wire line
- Fig. 4.27. Single-wire line topology
- Fig. 4.28. Representation of a single-wire line and its load used in the proposed approach
- Fig. 4.29. Procedure for estimating the phase difference $\Delta\varphi_e$ between \bar{V}_1 and \bar{V}'_2
- Fig. 4.30. PI-schematization of an electric line, resulting from the two-port model matrix
- Fig. 4.31. 4-nodes power network configuration adopted for both the algorithms presented
- Fig. 4.32. Measurement points when applying the two terminals algorithm to the 4-nodes power network configuration
- Fig. 4.33. Representation of a single-wire line and its load used in the proposed approach
- Fig. 4.34. Trend of the resistance and the reactance with respect to the cross section of a medium voltage cable (8.7-15 kV)
- Fig. 4.35. Suggested measurement setup and Acquisition System (AS) applied on the 4-nodes power network configuration
- Fig. 4.36. Amplitude (mrad) of the 95% confidence interval of the phase displacement $\Delta\varphi_{12}$, considering only the effect of ITs with respect to the different accuracy classes, for the 4 analyzed cases
- Fig. 4.37. Amplitude (mrad) of the 95% confidence interval of the phase displacement $\Delta\varphi_{13}$, considering only the effect of ITs with respect to the different accuracy classes, for the 4 analyzed cases
- Fig. 4.38. Amplitude (mrad) of the 95%-confidence interval of the phase displacement $\Delta\varphi_{12}$, when only the effect of the percentage variation of the branches length from the rated values are considered
- Fig. 4.39. Amplitude (mrad) of the 95%-confidence interval of the phase displacement $\Delta\varphi_{13}$, when only the effect of the percentage variation of the per-unit length reactance from the rated values are considered
- Fig. 4.40. Schematic of a typical setup for the measurement of three-phase system of symmetric voltages
- Fig. 4.41. PDF of $|\bar{V}_R|$ when three 0.1 class LPVTs are considered (case #1)
- Fig. 4.42. PDF of $|\bar{V}_R|$ when three 0.2 class LPVTs are considered (case #6)
- Fig. 4.43. PDF of $|\bar{V}_R|$ when three 0.5 class LPVTs are considered (case #11)
- Fig. 4.44. Schematic of the measurement setup adopted for the residual voltage measurement
- Fig. 4.45. Graphical representation of the measurements and their 95 % confidence intervals, in the case of tests #2, #3 and #4
- Fig. 4.46. PDF of $|\bar{V}_R|_N$ for case #2
- Fig. 4.47. PDF of a generic Nakagami distribution for several m and ω (o) parameters

LIST OF TABLES

Table 2.1.	Temperature categories for Instrument Transformers
Table 2.2.	List of tests, to be performed on ITs, defined in IEC 61869-1 and 6
Table 2.3.	Rated quantities defined in the Standards for inductive current and voltage transformers
Table 2.4.	Limits of the ratio error and phase displacement for inductive current transformers
Table 2.5.	Limits of the ratio error and phase displacement for inductive voltage transformers
Table 2.6.	Limits of the ratio error and phase displacement for protective inductive current transformers
Table 2.7.	Limits of the ratio error and phase displacement for protective inductive voltage transformers
Table 2.8.	Rated quantities defined in the Standards for low-power current and voltage transformers
Table 2.9.	Limits of the ratio error and phase displacement for protective LPVTs
Table 2.10.	Limits of the ratio error and phase displacement for low-power current transformers
Table 2.11.	
Table 2.12.	List of low/medium voltage phenomena and events
Table 2.13.	Percentage of the maximum value of each single harmonic allowed over the voltage supply
Table 4.1.	Repeated measurements of the 600 V output value provided by the Calibrator to the reference divider and measured with the multimeter 3458A
Table 4.2.	Repeated measurements of the 57V output value provided by the Calibrator to the resistance divider, measured with the multimeter 3458A
Table 4.3.	Repeated measurements of the 57V output value given from the Calibrator to the multimeter 3458A
Table 4.4.	Repeated measurements of the 600 V output value given from the Calibrator to the multimeter 3458A
Table 4.5.	Characteristics of the two transformers under test
Table 4.6.	Ratio error for different temperatures for the transformer A
Table 4.7.	Phase displacement for different ambient temperatures for the transformer A
Table 4.8.	Ratio error for different temperatures for the transformer B
Table 4.9.	Phase displacement for different ambient temperatures for the transformer B
Table 4.10.	Results of the metrological characterization of the setup
Table 4.11.	Characteristics of the two transformers under test
Table 4.12.	Thresholds of the ratio and phase errors for different percentages of the rated current
Table 4.13.	Ratio error for different temperatures for transformer A, at 100 % of the rated current
Table 4.14.	Phase displacement for different temperatures for transformer A, at 100 % of the rated current
Table 4.15.	Ratio error for different temperatures for transformer A, at 20 % of the rated current
Table 4.16.	Phase displacement for different temperatures for transformer A, at 20 % of the rated current
Table 4.17.	Ratio error for different temperatures for transformer B, at 100 % of the rated current
Table 4.18.	Phase displacement for different temperatures for transformer B, at 100 % of the rated current
Table 4.19.	Ratio error for different temperatures for transformer B, at 20 % of the rated current
Table 4.20.	Phase displacement (mrad) for different temperatures for transformer B, at 20 % of the rated current
Table 4.21.	Accuracy specification of the Calibrator Fluke 6105a

Table 4.22.	Main Characteristics of the Rogowski coils under test
Table 4.23.	Main characteristics of the NI 9238
Table 4.24.	List of all the performed test: 36 for each RUT
Table 4.25.	Resistive burden characterization results
Table 4.26.	Test #1 results. Used to determine the actual ratio of the Rogowski coils
Table 4.27.	Phase Error results for tests #1, #13, and #28
Table 4.28.	Phase displacement computation results for all the accuracy vs. temperature + position test combinations
Table 4.29.	Per unit length parameters for the three types of cable
Table 4.30.	Actual and Estimated voltage phase difference for different loads in a 5000 m length, 50 mm ² section cable
Table 4.31.	Actual and Estimated voltage phase difference for different loads in a 7500 m length, 50 mm ² section cable
Table 4.32.	Actual and Estimated voltage phase difference for different loads in a 10000 m length, 50 mm ² section cable
Table 4.33.	Actual and Estimated voltage phase difference for different loads in a 5000 m length, 95 mm ² section cable
Table 4.34.	Actual and Estimated voltage phase difference for different loads in a 7500 m length, 95 mm ² section cable
Table 4.35.	Actual and Estimated voltage phase difference for different loads in a 10000 m length, 95 mm ² section cable
Table 4.36.	Actual and Estimated voltage phase difference for different loads in a 5000 m length, 240 mm ² section cable
Table 4.37.	Actual and Estimated voltage phase difference for different loads in a 7500 m length, 240 mm ² section cable
Table 4.38.	Actual and Estimated voltage phase difference for different loads in a 10000 m length, 240 mm ² section cable
Table 4.39.	Lengths of the branches in the different considered cases
Table 4.40.	Actual phase displacements among the nodes φ_{ij} and phase errors $\Delta\varphi_{ij}$ introduced by the two methods, for the Case #1 and for different loads
Table 4.41.	Actual phase displacements among the nodes φ_{ij} and phase errors $\Delta\varphi_{ij}$ introduced by the two methods, for the Case #4 and for different loads
Table 4.42.	Ratio errors and phase errors for CT and VT
Table 4.43.	Amplitude (mrad) of the 95 %-confidence interval of the phase displacement $\Delta\varphi_{12}$, when all the sources of uncertainty are considered
Table 4.44.	Amplitude (mrad) of the 95 %-confidence interval of the phase displacement $\Delta\varphi_{13}$, when all the sources of uncertainty are considered
Table 4.45.	List of the phasor values for the 15 tests
Table 4.46.	Mean value and variance of $ \bar{V}_R $ for the #15 tests applying the MC method and the proposed expression
Table 4.47.	List of the phasor values for each of the 20 tests performed
Table 4.48.	Residual voltage measurement results comparison between simulations and actual tests
Table 4.49.	95 %-confidence interval limits for the mean values $ \bar{V}_R _W$ and $ \bar{V}_R _N$

LIST OF ACRONYMS

CD	Capacitive Divider
CLT	Central Limit Theorem
CT	Current Transformer
CVT	Capacitive-type Voltage Transformer
DAQ	Data AcQuisition Board
GUM	Guide to the expression of Uncertainty in Measurements
HV	High Voltage
IED	Intelligent Electronic Device
IT	Instrument Transformer
JCGM	Joint Committee for Guide in Metrology
LPCT	Low-Power Current Transformers
LPIT	Low-Power Instrument Transformers
LPVT	Low-Power Voltage Transformers
MC	Monte Carlo
MCM	Monte Carlo Method
MV	Medium Voltage
OVT	Optical-type Voltage Transformer
PC	Personal Computer
PDF	Probability Density Function
PLL	Phase Locked Loop
PMU	Phasor Measurement Unit
RUT	Rogowski Under Test
TC	Technical Committee
VT	Voltage Transformer